UNIVERSITY OF CALIFORNIA, SAN DIEGO

DETERMINANTS OF ACTIVE AND PASSIVE TENSION IN SKELETAL MUSCLE

A dissertation submitted in partial satisfaction of the

requirements for the degree Doctor of Philosophy

in

Bioengineering

by

Taylor M. Winters

Committee in charge:

Professor Samuel R. Ward, Chair
Professor Robert L. Sah, Co-Chair
Professor Richard L. Lieber
Professor Simon Schenk
Professor Shyni Varghese

2012

The dissertation of Taylor M. Winters is approved, and it is acceptable in quality and form for publication on microfilm and electronically:

_____

_____

_____

_____

_____
Co-Chair

_____
Chair

University of California, San Diego

2012

TABLE OF CONTENTS

LIST OF TABLES

LIST OF FIGURES

ACKNOWLEDGMENTS

I would like to first and foremost thank my doctoral adviser and mentor, Dr. Samuel Ward, for always supporting, believing, and guiding me. He always pushed me to be the best and allowed me to pursue my own ideas. I am also grateful for the guidance and enthusiasm of Dr. Lieber. I would also like to acknowledge the current and past members of the Lieber/Ward Lab who have made this work possible, which includes Shannon Bremner, who could fix any issue, David Gokhin, who could answer all of my muscle-related questions, and Trevor Kingsbury, Alan Kwan, Genero Sepulveda, and Eric Chehab, who could always made me appreciate my time in lab. Finally, I would like to thank my wife and family for their irreplaceable support.

Chapter 2, in full, is a reprint of the published article "Whole Muscle Length-Tension Relationships Are Accurately Modeled as Scaled Sarcomeres in Rabbit Hindlimb Muscles." Winters TM, Takahashi M, Lieber RL, Ward SR. *Journal of Biomechanics*, 4(44), 109-115, 2011. The dissertation author was the primary investigator and author of this paper.

Chapter 3, in full, is currently being prepared for submission for publication of the material as it may appear in Journal of Biomechanics, 2012, Winters TM, Lieber RL, Ward SR. The dissertation author was the primary investigator and author of this paper.

Chapter 4, in full, is currently being prepared for submission for publication of the material as it may appear in Journal of Biomechanics, 2012, Winters TM, Yamaguchi T, Masuda K, Lieber RL, Ward SR. The dissertation author was the primary investigator and author of this material.

VITA

2007	B.S. in Bioengineering, *cum laude* University of California, San Diego, La Jolla, California
2008	M.S. in Bioengineering University of California, San Diego, La Jolla, California
2008-2009	Graduate Teaching Assistant University of California, San Diego, La Jolla, California
2008-2012	Graduate Student Researcher Muscle Physiology Labratory University of California, San Diego, La Jolla, California
2012	Ph.D., Bioengineering University of California, San Diego, La Jolla, California

Journal Articles

Winters TM, Yamaguchi T, Masuda K, Lieber RL, Ward SR. Determinants of Active and Passive Tension Following Tenotomy. *In Preparation*.

Winters TM, Lieber RL, Ward SR. Nonlinear Scaling of Passive Tension in Skeletal Muscle. *In Preparation*.

Winters TM, Lim M, Takahashi M, Fridén J, Lieber RL, Ward SR. Muscle Architecture Determines Active and Passive Tension-Generating Impairments During Surgical Release. *Submitted Journal of Biomechanics*.

Winters TM, Sepulveda GS, Cottler PS, Kaufman KR, Lieber RL, Ward SR. Correlation Between Force and Intramuscular Pressure During Dynamic Contractions in Rabbit Tibialis Anterior Muscle with an Intact Anterior Compartment. *Submitted Muscle and Nerve*.

Franko OI, Winters TM, Tirrell TF, Hentzen ER, Lieber RL. Moment arms of the human digital flexors. *Journal of Biomechanics*, 44(10), 1987-1990, 2011. (PMID: 21561624)

Winters TM, Takahashi M, Lieber RL, Ward SR. Whole Muscle Length-Tension Relationships Are Accurately Modeled as Scaled Sarcomeres in Rabbit Hindlimb Muscles. *Journal of Biomechanics*, 4(44), 109-115, 2011. (PMID 20889156)

Ward SR, Winters TM, Blemker SS. The Architectural Design of the Gluteal Muscle Group: Implications for Movement and Rehabilitation. *Journal of Orthopaedic and Sports Physical Therapy*, 40(2), 95-102, 2010. (PMID: 20118527)

Winters TM, Sepulveda GS, Cottler PS, Kaufman KR, Lieber RL, Ward SR. Correlation Between Isometric Force and Intramuscular Pressure in Rabbit Tibialis Anterior Muscle with an Intact Anterior Compartment. *Muscle and Nerve*, 40(1), 79-85, 2009. (PMID: 19533654)

Ward SR, Takahashi M, Winters TM, Kwan A, Lieber RL. A novel muscle biopsy clamp yields accurate in vivo sarcomere length values. *Journal of Biomechanics*, 19;42(2) 193-196, 2009.

ABSTRACT OF THE DISSERTATION

DETERMINANTS OF ACTIVE AND PASSIVE TENSION IN SKELETAL MUSCLE

by

Taylor M. Winters

Doctor of Philosophy in Bioengineering

University of California, San Diego, 2012

Professor Samuel R. Ward, Chair
Professor Robert L. Sah, Co-Chair

Structure-function relationships are paramount to predicting *in vivo* muscle function. Muscle architecture is commonly used to predict both active and passive performance. Although these relationships are assumed to be true for active tension, architectural-based predictions of passive tension are unable to capture muscle-specific differences. Passive tension is thought to arise from the resistive stretch of titin and collagen, but the relative importance of these load-bearing proteins and muscle architecture is unclear. The purpose of this work was to investigate the ability of biochemical and architectural parameters to predict active and passive properties of skeletal muscle at different size scales and strains. To robustly evaluate these predictors, functional changes were induced via tenotomy and the morphologic parameters were reevaluated to refine the active and passive models. An approach combining mechanical testing, biochemical assays, and computation modeling was implemented to show that both active and passive performance characteristics can be accurately predicted using a combination of muscle architecture and protein composition under both healthy and pathologic conditions.

CHAPTER 1

INTRODUCTION

Skeletal muscle represents the classic biological example of a structure-function relationship. The production of force within muscle is intimately linked to the physical arrangement of muscle components, from the micro to the macro scale. Therefore, to appropriately discuss muscle function, structures that mediate that force must be identified and closely examined.

1.1 Structure-Function Relationship in Skeletal Muscle

1.1.1 Active Tension

The ability for muscles to generate force results from the highly coordinated interactions between the actin thin filaments and the myosin thick filaments (myofilaments) in sarcomeres. These filaments are organized into a repeating array, the functional unit known as the sarcomere. Sarcomeres are arranged serially into myofibrils, which are packed radially inside muscle fibers. These fibers compose fascicles, and in turn, fascicles compose whole muscles (Fig. 1.1).

The fundamental structure-function property that relates sarcomere length to active force production is the length-tension relationship (Fig. 1.2), which is derived

from isometric experiments (where sarcomere length is held constant) [1-4]. This length-tension relationship is dictated by the classic sliding filament model, which states that active muscle force is proportional to the amount of overlap between thin and thick filaments [5, 6]. Analysis and application of the sliding filament model is the theoretical foundation of active muscle function [7].

Three characteristic regions are apparent on the sarcomere length-tension curve: the ascending limb (shallow & steep), plateau, and descending limb. Each limb is associated with varying amounts of myofilament overlap. When overlap is optimized, force production is maximized; this represents the plateau region of the length-tension curve (Fig. 1.2; Region 2). As sarcomere length increases, filament overlap decreases, which results in force reduction; this corresponds to the descending limb (Fig. 1.2; Region 3). Similarly, as sarcomere length decreases from optimal length, actin filaments interfere with each other, attenuating force production due to decreased overlap; this represents the shallow portion of the ascending limb. Finally, if sarcomere length is reduced further, hypothetically, the thick filament collides with the Z-disk (the protein assembly where thin filaments are anchored), and force production is rapidly diminished; this corresponds to the steep portion of the ascending limb (Fig. 1.2; Region 1). This theoretical relationship has been shown to be experimentally true in frog fibers [2] and mouse fibers [8].

The length-tension relationship of a muscle can be measured by imposing fixed-end (isometric) contractions at a series of sarcomere lengths [9]. Sarcomere length can be determined using a real-time approach, such as optical methods [10] or using laser diffraction [11].

In comparison to a sarcomere length-tension curve, whole muscle length-tension curves have a slightly different appearance. Sarcomere and fiber length

heterogeneities within a whole muscle result in a smoothing and broadening of the length-tension relationship [12].

1.1.2 Passive Tension

Muscle doesn't simply produce force through active contraction; it can also provide resistance to stretch in the absence of activation. This resistance is known as passive tension. Thus, a passive length tension curve may be added to the active length tension curve described above.

Magid and Law [13] demonstrated that the origin of passive tension in frog muscle was within the myofibril and was not extracellular as previously believed [14-16]. From this result, a megadalton sized protein known as titin or connectin [17, 18] was concluded to be the primary source of passive tension. Titin spans the M-line to the Z-disc [19] and contains an extensible I-band region [20], which makes it a prime candidate for this role. Experiments in which titin was enzymatically removed yielded more compliant fibers [21]. Furthermore, titin was found to have many splice variants with much of the variation in the length of the extensible PEVK region, which can result in muscle-specific titin sizes. To probe this issue further, the size and corresponding length of titin was related to the stiffness, with shorter isoforms being stiffer [22, 23]. This presented strong evidence for titin bearing considerable muscle passive tension.

Despite the attention afforded to titin, data still suggests that the extracellular matrix (ECM) is important for passive tension development [24, 25]. ECM is composed of collagen that provide stiffness, elastins that provide elasticity, fibroblasts that synthesize, maintain, and provide the structural framework, as well as many other

proteins and cells. Collagen content, isoform distribution, and crosslinking have all been shown to have roles in passive load-bearing [24, 25]. Although ECM may not be functionally relevant at smaller size scales (e.g., a muscle fiber), it appears to play a significant role at larger size scales (e.g., fascicles and whole muscles). This is due to the hierarchical structure of the connective tissue matrix: it ensheathes whole muscle (epimysium), surrounds fiber bundles (perimysium) and provides inter-fibrillar connections (endomysium). Thus, ECM has a more significant presence at larger scales. ECM provides structural support at each level, and also provides a route of transmitting force to the external world.

The influence of each protein on passive tension is known to be strain dependent. Titin has been shown to dominate at short lengths, while collagen dominates at long lengths [26]. With small strains, the I-band region of titin produces force, but when strained by a factor of 3-4 [27, 28], it is forcibly detached from its anchor points in the A-band [27]. Along with the stretching of unique domains within titin, this results in a force plateau at longer lengths because more domains of titin become extensible. In contrast, the contribution of collagen is small at short strains due to crimping of the collagen fibril, but as strain increases, the uncrimping produces tension at higher strains [29-32].

The role of ECM in muscle function has been largely neglected in favor of contractile studies, but new emerging evidence suggests that ECM plays a large role in muscle function, especially during pathology. Alterations to the ECM are a hallmark of nearly every case of myopathy or altered muscle use, from diabetes and muscular dystrophies to exercise and aging, highlighting its significance to proper muscle function [33-35].

1.1.3 Muscle Architecture

Similar to the organization of skeletal muscle at the microscopic level, the macroscopic level also displays a high level of structural organization. Skeletal muscle architecture is defined as "the arrangement of muscle fibers relative to the axis of force generation" [36] and is the main determinant of active muscle function at the whole muscle level [37]. The physiological cross-sectional area (PCSA) of a muscle is the best predictor of a muscle's maximum force generating capacity [38]. Similarly, the normalized fiber length of a muscle (experimentally measured fiber length normalized to a ratio of optimal sarcomere length and measured sarcomere length) predicts a muscle's maximum contractile velocity [39]. These architectural relationships have lead researchers to speculate that a similar relationship exists between the normalized fiber length of a muscle and the excursion (width) of its length-tension curve (Fig. 2), but this has never been explicitly verified. This insinuation also suggests that a whole muscle behaves functionally as a series of sarcomeres.

1.2 Musculoskeletal Modeling

As muscle force is difficult to measure in vivo, musculoskeletal models are necessary to understand both muscle function and human movement. However, it is unclear what level of complexity is needed in a model to accurately predict whole muscle function. Due to this discrepancy, the literature varies widely in the level of complexity in the models published. These models range from scaling the functional characteristics of a sarcomere up to whole muscle (scaled sarcomere model; [40]) to finite element analyses that incorporates tendon, aponeurosis, and constitutive muscle

properties [41]. The more complex models often emphasize interactions between muscles and body segments over the properties of any one muscle. Further, it has been suggested that simple models are inadequate and that more complex models are "better" without providing objective criteria for such statements. Despite this criticism, simple models are commonly used in the literature due to their ease of use and low computing power, but have been met with varied success.

Current estimates of whole muscle function either rely on a generic model of passive tension [42]. Using a conceptual, Hill-type model, the passive element produces at generic, non-dimensional length-tension curve. Therefore, by scaling this curve by a muscle's PCSA and normalized fiber length, it can be applied to any muscle. However, this model does not account for muscle-specific differences in load-bearing proteins or the organization of connective tissue within the muscle. Therefore, it is unclear whether simple generic models scaled by architectural parameters are adequate to predict active and passive function in whole muscle.

1.3 Muscle Plasticity

Skeletal muscle is an adaptive tissue that is able to remodel its properties based on its usage pattern. High loads placed on a muscle will result in hypertrophy to increase the maximum force output [43, 44]. Conversely, muscles that are not subject to use undergo fiber atrophy. This can result from immobilization, space flight, or tendon rupture [45]. Muscle atrophy is an active process in which proteins are selectively targeted for degradation to conserve the high-energy demand required for muscle upkeep. Moreover, muscles undergoing atrophy are often subject to a fibrotic response.

In addition to adding sarcomeres in parallel, muscle is also capable of adding sarcomeres in series to increase excursion via longer fibers. Muscles that are immobilized in a shortened position reduce the number of sarcomeres in series, while muscles immobilized in a lengthened position add sarcomeres [46, 47]. Muscles remodel in this manner to remain at the same point on the sarcomere length tension curve [48]. This property of muscle has important consequences during surgical operations in which muscle length is altered [49].

Muscle remodeling can also produce a change in fiber types, which can have important functional consequences for the muscle. Animal muscle has four fiber types, which are based largely on the myosin heavy chain isoform expressed (human expresses three of these). Type I, or slow, fibers have slower crossbridge cycling rates, produce less force than other fiber types, and are highly fatigue resistant. Conversely, fast fibers (Types IIA, IIX, and IIB) have faster crossbridge cycling rates, are capable of producing larger forces than type I fibers, and can vary in their fatigability depending on fiber type. The proportion of fast to slow fibers within a muscle depends heavily on muscle function. With an altered usage pattern, the proportion of fiber types within a muscle can shift to a slower phenotype with over-activity or to a faster phenotype with decreased use. The potential magnitude of these changes is controversial.

Aside from remodeling that occurs with age, exercise, and injury, pathologic muscles display a disconnect between the previously mentioned structure-function relationships. Changes in the normalized fiber length and PCSA were unable to predict the functional outcome of a muscle following a tendon transfer. However, it is unclear as to the mechanism of this uncoupling. Therefore, the relationships between structure and function may need to be evaluated following pathology.

1.4 Clinical Significance

Following pathology and its associated uncoupling of known structure-function relationships, current musculoskeletal models also break down. As buckle-transducers and similar testing protocols are highly invasive, muscle biopsies are commonly used to study muscle adaption following pathology. This involves the dissection of a small bundle of fibers that may be stored for later testing. Typically, (immuno)-histological sectioning and staining is completed on these biopsies to uncover changes in fiber type, the reorganization of specific proteins, and the general morphology of the tissue. However, biopsies can be passively tested as well to evaluate the functional adaption.

Fiber bundle passive tension moduli have been shown to be altered in cerebral palsy [50], desminopathy [51], intervertebral disc degeneration [52], and spasticity [53]. Several studies have attempted to extrapolate the functional conclusions determined at the bundle level to the whole muscle level [54, 55]. However, it is unclear whether changes at the bundle level accurately mimic those occurring at the whole muscle level.

Therefore, the overarching objective of this dissertation was to identify the key structural determinants of active and passive tension to provide a robust model for predicting function during normal and pathologic conditions. Specifically, Chapter 2 of this dissertation evaluates the use of a simplistic model to predict active and passive function based on sarcomere characteristics and architectural data. In Chapter 3, the key mediators of passive tension were identified at various size scales, and the relative contributions of these parameters were used to generate a new model of passive

tension that relies on morphologic and biochemical data. Finally, in Chapter 4, the models developed in Chapters 2 and 3 are robustly evaluated by inducing muscle remodeling via tenotomy of the distal tendon. The predictors of active and passive tension are re-evaluated and both models are reevaluated to be applicable under both healthy and pathologic conditions

1.5 References

1. Edman, K.A., *The relation between sarcomere length and active tension in isolated semitendinosus fibres of the frog.* J Physiol, 1966. **183**(2): p. 407-17.

2. Gordon, A.M., A.F. Huxley, and F.J. Julian, *The variation in isometric tension with sarcomere length in vertebrate muscle fibres.* J Physiol, 1966. **184**(1): p. 170-92.

3. Huxley, A.F., *Muscle structure and theories of contraction.* Prog Biophys Biophys Chem, 1957. **7**: p. 255-318.

4. Gordon, A.M., A.F. Huxley, and F.J. Julian, *Tension development in highly stretched vertebrate muscle fibres.* J Physiol, 1966. **184**(1): p. 143-69.

5. Huxley, A.F. and R. Niedergerke, *Structural changes in muscle during contraction; interference microscopy of living muscle fibres.* Nature, 1954. **173**(4412): p. 971-3.

6. Huxley, H. and J. Hanson, *Changes in the cross-striations of muscle during contraction and stretch and their structural interpretation.* Nature, 1954. **173**(4412): p. 973-6.

7. Lieber, R.L., *Skeletal Muscle Structure, Function & Plasticity: The Physiological Basis of Rehabilitation*. 2nd ed. 2002, Philadelphia: Lippincott Williams & Wilkins. xii, 369 p.

8. Edman, K.A., *Contractile properties of mouse single muscle fibers, a comparison with amphibian muscle fibers.* J Exp Biol, 2005. **208**(Pt 10): p. 1905-13.

9. Rassier, D.E., B.R. MacIntosh, and W. Herzog, *Length dependence of active force production in skeletal muscle.* J Appl Physiol, 1999. **86**(5): p. 1445-57.

10. Roos, K.P. and A.J. Brady, *Individual sarcomere length determination from isolated cardiac cells using high-resolution optical microscopy and digital image processing.* Biophys J, 1982. **40**(3): p. 233-44.

11. Lieber, R.L., Y. Yeh, and R.J. Baskin, *Sarcomere length determination using laser diffraction. Effect of beam and fiber diameter.* Biophys J, 1984. **45**(5): p. 1007-16.

12. Sinclair, P.J., *Forward dynamic modelling of cycling for people with spinal cord injury*, in *School of Exercise and Sport Science*. 2001, The University of Sydney: Lidcombe.

13. Magid, A. and D.J. Law, *Myofibrils bear most of the resting tension in frog skeletal muscle.* Science, 1985. **230**(4731): p. 1280-2.

14. Purslow, P.P., *Strain-induced reorientation of an intramuscular connective tissue network: implications for passive muscle elasticity.* J Biomech, 1989. **22**(1): p. 21-31.

15. Ramsey, R.W. and S.F. Street, *The isometric length-tension diagram of isolated skeletal muscle fibers of the frog.* J. cell. comp. Physiol., 1940. **15**: p. 11–34.

16. Borg, T.K. and J.B. Caulfield, *Morphology of connective tissue in skeletal muscle.* Tissue Cell, 1980. **12**(1): p. 197-207.

17. Maruyama, K., *Connectin, an elastic filamentous protein of striated muscle.* Int Rev Cytol, 1986. **104**: p. 81-114.

18. Wang, K., *Sarcomere-associated cytoskeletal lattices in striated muscle. Review and hypothesis.* Cell Muscle Motil, 1985. **6**: p. 315-69.

19. Maruyama, K., et al., *Connectin filaments link thick filaments and Z lines in frog skeletal muscle as revealed by immunoelectron microscopy.* J Cell Biol, 1985. **101**(6): p. 2167-72.

20. Trombitas, K., J.P. Jin, and H. Granzier, *The mechanically active domain of titin in cardiac muscle.* Circ Res, 1995. **77**(4): p. 856-61.

21. Funatsu, T., H. Higuchi, and S. Ishiwata, *Elastic filaments in skeletal muscle revealed by selective removal of thin filaments with plasma gelsolin.* The Journal of cell biology, 1990. **110**(1): p. 53-62.

22. Horowits, R., *Passive force generation and titin isoforms in mammalian skeletal muscle.* Biophysical journal, 1992. **61**(2): p. 392-8.

23. Freiburg, A., et al., *Series of exon-skipping events in the elastic spring region of titin as the structural basis for myofibrillar elastic diversity.* Circulation research, 2000. **86**(11): p. 1114-21.

24. Prado, L.G., et al., *Isoform diversity of giant proteins in relation to passive and active contractile properties of rabbit skeletal muscles.* J Gen Physiol, 2005. **126**(5): p. 461-80.

25. Kovanen, V., H. Suominen, and E. Heikkinen, *Mechanical properties of fast and slow skeletal muscle with special reference to collagen and endurance training.* J Biomech, 1984. **17**(10): p. 725-35.

26. Granzier, H.L. and T.C. Irving, *Passive tension in cardiac muscle: contribution of collagen, titin, microtubules, and intermediate filaments.* Biophys J, 1995. **68**(3): p. 1027-44.

27. Wang, K., et al., *Viscoelasticity of the sarcomere matrix of skeletal muscles. The titin-myosin composite filament is a dual-stage molecular spring.* Biophys J, 1993. **64**(4): p. 1161-77.

28. Granzier, H.L. and K. Wang, *Passive tension and stiffness of vertebrate skeletal and insect flight muscles: the contribution of weak cross-bridges and elastic filaments.* Biophys J, 1993. **65**(5): p. 2141-59.

29. Diamant, J., et al., *Collagen; ultrastructure and its relation to mechanical properties as a function of ageing.* Proc R Soc Lond B Biol Sci, 1972. **180**(60): p. 293-315.

30. Franchi, M., et al., *Tendon crimps and peritendinous tissues responding to tensional forces.* Eur J Histochem, 2007. **51 Suppl 1**: p. 9-14.

31. Franchi, M., et al., *Crimp morphology in relaxed and stretched rat Achilles tendon.* J Anat, 2007. **210**(1): p. 1-7.

32. Benjamin, M., E. Kaiser, and S. Milz, *Structure-function relationships in tendons: a review.* J Anat, 2008. **212**(3): p. 211-28.

33. Kang, L., et al., *Diet-induced muscle insulin resistance is associated with extracellular matrix remodeling and interaction with integrin alpha2beta1 in mice.* Diabetes. **60**(2): p. 416-26.

34. Foidart, M., J.M. Foidart, and W.K. Engel, *Collagen localization in normal and fibrotic human skeletal muscle.* Arch Neurol, 1981. **38**(3): p. 152-7.

35. Gao, Y., et al., *Age-related changes in the mechanical properties of the epimysium in skeletal muscles of rats.* J Biomech, 2008. **41**(2): p. 465-9.

36. Gans, C. and W.J. Bock, *The functional significance of muscle architecture--a theoretical analysis.* Ergeb Anat Entwicklungsgesch, 1965. **38**: p. 115-42.

37. Burkholder, T.J., et al., *Relationship between muscle fiber types and sizes and muscle architectural properties in the mouse hindlimb.* J Morphol, 1994. **221**(2): p. 177-90.

38. Powell, P.L., et al., *Predictability of skeletal muscle tension from architectural determinations in guinea pig hindlimbs.* J Appl Physiol, 1984. **57**(6): p. 1715-21.

39. Bodine, S.C., et al., *Architectural, histochemical, and contractile characteristics of a unique biarticular muscle: the cat semitendinosus.* J Neurophysiol, 1982. **48**(1): p. 192-201.

40. Huijing, P.A., A.A. van Lookeren Campagne, and J.F. Koper, *Muscle architecture and fibre characteristics of rat gastrocnemius and semimembranosus muscles during isometric contractions.* Acta Anat (Basel), 1989. **135**(1): p. 46-52.

41. Blemker, S.S. and S.L. Delp, *Rectus femoris and vastus intermedius fiber excursions predicted by three-dimensional muscle models.* J Biomech, 2006. **39**(8): p. 1383-91.

42. Zajac, F.E., *Muscle and tendon: properties, models, scaling, and application to biomechanics and motor control.* Crit Rev Biomed Eng, 1989. **17**(4): p. 359-411.

43. Roig, M., et al., *The effects of eccentric versus concentric resistance training on muscle strength and mass in healthy adults: a systematic review with meta-analysis.* British journal of sports medicine, 2009. **43**(8): p. 556-68.

44. Hather, B.M., et al., *Influence of eccentric actions on skeletal muscle adaptations to resistance training.* Acta physiologica Scandinavica, 1991. **143**(2): p. 177-85.

45. Lecker, S.H., et al., *Multiple types of skeletal muscle atrophy involve a common program of changes in gene expression.* The FASEB journal : official publication of the Federation of American Societies for Experimental Biology, 2004. **18**(1): p. 39-51.

46. Williams, P.E. and G. Goldspink, *The effect of immobilization on the longitudinal growth of striated muscle fibres.* J Anat, 1973. **116**(Pt 1): p. 45-55.

47. Williams, P.E. and G. Goldspink, *Changes in sarcomere length and physiological properties in immobilized muscle.* J Anat, 1978. **127**(Pt 3): p. 459-68.

48. Tabary, J.C., et al., *Physiological and structural changes in the cat's soleus muscle due to immobilization at different lengths by plaster casts.* The Journal of Physiology, 1972. **224**(1): p. 231-44.

49. Boakes, J.L., et al., *Muscle adaptation by serial sarcomere addition 1 year after femoral lengthening.* Clinical orthopaedics and related research, 2007. **456**: p. 250-3.

50. Smith, L.R., et al., *Hamstring contractures in children with spastic cerebral palsy result from a stiffer extracellular matrix and increased in vivo sarcomere length.* J Physiol, 2011. **589**(Pt 10): p. 2625-39.

51. Meyer, G.A. and R.L. Lieber, *Skeletal Muscle Fibrosis Develops in Response to Desmin Deletion.* Am J Physiol Cell Physiol, 2012.

52. Brown, S.H., et al., *ISSLS prize winner: Adaptations to the multifidus muscle in response to experimentally induced intervertebral disc degeneration.* Spine (Phila Pa 1976), 2011. **36**(21): p. 1728-36.

53. Friden, J. and R.L. Lieber, *Spastic muscle cells are shorter and stiffer than normal cells.* Muscle Nerve, 2003. **27**(2): p. 157-64.

54. Ward, S.R., et al., *Passive mechanical properties of the lumbar multifidus muscle support its role as a stabilizer.* J Biomech, 2009. **42**(10): p. 1384-9.

55. Ward, S.R., et al., *Architectural analysis and intraoperative measurements demonstrate the unique design of the multifidus muscle for lumbar spine stability.* J Bone Joint Surg Am, 2009. **91**(1): p. 176-85.

56. Gillies, A.R. and R.L. Lieber, *Structure and function of the skeletal muscle extracellular matrix.* Muscle Nerve. **44**(3): p. 318-31.

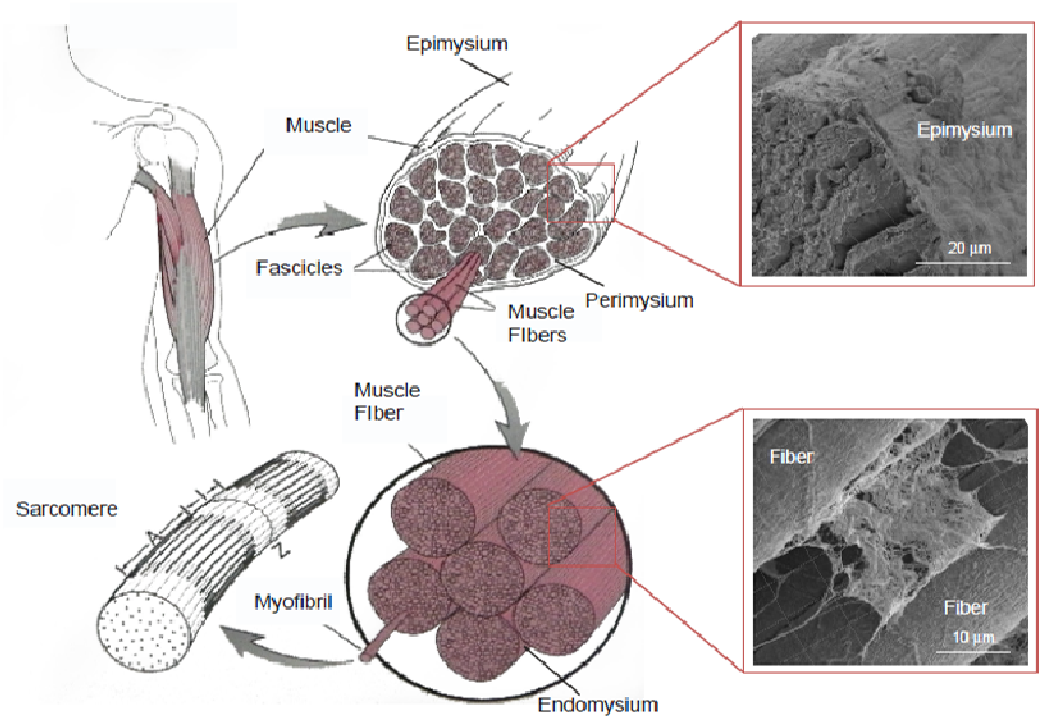

Figure 1.1: Diagram of the hierarchical organization of muscle. Whole muscle is ensheathed by a connective tissue matrix (epimysium; top inset). Muscle can be subdivided into fascicles, which are bundles of fibers surrounded by perimysium. Fibers are connected by endomysium (bottom inset) and are composed of radially packed myofibrils. Finally, myofibrils consist of serially arranged sarcomeres (the smallest functional unit of muscle). Schematic from [7] and SEM images from [56].

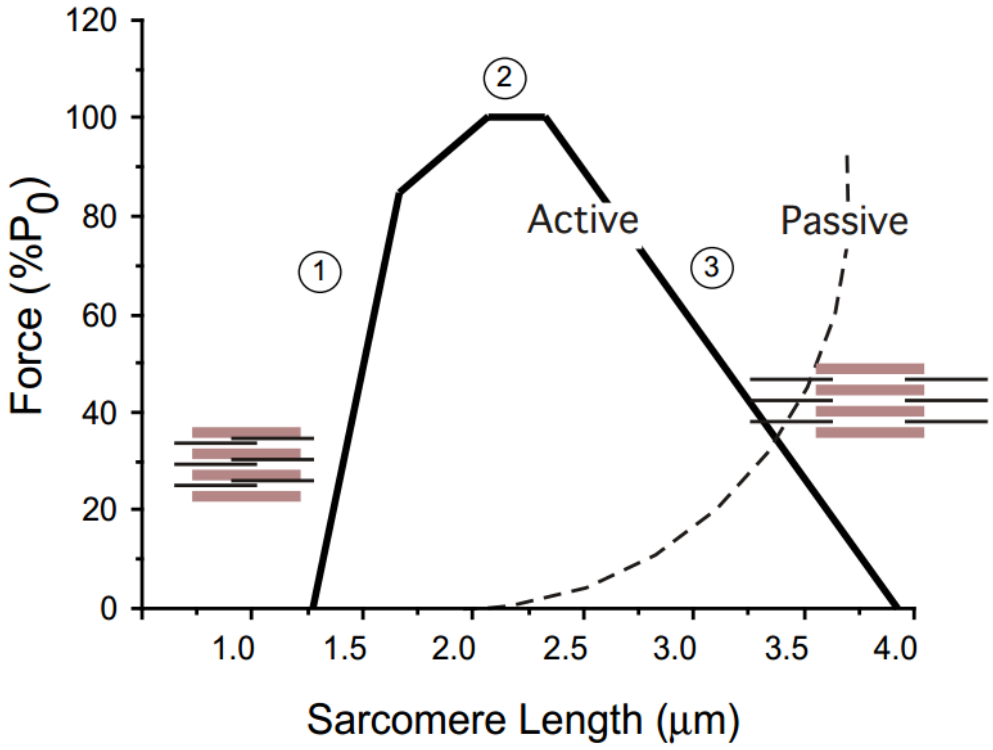

Figure 1.2: The length-tension relationship in muscle. The amount of force produced by a muscle is directly proportional to the amount of overlap between actin and myosin. Force is optimized on the plateau, but as sarcomere length increases or decreases, overlap decreases as does force production [1]. Schematic from [7].

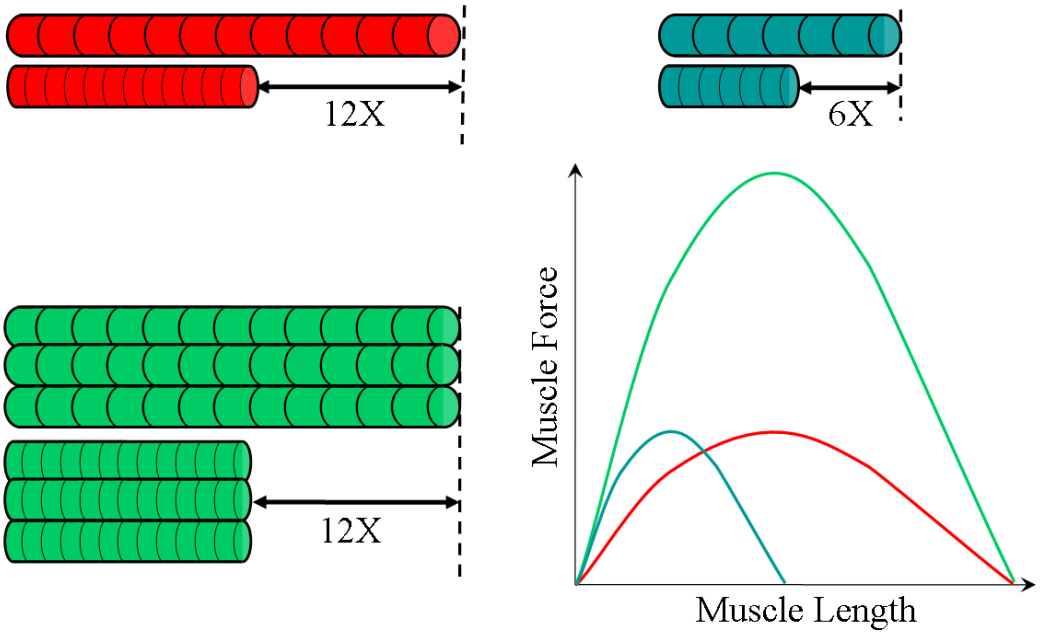

Figure 1.3: The structure-function relationship for muscle architecture. A hypothetical muscle with one fiber (red & blue) will have a third of the maximum force generating capacity of a muscle with three fibers (green). This relationship between PCSA and peak force output has lead to the hypothesis that a muscle with 12 sarcomeres in series (red & green) will have twice the excursion (width of the length-tension curve) of a muscle with 6 sarcomeres in series (blue).

CHAPTER 2

WHOLE MUSCLE LENGTH-TENSION RELATIONSHIPS ARE ACCURATELY MODELED AS SCALED SARCOMERES IN RABBIT HINDLIMB MUSCLES

2.1 Abstract

An *a priori* model of the whole active muscle length-tension relationship was constructed utilizing only myofilament length and serial sarcomere number for rabbit tibialis anterior (TA), extensor digitorum longus (EDL), and extensor digitorum II (EDII) muscles. Passive tension was modeled with a two-element Hill-type model. Experimental length-tension relations were then measured for each of these muscles and compared to predictions. The model was able to accurately capture the active - tension characteristics of experimentally-measured data for all muscles (ICC=0.88±0.03). Despite their varied architecture, no differences in predicted *versus* experimental correlations were observed among muscles. In addition, the model demonstrated that excursion, quantified by full-width-at-half-maximum (FWHM) of

the active length-tension relationship, scaled linearly (slope=0.68) with normalized muscle fiber length. Experimental and theoretical FWHM values agreed well with an intraclass correlation coefficient of 0.99 ($p < 0.001$). In contrast to active tension, the passive tension model deviated from experimentally-measured values and thus, was not an accurate predictor of passive tension (ICC=0.70±0.07). These data demonstrate that modeling muscle as a scaled sarcomere provides accurate active functional predictions for rabbit TA, EDL, and EDII muscles and call into question the need for more complex modeling assumptions often proposed.

2.2 Introduction

Modeling muscle force generation is necessary to understand both muscle function and human movement. Musculoskeletal models vary in their levels of complexity. Early models used simplistic representations of muscle to estimate function [1-3]. However, it has been suggested that these simple models are inadequate. Herzog and ter Keurs [4] suggested that the width of the computationally-derived length-tension relationship of the human rectus femoris was much wider than estimated by a simple scaled sarcomere model. By introducing fiber length variability into their model, Ettema and Huijing [5] improved and more closely matched modeled and experimentally-measured muscle length-tension relationships. Blemker and Delp [6] further developed the idea of introducing complexities with a three-dimensional finite element model that incorporated tendon, aponeurosis, and constitutive muscle properties. The authors claim that it was critical to use this model over the lumped

parameter model used in Delp et al. [7] in order for their data to match knee extension moment arm-joint angle data from Buford et al. [8].

Despite claims that simple models cannot appropriately capture muscle performance, they have been used extensively in the literature [2, 7, 9-10]. Huijing et al. [11] modeled a muscle fiber as a scaled sarcomere and compared the results to experimentally-measured active length-tension data. The authors correctly predicted the characteristics of rat medial gastrocnemius, but were unable to accurately represent the semimembranosus. This discrepancy may stem from the vastly different architecture between the two muscles, but this idea has not been tested experimentally.

Current passive tension models typically rely on a generic curve [12] that is scaled by a muscle's architectural parameters [7, 13]. These models do not incorporate any mechanism of passive load-bearing and do not consider potential load-bearing protein differences amongst muscles [14-15].

Thus, most of the predictions of musculoskeletal models are not accompanied by explicit validations. As a result, it is often stated that a more complex model is "better" without providing objective criteria for such a statement. It is surprising that whole muscle isometric mechanical properties have not been validated against structurally-based predictions, given the popularity of the approach and the large number of architectural data sets in the literature. Therefore, the purposes of this study were: (1) to determine whether the experimentally-measured muscle length-tension relationship could be explained by modeling muscles based solely on their architecture and myofilament dimensions, and (2) to determine experimentally

whether normalized fiber length scales linearly with muscle excursion as is often claimed.

2.3 Methods

2.3.1 Theoretical Model

To provide the *a priori* framework for the muscle length-tension relationship, three assumptions were made: (1) all muscle fibers are functionally in parallel; (2) all fibers and sarcomeres are identical; (3) muscle strain is uniformly distributed among sarcomeres and fibers. Therefore, any change in muscle length corresponds to an equivalent fiber length change. Actin filament length for rabbit striated muscle was based on the literature (1.16 μm, [16]) while myosin filament length was assumed to be 1.60 μm, the same length observed for all vertebrates [17]. Sarcomere dimensions included Z-disk widths and length of the bare zone of the myosin filament (0.05 μm and 0.20 μm, respectively; [18]). Using these assumptions, peak force was predicted at optimal sarcomere length (L_{s0}=2.50 μm). Relative tension developed at the point of interaction between the myosin filament and the Z-disks (1.70 μm) was determined by the number of cross-bridges that are formed in the zone of single overlap between actin and myosin filaments (67.59%; [19]). Reduction in length from this point was assumed to mimic experimental data [20-22] and achieve zero force at 1.27 μm. Finally, the zero-force point of the descending limb (4.02 μm) was calculated as the sum of the myosin filament, actin filament, and Z-disk widths. Subsequently, the sarcomere length-tension relationship was scaled to the fiber length-tension

relationship by multiplying all sarcomere length values by serial sarcomere number (calculated by dividing literature values for normalized fiber length by optimal sarcomere length). Based on the assumptions above, the width of the fiber length-tension relationship is equal to the width of the muscle length-tension relationship. This allows the fiber length-tension relationship (centered at optimal fiber length) to be aligned with optimal muscle length to yield the muscle length-tension relationship.

Passive tension was modeled using the two-element Hill-type model [1, 12] consisting of a contractile element in parallel with a passive elastic element. When not activated, the muscle is assumed to develop force in the passive element for muscle lengths greater than optimal length (L_0). The passive length-tension relationship is generated using the generic non-dimensional model popularized by Zajac [12] and scaled by literature values for optimal muscle length for each muscle [23-24]).

2.3.2 Experimental Validation of Theoretical Prediction

The tibialis anterior (TA; n=10), extensor digitorum longus (EDL; n=7), and extensor digitorum II (EDII; n=14) muscles of New Zealand White rabbits (mass=2.6±0.5 kg) were chosen due to their range of normalized fiber lengths (38.08 mm, 15.34 mm, and 10.71 mm, respectively; [23-24]. Animal preparation and measurement of isometric contractile properties were performed as previously described [25-26]. Briefly, rabbits were anesthetized with 5% isoflurane and a subcutaneous injection of a ketamine-xylazine cocktail (50 and 5 mg/kg body mass, respectively) and maintained on 2% isoflurane anesthesia. Heart rate and oxygen

saturation were monitored (VetOx, Heska Co., Fort Collins, CO) throughout the test duration. A mid-line incision was made from the mid-thigh to the ankle. Steinmann pins (3.2 mm) were drilled at the lateral femoral condyle and proximal to the malleoli and secured to a custom-made jig to immobilize the leg. For the TA and EDL, the biceps femoris was split, exposing the peroneal nerve; for the EDII, the tibial nerve was exposed. A cuff electrode was placed around the nerve for direct stimulation (Pulsar 6Bp Stimulator; FHC, Bowdoinham, ME). Suture markers were placed at the distal and proximal muscle-tendon junctions to define muscle length and measure it at the neutral position (knee and ankle joints at 90°). The distal TA, EDL, or EDII tendon was transected, released from the extensor retinaculum (for TA and EDL), and clamped to a servomotor (Cambridge Model 310B; Aurora Scientific, Aurora, ON, Canada) at the muscle-tendon junction and aligned with the force-generating axis of the motor [27]. Muscle temperature was maintained at 37°C with radiant heat, mineral oil, and a servo-temperature controller (Model 73A; YSI, Yellow Springs, OH).

The length-tension protocol consisted of a series of 100 Hz tetanic contractions (pulse width: 0.3 ms; amplitude: 10 V) over a 640 ms period. Two minute rest intervals were interposed between contractions to minimize fatigue. Measurements began at neutral muscle length (L_n) and ranged from -40%L_{fn} to 40%L_{fn} in increments of 5%L_{fn} (L_{fn}: normalized fiber length). Length and force were acquired for each contraction using a data acquisition board (610E series; National Instruments, Austin, TX) and a custom-written LabView program (National Instruments) at 4 kHz per channel. Passive tension at each muscle length was obtained by measuring the

baseline (preactivation) force. Typical experimental muscle force traces for the TA, EDL, and EDII are shown in Fig. 2.1.

Upon completion of testing, animals were euthanized with pentobarbital (Euthasol; Virbac AH, Fort Worth, TX), skinned, transected at the sacrum, and fixed for 3-5 days in 10% buffered formalin with hips, knees, and ankles held in 90 degrees of flexion and abduction (chosen arbitrarily) for architectural determination, according to the methods of Sacks and Roy [28] as modified by Lieber and Blevins [23]. Mean sarcomere length (L_s), muscle length, and fiber length (for the purpose of this study, fiber length refers to the normalized length of the dissected muscle fascicles) were measured. Muscle length and fiber length were normalized to L_{s0} to enable comparison among muscles by eliminating variability resulting from differences in joint fixation angle [28]. Active and passive force were converted to relative tension by normalizing to experimentally-measured peak active tension (P_0) to compare among muscles of different sizes. The relative muscle length-tension relationship was scaled by the experimentally-measured optimal muscle length obtained from architecture to compare experimental measurements with theoretical predictions.

2.3.3 Data Analysis

Piecewise linear regression and intraclass correlation coefficients (ICC) were used to characterize agreement between experimental and theoretical values of relative active and passive tension (SPSS, Chicago, IL). For active tension, ICC was used to quantify the level of experiment-model agreement for both the ascending (lengths less

than or equal to L_0) and descending limbs (lengths greater than L_0) of the length-tension relationship. Paired t-tests were used to compare correlations between the two limbs. ANOVA was used to detect differences in correlations among muscles.

Due to assumptions listed for the theoretical model, the relative fiber length-tension relationships for all three muscles were expected to coincide. To test this idea, the relative muscle length-tension relationship was scaled to a fiber length-tension relationship by multiplying by the muscle length/fiber length ratio. Experimental measurements and theoretical predictions were then compared.

Full-width-at-half-maximum (FWHM) was chosen as a measure of excursion. However, data were not captured at exactly 50%P_0 for all trials, thus raw data were fit to a second order polynomial (r^2=0.94±0.05) to permit calculation of FWHM. Linear regression was performed to investigate the relationship between FWHM and normalized fiber length. Subsequently, FWHM was normalized to optimal sarcomere length to facilitate comparisons among species as well as validate the regression findings of this study. Normalization was necessary as thin filament length varies among species and alters the width of the length-tension relationship [17]. Studies were chosen that did not require extrapolation to the half-maximum point at long or short lengths: this resulted in data that included the rat soleus and medial gastrocnemius [29]; cat soleus, extensor digitorum longus, and superficial vastus lateralis [30]; and rabbit digastric [31]; [32] muscles. Using the methods above, a theoretically derived FWHM and normalized fiber length was predicted for each muscle. The results obtained from the different species were compared to predictions

using ICC. Significance was set to $p < 0.05$ and data are presented as mean±SEM (standard error of the mean).

2.4 Results

The muscle length-tension relationship had the classic shape of an inverted parabola (Fig. 2.2). Literature values of normalized fiber length (TA: 38.08 mm, EDL: 15.34 mm, EDII: 10.71 mm; [23-24]) agreed well with measured lengths (TA: 38.47±2.94 mm, EDL: 15.34±1.06 mm, EDII: 10.47±1.01 mm) and predicted FWHM matched experimental FWHM (ICC=0.99).

Experimental isometric length-tension values obtained from TA, EDL, and EDII agreed well with theoretical predictions for active tension (average ICC = 0.88±0.03, $p < 0.05$, Fig. 2.2, Table 2.1) with 88% of the variability in the length-tension relationship explained by the model. Experimental data for the descending limb had consistently higher ICC values compared to the ascending limb (TA: p=0.034; EDL: p=0.033; EDII: p=0.001; Table 2.1). However, there were no significant differences in the correlation among the muscle's theoretical and experimental length-tension values (ICC: p=0.228; Table 2.1). When comparing relative fiber length-tension relationships, agreement between active experimental and theoretical values remained and the data sets were not different among muscles (Fig. 2.3). However, theoretical passive tension did not accurately predict the experimental data (dotted lines, Fig. 2.2 and 2.3; ICC=0.70±0.07, Table 2.1).

Because the model predicted almost 90% of the variability in the active tension data, it was extended to a linear regression of FWHM and normalized fiber length (Fig. 2.4A). Theoretical data yielded a slope of 0.68, with similar results for each individual muscle's raw data (TA: slope=0.73, r^2=0.75; EDL: slope=0.71, r^2=0.63; EDII: slope=0.74, r^2=0.67). When normalized FWHM results were compared to literature values, the model explained 88% of the variance in the literature values for all species considered (Fig. 2.4B). The effect of normalizing FWHM to optimal sarcomere length allowed comparisons among different species (rat, cat, and rabbit) without altering the linear relationship of the original theoretical regression.

2.5 Discussion

This study demonstrated that modeling rabbit whole muscle length-tension relationship as a scaled sarcomere explained 88% of the variation in experimentally-measured active tension data for TA, EDL, and EDII. The model succeeded in capturing functional characteristics of the given muscles while requiring only two variables: (1) myofilament length and (2) normalized fiber length (or serial sarcomere number). Previous studies have shown both filament-level [33] and fiber length [29, 34-35] changes are reflected in whole muscle function. Thus, our findings suggest that, to a first approximation, these muscles can be considered to act isometrically as a scaled sarcomere. These results could not be extended accurately to the modeling of passive tension using a simple two-element Hill-type model of skeletal muscle.

Morgan [36] admits that "it is tempting to model a whole muscle simply as a scaled sarcomere," but factors such as internal motion, tendon compliance, and sarcomere heterogeneity complicate the situation. Our study, however, suggests that additional complexities would do little to improve the experiment-model correlation since only 12% of the experimental variability is unexplained. This idea is further supported by the work of Sinclair [37]. By examining the effect of modeling fiber length distributions and comparing the results to those experimentally-measured by Huijing et al. [11], Sinclair found that a homogeneous distribution of fiber lengths better predicted the length-tension properties of muscle at extreme lengths than more heterogeneous distributions. Yet, for the normal operating range of the rat semimembranosus (i.e. closer to optimum length), heterogeneous fiber and sarcomere length distributions provided little benefit beyond that of the scaled sarcomere model. Therefore, under normal conditions, the marginal benefits of added model complexities are low. This is applicable to most muscles since their operational range do not cover the entire length-tension relationship [38], but more sophisticated models may be needed to examine muscles that operate over a wider range of sarcomere lengths (e.g. human biceps brachii muscle; [39]).

Delp et al. found success in employing the computationally-inexpensive cost of assumptions inherent in the scaled sarcomere (active) and adapted Hill-type (passive) models with the creation of the modeling software packages SIMM [40] and OpenSim [13]. Despite optimistic results from both [41-42], the overall accuracy of treating a muscle as a scaled sarcomere has been questioned. Herzog and ter Keurs [4] found a large discrepancy between the length-tension relationship of the rectus femoris and

that of the scaled sarcomere model. This difference may be explained by a lack of direct muscle force and length measurements in their experimental results, joint-dependent neural activation, overestimation of hip or knee moment arms, or underestimation of the series elastic component's stiffness. The theoretical basis of the scaled sarcomere model has been criticized as well [36, 43], but again, in no case has the model been directly compared to experimental data.

The differences in muscle architecture (e.g. L_{fn} and pennation angle) between the three muscles did not change the level of agreement between experimental and modeled length-tension relationships. In contrast, Huijing et al. [11] found experiment-model differences for a parallel-fibered muscle (rat semimembranosus; 2°), but not for a pennate muscle (rat medial gastrocnemius; 21°). These authors later concluded that for a parallel-fibered muscle, sarcomere length heterogeneity was, potentially, the main contributor to the width of the length-tension relationship [44]. This may help explain the experiment-model discrepancy exhibited by the rat semimembranosus. This idea may be further supported by the current study, in which a parallel-fibered muscle (TA: 2.54±0.47°) exhibited low L_s heterogeneity (coefficient of variation: 4.42±0.93%) and strong experiment-model agreement.

The sarcomere length-tension relationship defined by Gordon et al. [20] was defined by experimentally controlling sarcomere length using a high-speed feedback controller. For a fixed-end contraction, as employed in the current study, the term "isometric" refers to fixed muscle (or fiber) length, not fixed sarcomere length. When single fiber experiments were performed without controlling sarcomere length, the plateau region of the length-tension relationship is often more broad, more curved in

shape, and the descending limb extended to longer lengths [45-47]. However, these are not universal findings, as several studies of fixed-end contraction have matched the predicted sarcomere length-tension relationship [48-49].

The large difference in L_{fn} across muscles facilitated the extension of the active tension model to examine the relationship between excursion and L_{fn}. The results displayed a clear linear relationship between excursion and L_{fn}, demonstrating that a 1 mm change in L_{fn} corresponded to a 0.68 mm change in excursion. When extended to normalized excursion of rat and cat, the regression is not altered—validating the current relationship while suggesting that it may be extrapolated to other species without change. This general finding is reminiscent of the relationship between maximum tetanic tension and physiological cross sectional area that yielded specific tension for mammalian muscle [50].

The inability of the passive model to accurately reflect the experimental data stems from a divergence in both (1) the slope and (2) the position of the two curves. The slope of the theoretical model is fixed at a constant relative stiffness (dotted line, Fig. 2.3) and relies upon architectural properties for passive tension calculation. However, recent work has shown that a main determinant of passive tension is a muscle's protein composition, both myofibrillar and extramyofibrillar, and not muscle architecture [14-15]. The deviation in position results from the model's assumption that passive tension is first developed at L_0. This is not the case for all muscles. Thus, a more accurate model must incorporate a muscle-specific stiffness that depends on the muscle's protein composition and alters the position in which passive tension is developed.

The current study has several limitations. First, disruption of the myofascial compartment has been reported to result in a decrease in maximal force production and an increase in the length range between optimal muscle length and active slack length—thus lowering the slope of the ascending limb [51-52]. The patency of the anterior compartment may have widened the length-tension relationship at the extreme lengths, artificially improving the experiment-model correlations. Second, the data are explained in terms of relative force production, rather than absolute stress. This is consistent with other scaled sarcomere models [4, 9], in which a predicted model is compared to experimental results. This study does not attempt to correlate the modeled absolute stress with those measured *in vivo*. Third, real-time changes in sarcomere length were not measured during whole muscle contractions and thus, were not correlated with muscle length. These methods would be difficult to perform but have been executed by Llewellyn et al. [53].

In addition to the limitations, several cautions regarding the data must be made. First, the muscles chosen in this study do not follow complex three-dimensional trajectories. Thus, the relationships presented in this study may not extend to modeling more architecturally complex muscles such as the rectus femoris or gluteus maximus. Second, maximal activation was used in the current study. It is known that submaximal activation distorts the length-tension relationship [54]. The purpose of the current study was to investigate a simple theoretical relationship and its ability to recreate a whole muscle's function. Thus, caution must be taken when extrapolating these data for physiological applications and other instances where sub-maximal activation might occur. In other words, the sarcomere length-tension

relationship may not approximate the physiological length-tension relationship for everyday muscle function. Third, contraction-induced strain for the distal portion of the current system was less than 2% of muscle length, providing support that peak tension did occur at optimal length. This compliance would only underestimate the active tension by less than 8% across the length-tension relationship, if an offset did occur. Any proximal shortening may further contribute to this underestimation, but was not quantified. Therefore, for physiological muscle contractions, fiber shortening may be more substantial than experienced when clamped at the muscle-tendon junction [55-57]. Finally, it is important to note that this study was performed under isometric conditions. Therefore, extrapolation to dynamic conditions must be made with caution.

In summary, these data demonstrate that, for the rabbit TA, EDL, and EDII muscles, modeling active muscle properties as a scaled sarcomere provide an accurate estimate of the whole muscle length-tension relationship, while a simple model of passive tension is unable to model experimental results. In addition, model and experimental active tension demonstrate that there is a linear relationship between muscle excursion and normalized fiber length and its scaling factor is 0.68 mm excursion per mm of fiber length.

2.6 Acknowledgements

I would like to acknowledge my co-authors from Chapter 2, which is a reprint of the material as it appears in Journal of Biomechanics, 2012, Winters TM, Takahashi

M, Lieber RL, Ward SR. No authors had competing interests regarding the publication of this research.

We thank Shannon Bremner for her expertise in the development of the LabView program, Alan Kwan and Genaro Sepulveda for technical assistance, and Gretchen Meyer for her critical review of the data. We acknowledge grant support by the Department Veterans Affairs and NIH/NICHD grants HD31476, HD048501, and HD050837.

2.7 References

1. Hill, A.V., *The heat of shortening and the dynamic constants of muscle.* Proceedings of the Royal Society London Series B, 1938. **128**: p. pp. 136-195.

2. Morgan, D.L., S. Mochon, and F.J. Julian, *A quantitative model of intersarcomere dynamics during fixed-end contractions of single frog muscle fibers.* Biophys J, 1982. **39**(2): p. 189-96.

3. Kaufman, K.R., K.N. An, and E.Y. Chao, *Incorporation of muscle architecture into the muscle length-tension relationship.* J Biomech, 1989. **22**(8-9): p. 943-8.

4. Herzog, W. and H.E. ter Keurs, *Force-length relation of in-vivo human rectus femoris muscles.* Pflugers Arch, 1988. **411**(6): p. 642-7.

5. Ettema, G.J. and P.A. Huijing, *Effects of distribution of muscle fiber length on active length-force characteristics of rat gastrocnemius medialis.* Anat Rec, 1994. **239**(4): p. 414-20.

6. Blemker, S.S. and S.L. Delp, *Rectus femoris and vastus intermedius fiber excursions predicted by three-dimensional muscle models.* J Biomech, 2006. **39**(8): p. 1383-91.

7. Delp, S.L., et al., *An interactive graphics-based model of the lower extremity to study orthopaedic surgical procedures.* IEEE Trans Biomed Eng, 1990. **37**(8): p. 757-67.

8. Buford, W.L., Jr., et al., *Muscle balance at the knee--moment arms for the normal knee and the ACL-minus knee.* IEEE Trans Rehabil Eng, 1997. **5**(4): p. 367-79.

9. Herzog, W., S.K. Abrahamse, and H.E. ter Keurs, *Theoretical determination of force-length relations of intact human skeletal muscles using the cross-bridge model.* Pflugers Arch, 1990. **416**(1-2): p. 113-9.

10. Meijer, K., et al., *The isometric knee extension moment-angle relationship: experimental data and predictions based on cadaver data.* J Appl Biomech, 1998. **14**(1): p. 62-79.

11. Huijing, P.A., A.A. van Lookeren Campagne, and J.F. Koper, *Muscle architecture and fibre characteristics of rat gastrocnemius and semimembranosus muscles during isometric contractions.* Acta Anat (Basel), 1989. **135**(1): p. 46-52.

12. Zajac, F.E., *Muscle and tendon: properties, models, scaling, and application to biomechanics and motor control.* Crit Rev Biomed Eng, 1989. **17**(4): p. 359-411.

13. Delp, S.L., et al., *OpenSim: open-source software to create and analyze dynamic simulations of movement.* IEEE Trans Biomed Eng, 2007. **54**(11): p. 1940-50.

14. Magid, A. and D.J. Law, *Myofibrils bear most of the resting tension in frog skeletal muscle.* Science, 1985. **230**(4731): p. 1280-2.

15. Prado, L.G., et al., *Isoform diversity of giant proteins in relation to passive and active contractile properties of rabbit skeletal muscles.* J Gen Physiol, 2005. **126**(5): p. 461-80.

16. Ringkob, T.P., D.R. Swartz, and M.L. Greaser, *Light microscopy and image analysis of thin filament lengths utilizing dual probes on beef, chicken, and rabbit myofibrils.* J Anim Sci, 2004. **82**(5): p. 1445-53.

17. Walker, S.M. and G.R. Schrodt, *I segment lengths and thin filament periods in skeletal muscle fibers of the Rhesus monkey and the human.* Anat Rec, 1974. **178**(1): p. 63-81.

18. Huxley, H.E., *Electron Microscope Studies on the Structure of Natural and Synthetic Protein Filaments from Striated Muscle.* J Mol Biol, 1963. **7**: p. 281-308.

19. Stephenson, D.G., A.W. Stewart, and G.J. Wilson, *Dissociation of force from myofibrillar MgATPase and stiffness at short sarcomere lengths in rat and toad skeletal muscle.* J Physiol, 1989. **410**: p. 351-66.

20. Gordon, A.M., A.F. Huxley, and F.J. Julian, *The variation in isometric tension with sarcomere length in vertebrate muscle fibres.* J Physiol, 1966. **184**(1): p. 170-92.

21. Elmubarak, M.H. and K.W. Ranatunga, *Temperature sensitivity of tension development in a fast-twitch muscle of the rat.* Muscle Nerve, 1984. **7**(4): p. 298-303.

22. Roots, H., G.W. Offer, and K.W. Ranatunga, *Comparison of the tension responses to ramp shortening and lengthening in intact mammalian muscle fibres: crossbridge and non-crossbridge contributions.* J Muscle Res Cell Motil, 2007. **28**(2-3): p. 123-39.

23. Lieber, R.L. and F.T. Blevins, *Skeletal muscle architecture of the rabbit hindlimb: functional implications of muscle design.* J Morphol, 1989. **199**(1): p. 93-101.

24. Takahashi, M., S.R. Ward, and R.L. Lieber, *Intraoperative single-site sarcomere length measurement accurately reflects whole-muscle sarcomere length in the rabbit.* J Hand Surg [Am], 2007. **32**(5): p. 612-7.

25. Lieber, R.L. and J. Fridén, *Muscle damage is not a function of muscle force but active muscle strain.* J Appl Physiol, 1993. **74**(2): p. 520-6.

26. Lieber, R.L., T.M. Woodburn, and J. Fridén, *Muscle damage induced by eccentric contractions of 25% strain.* J Appl Physiol, 1991. **70**(6): p. 2498-507.

27. Davis, J., K.R. Kaufman, and R.L. Lieber, *Correlation between active and passive isometric force and intramuscular pressure in the isolated rabbit tibialis anterior muscle.* J Biomech, 2003. **36**(4): p. 505-12.

28. Sacks, R.D. and R.R. Roy, *Architecture of the hind limb muscles of cats: functional significance.* J Morphol, 1982. **173**(2): p. 185-95.

29. Walmsley, B. and U. Proske, *Comparison of stiffness of soleus and medial gastrocnemius muscles in cats.* J Neurophysiol, 1981. **46**(2): p. 250-9.

30. Witzmann, F.A., D.H. Kim, and R.H. Fitts, *Hindlimb immobilization: length-tension and contractile properties of skeletal muscle.* J Appl Physiol, 1982. **53**(2): p. 335-45.

31. Muhl, Z.F., *Active length-tension relation and the effect of muscle pinnation on fiber lengthening.* J Morphol, 1982. **173**(3): p. 285-92.

32. Muhl, Z.F. and J.H. Newton, *Change of digastric muscle length in feeding rabbits.* J Morphol, 1982. **171**(2): p. 151-7.

33. Gokhin, D.S., et al., *Reduced thin filament length in nebulin-knockout skeletal muscle alters isometric contractile properties.* Am J Physiol Cell Physiol, 2009. **296**(5): p. C1123-32.

34. Williams, P.E. and G. Goldspink, *The effect of denervation and dystrophy on the adaptation of sarcomere number to the functional length of the muscle in young and adult mice.* J Anat, 1976. **122**(Pt 2): p. 455-465.

35. Bodine, S.C., et al., *Architectural, histochemical, and contractile characteristics of a unique biarticular muscle: the cat semitendinosus.* J Neurophysiol, 1982. **48**(1): p. 192-201.

36. Morgan, D.L., *From sarcomeres to whole muscles.* J Exp Biol, 1985. **115**: p. 69-78.

37. Sinclair, P.J., *Forward dynamic modelling of cycling for people with spinal cord injury*, in *School of Exercise and Sport Science*. 2001, The University of Sydney: Lidcombe.

38. Burkholder, T.J. and R.L. Lieber, *Sarcomere length operating range of vertebrate muscles during movement.* J Exp Biol, 2001. **204**(Pt 9): p. 1529-36.

39. Ismail, H.M. and K.W. Ranatunga, *Isometric tension development in a human skeletal muscle in relation to its working range of movement: the length-tension relation of biceps brachii muscle.* Exp Neurol, 1978. **62**(3): p. 595-604.

40. Delp, S.L. and J.P. Loan, *A graphics-based software system to develop and analyze models of musculoskeletal structures.* Comput Biol Med, 1995. **25**(1): p. 21-34.

41. Higginson, J.S., et al., *Muscle contributions to support during gait in an individual with post-stroke hemiparesis.* J Biomech, 2006. **39**(10): p. 1769-77.

42. Xiao, M. and J.S. Higginson, *Muscle function may depend on model selection in forward simulation of normal walking.* J Biomech, 2008. **41**(15): p. 3236-42.

43. Allinger, T.L., W. Herzog, and M. Epstein, *Force-length properties in stable skeletal muscle fibers--theoretical considerations.* J Biomech, 1996. **29**(9): p. 1235-40.

44. Willems, M.E. and P.A. Huijing, *Heterogeneity of mean sarcomere length in different fibres: effects on length range of active force production in rat muscle.* Eur J Appl Physiol Occup Physiol, 1994. **68**(6): p. 489-96.

45. ter Keurs, H.E., T. Iwazumi, and G.H. Pollack, *The sarcomere length-tension relation in skeletal muscle.* J Gen Physiol, 1978. **72**(4): p. 565-92.

46. Altringham, J.D. and R. Bottinelli, *The descending limb of the sarcomere length-force relation in single muscle fibres of the frog.* J Muscle Res Cell Motil, 1985. **6**(5): p. 585-600.

47. Granzier, H.L. and G.H. Pollack, *The descending limb of the force-sarcomere length relation of the frog revisited.* J Physiol, 1990. **421**: p. 595-615.

48. Julian, F.J. and R.L. Moss, *Sarcomere length-tension relations of frog skinned muscle fibres at lengths above the optimum.* J Physiol, 1980. **304**: p. 529-39.

49. Julian, F.J. and D.L. Morgan, *Tension, stiffness, unloaded shortening speed and potentiation of frog muscle fibres at sarcomere lengths below optimum.* J Physiol, 1981. **319**: p. 205-17.

50. Powell, P.L., et al., *Predictability of skeletal muscle tension from architectural determinations in guinea pig hindlimbs.* J Appl Physiol, 1984. **57**(6): p. 1715-21.

51. Huijing, P.A. and G.C. Baan, *Myofascial force transmission causes interaction between adjacent muscles and connective tissue: effects of blunt dissection and compartmental fasciotomy on length force characteristics of rat extensor digitorum longus muscle.* Arch Physiol Biochem, 2001. **109**(2): p. 97-109.

52. Smeulders, M.J., et al., *Progressive surgical dissection for tendon transposition affects length-force characteristics of rat flexor carpi ulnaris muscle.* J Orthop Res, 2002. **20**(4): p. 863-8.

53. Llewellyn, M.E., et al., *Minimally invasive high-speed imaging of sarcomere contractile dynamics in mice and humans.* Nature, 2008. **454**(7205): p. 784-8.

54. Rack, P.M. and D.R. Westbury, *The effects of length and stimulus rate on tension in the isometric cat soleus muscle.* J Physiol, 1969. **204**(2): p. 443-60.

55. Fukunaga, T., et al., *Determination of fascicle length and pennation in a contracting human muscle in vivo.* J Appl Physiol, 1997. **82**(1): p. 354-8.

56. Fukunaga, T., et al., *In vivo behaviour of human muscle tendon during walking.* Proc Biol Sci, 2001. **268**(1464): p. 229-33.

57. Maganaris, C.N., V. Baltzopoulos, and A.J. Sargeant, *Human calf muscle responses during repeated isometric plantarflexions.* J Biomech, 2006. **39**(7): p. 1249-55.

Table 2.1: The scaled sarcomere model is able to accurately predict active experimental data. This prediction is stronger for the descending limb compared to the ascending limb. The passive model can only moderately predict experimental passive tension data because it is unable to capture muscle-specific differences.

Muscle	Portion of the length-tension relationship	Intraclass correlation coefficient (ICC)
		Mean ± SEM
TA[a]	Active ascending limb	0.81 ± 0.05
	Active descending limb	0.92 ± 0.02
	Active ascending+descending	0.85 ± 0.04
	Passive curve	0.60 ± 0.08
EDL[b]	Active ascending limb	0.81 ± 0.05
	Active descending limb	0.93 ± 0.03
	Active ascending+descending	0.86 ± 0.03
	Passive curve	0.78 ± 0.10
EDII[c]	Active ascending limb	0.81 ± 0.04
	Active descending limb	0.97 ± 0.01
	Active ascending+descending	0.90 ± 0.02
	Passive curve	0.73 ± 0.03

[a] Values represent mean ± standard error for $n=10$ animal subjects.
[b] Values represent mean ± standard error for $n=7$ animal subjects.
[c] Values represent mean ± standard error for $n=14$ animal subjects.

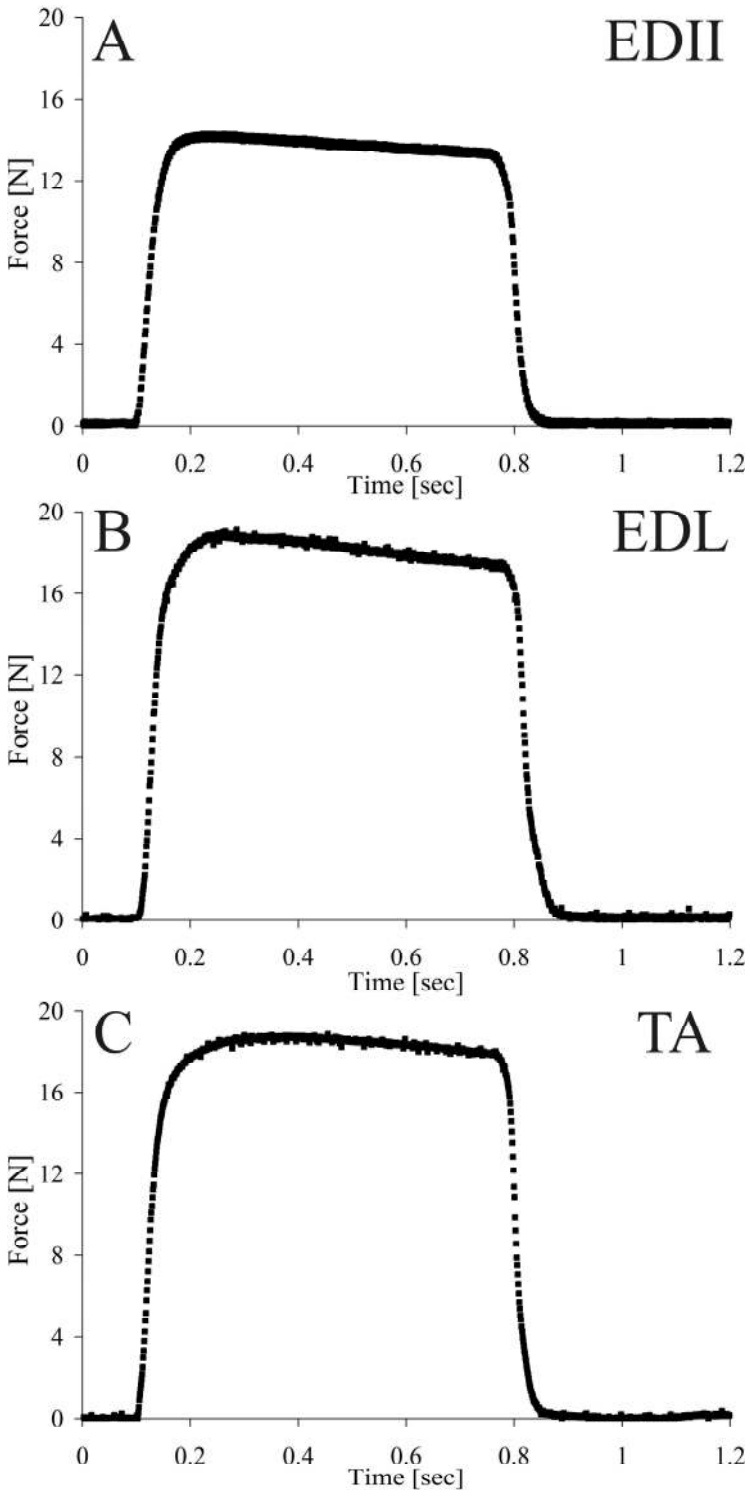

Figure 2.1: Sample record of muscle force (N) recordings from an isometric contraction at optimal length for (A) EDII, (B), EDL. (C) TA. Force-time recordings for all three muscles displayed no abnormalities. Average force values on the plateau were used to construct the length-tension relationship.

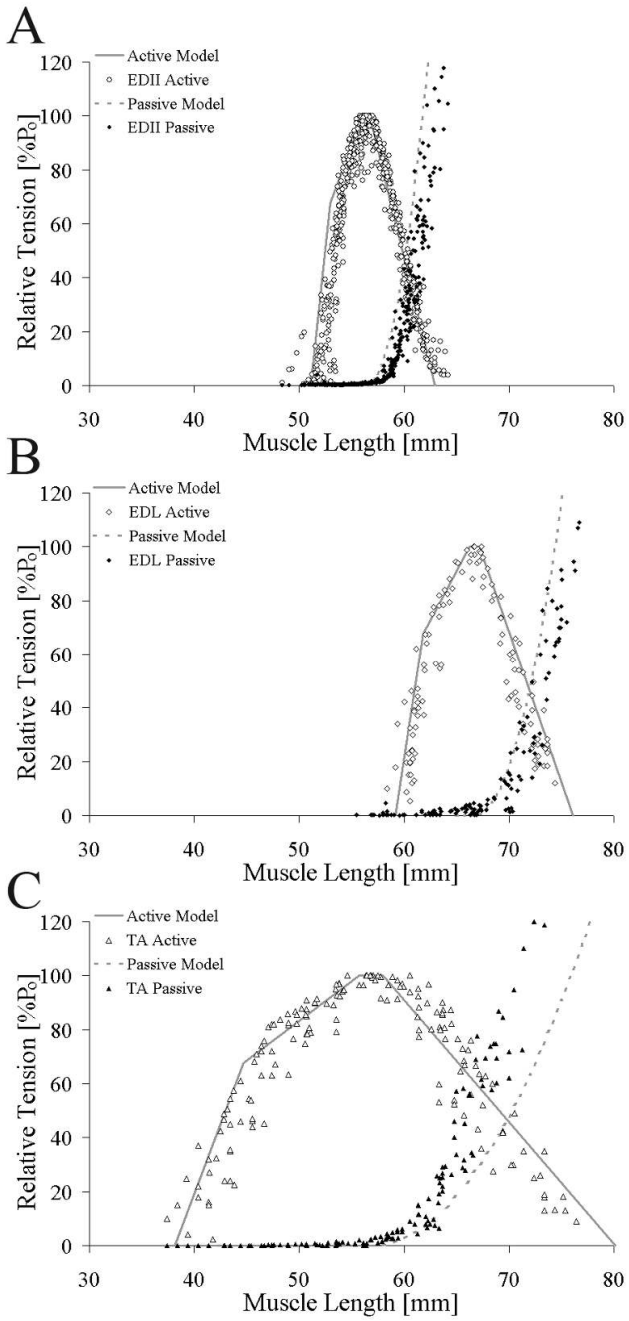

Figure 2.2: The scaled sarcomere model (solid gray line) accurately predicts experimentally measured whole muscle active tension (open symbols), but the passive model (dotted gray line) is unable to capture muscle-specific differences in experimental passive tension (filled symbols) for (A) EDII (○), (B) EDL (◊), and (C) TA (Δ). Theoretical and experimental data were highly correlated for all muscles (TA: r^2=0.81, ICC=0.84; EDL: r^2=0.90, ICC=0.86; EDII: r^2=0.87, ICC=0.89). Relative tension (muscle tension normalized to maximum tension) was plotted on the ordinate to facilitate comparison between muscles.

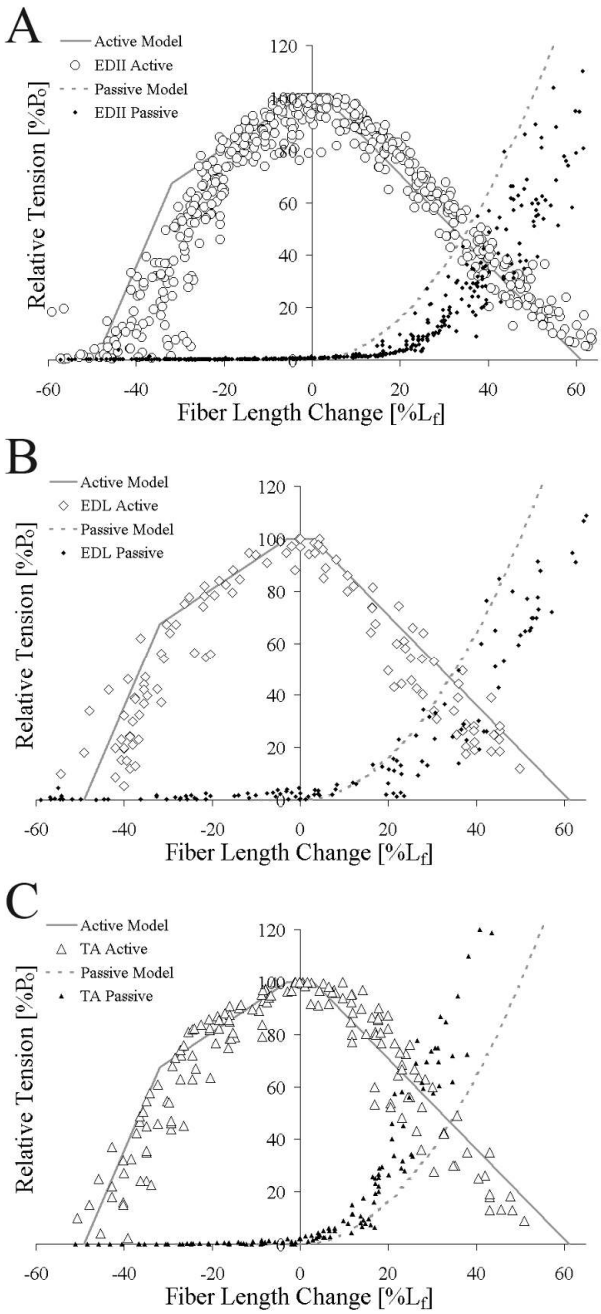

Figure 2.3: Relationship between active theoretical (solid gray line) and experimental (open symbols) relative fiber length-tension relationship and passive theoretical (dotted gray line) and experimental (filled symbols) relative fiber length-tension relationship for (A) EDII (○), (B) EDL (◊), (C) and TA (Δ). Theoretical and experimental data were highly correlated for all muscles and muscles were not significantly different from each other. Relative tension (muscle tension normalized to maximum tension) is plotted on the ordinate to facilitate comparison between muscles.

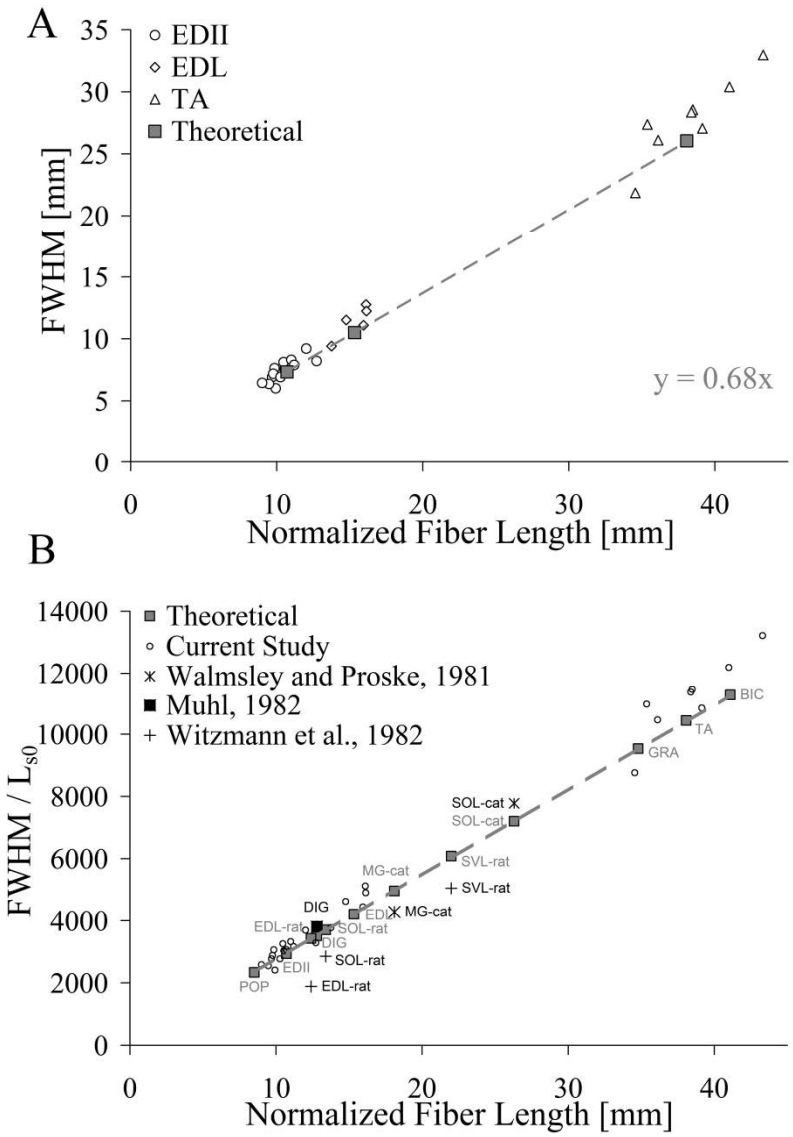

Figure 2.4: Full-width-at-half-maximum (the width of the length-tension relationship at 50% of maximum tension—a measure of muscle excursion) is accurately predicted by normalized fiber length. (A) Experimental data (open symbols: EDII (○), EDL (◊), and TA (Δ)) agree well with theoretical predictions (solid gray squares). The theoretical model predicted a linear relation (slope=0.68 mm/mm) between excursion and fiber length suggesting that a 1 mm increase in normalized fiber length extended FWHM by 0.68 mm. (B) Comparison of results with published literature across species. FWHM was normalized to the optimal sarcomere length of the species to facilitate comparisons among species. Data from Walmsley and Proske (+, Cat), Muhl (□, rabbit), and Witzmann et al. (✳, rat) agreed well with the results of this study. Abbreviations: POP: Popliteus; EDII: Extensor Digitorum II; EDL: Extensor Digitorum Longus; DIG: Digastric; SOL: Soleus; MG: Medial Gastrocnemius; SVL: Superficial Vastus Lateralis; GRA: Gracilis; TA: Tibialis Anterior; BIC: Biceps Femoris.

CHAPTER 3

NONLINEAR SCALING OF PASSIVE TENSION

3.1 Abstract

An understanding of passive mechanical properties is necessary for characterizing muscle function and treating pathologies. However, identifying sources of passive tension, the size scale in which they are functionally relevant and how passive tension scales from fiber and whole muscle is paramount to its understanding. To determine this, single fibers, fiber bundles, fascicles, and whole muscles were mechanically tested from three architecturally diverse muscles. Titin molecular weight and collagen content was quantified at each size scale, and muscle architecture was examined at the whole muscle level. To quantify the contribution of each variable to passive modulus, a multiple regression analysis was completed at each size scale. Passive moduli increased nonlinearly from fiber to whole muscle ($p < 0.001$), and this scaling relationship was muscle-specific ($p < 0.001$). Titin was the strongest predictor of passive tension at both the fiber and bundle level ($r^2 = 0.573$ and 0.225, $p = 0.001$ and 0.047, respectively) and at low strains ($r^2 = 0.573$ and 0.342, $p = 0.001$ and 0.013, respectively). With the addition of perimysium, collagen eclipsed titin at the fascicle and whole muscle level ($r^2 = 0.533$ and 0.608, $p < 0.001$ and $p = 0.023$, respectively),

and was also functionally relevant at high strains. Interestingly, at the whole muscle level, normalized fiber length was the strongest predictor of passive tension (r^2 = 0.880, $p < 0.001$), which suggests that stiffness may be designed to protect fibers from overstretching and damage. Finally, a model of passive tension was developed based on architectural and biochemical parameters and was shown to accurately predict whole muscle passive tension curves (ICC > 0.975, $p < 0.001$). These data provide insight into the sources of passive tension and suggest that a fundamental difference exists between fiber bundles and whole muscle, and thus, caution must be used when inferring whole muscle function from biopsy data.

3.2 Introduction

Passive tension is generated when a muscle is lengthened beyond its resting slack length. Longer lengths produce exponentially larger tensions and play a major role in providing resistive force, even in the absence of muscle activation. An understanding of passive mechanical properties is necessary for describing the function of different muscles [1-4], differentiating between healthy and pathologic muscle [5-8], and characterizing muscle adaption [9, 10]. However, identifying the sources of passive tension and at what size scale they are functionally relevant is paramount to its understanding.

Passive tension is attributed to the parallel action of the extracellular matrix (ECM) and intra-myofibrillar proteins (namely, titin, also known as connectin). The ECM of muscle is organized into three continuous levels: epimysium surrounds whole

muscles, perimysium binds fascicles into whole muscle, and endomysium outlines individual muscle cells [11]. These layers provide structural support and play an important role in force transmission between fibers and tendon [12]. Intracellularly, titin [13, 14], a ~3 MDa protein that spans the M-line to the Z-disc [15], is able to develop force with stretch due to an extensible I-band region [16].

Although the ECM and titin both contribute to passive tension, the relative contribution of each is muscle [2], size-scale [17], and strain dependent [18]. Titin has been shown to be passive load-bearing in fibers [19] and function at low muscle strains [18, 20]. Conversely, the ECM is thought to dominate at the fiber-bundle [17] and whole-muscle [21] level and act at high strains [22, 23]. At the whole muscle level, muscle architecture (i.e., the arrangement of muscle fibers within a muscle) is able to predict peak force [24] and excursion [25]. However, the relative contribution of titin, collagen, and architecture to predict passive stiffness is unclear.

The passive material properties of single fibers don't scale to the fiber-bundle level [4-6, 22, 23]. Differences that were not apparent at one size scale (e.g., a single fiber) became apparent at a different scale (a fiber bundle with endomysial connections), highlighting the importance of extracellular connections. With increasing size scale, additional layers of ECM are integrated into the sample, suggesting a highly nonlinear scaling relationship in skeletal muscle. Clinically, this idea suggests that extrapolating whole muscle function from bundle mechanics may not be appropriate. However, this idea has never been systematically tested.

Thus, the current study was designed to determine the passive mechanical properties of single muscle fibers, fiber bundles, fascicles, and whole muscle. Muscle

architecture and protein data were then used to determine the strongest predictors of passive modulus at each size scale. Finally, the data were analyzed within an anatomic length range to provide results pertinent to *in vivo* function as well as at short strains to evaluate the effect of strain on structural predictors.

3.3 Methods

3.3.1 Whole Muscle Mechanical Testing

The tibialis anterior (TA; n=6), extensor digitorum longus (EDL; n=6), and extensor digitorum of the second toe (EDII; n=6) muscles of New Zealand White rabbits (mass=2.68±0.04 kg) were chosen due to their varied architecture [10, 26]. Animal preparation and measurement of isometric contractile properties were performed as previously described [27, 28]. Briefly, rabbits were anesthetized using a subcutaneous injection of a ketamine-xylazine cocktail (35 and 5 mg/kg, respectively) and maintained on 2% isoflurane (IsoFlo; Abbott Laboratories, North Chicago, IL) at 2 L/min through a face-mask. Heart rate and oxygen saturation were monitored (VetOx, Heska Co., Fort Collins, CO) throughout the test. A mid-line incision was made from the mid-thigh to the ankle to expose the muscle. The hindlimb was immobilized in a custom jig via tightened screws at the lateral femoral condyle and malleoli. Suture markers were placed at the distal and proximal muscle-tendon junctions to define muscle length (L_m). The distal tendon was transected, released from the extensor retinaculum (for TA and EDL), and clamped to a servomotor (Cambridge Model 310B; Aurora Scientific, Aurora, ON, Canada) at the muscle-

tendon junction and aligned with the force-generating axis of the motor [28]. For TA and EDL testing, both tendons were cut to avoid confounding effects of the other muscle. Muscle temperature was maintained at 37°C with radiant heat and a servo-temperature controller (Model 73A; YSI, Yellow Springs, OH). Muscle and tendon tissue were regularly irrigated with isotonic saline to prevent dehydration.

The length-tension protocol consisted of a series of passive stretches with three-minute rest intervals interposed between to allow for passive stress relaxation. Measurements began at the muscle length at which the hip and knee were at 90° and the ankle was at 0° dorsiflexion and ranged from -5% to 40% L_{fn} in increments of 5 % L_{fn} (L_{fn}: normalized fiber length). Passive tension at each muscle length was obtained by measuring the baseline (preactivation) force. Force and length were acquired for each contraction using a data acquisition board (610E series; National Instruments, Austin, TX) and a custom-written LabView program (National Instruments) at 4 kHz per channel.

Upon completion of testing, animals were euthanized with pentobarbital (Euthasol; Virbac AH, Fort Worth, TX) and muscles were removed. The muscles were blotted dry and weighed for mass. The muscles were then divided longitudinally into two sections. One half (randomized) was fixed for 3-5 days in 10% buffered formalin for architectural determination. The distal one-third of the other section was removed and placed into a glycerinated storage solution (composed of 170.0-mM KPropionate, 5.0-mM K_3EGTA, 5.3-mM $MgCl_2$, 10.0-mM imidazole, 21.2-mM Na_2ATP, 1.0-mM NaN_3, 2.5-mM glutathione, 50-µM leupeptin, and 50% (v/v) glycerol) at -20°C for up to four weeks [5, 6, 29].

3.3.2 Fiber, Bundle, and Fascicle Mechanical Testing

The muscle section was removed from the storage solution and transferred to a chilled relaxing solution maintained at pCa 8.0 and pH 7.1, consisting of the following: 59.4-mM imidazole, 86.0-mM KCH_4O_3S, 0.13-mM $Ca(KCH_4O_3S)_2$, 10.8-mM $Mg(KCH_4O_3S)_2$, 5.5-mM K_3EGTA, 1.0-mM KH_2PO_4, 5.1-mM Na_2ATP, and 50.0-μM leupeptin. Single fiber, fiber bundle (approximately 20 fibers), and fascicle (approximately 300 fibers and defined by natural ECM divisions) segments and their constitutive ECM were carefully dissected from the same muscle. Each sample (1.5-3.0 mm in length) was mounted in a chamber in a custom apparatus at room temperature (20°C). Using 10-0 monofilament nylon suture, samples were secured to a force transducer (Model 405A for fibers and bundles and 404A for fascicles, Aurora Scientific, Ontario, Canada) on one end and to a titanium wire rigidly attached to a rotational bearing (Newport MT-RS; Irvine, CA) on the other end (Fig. 3.1). Segments displaying obvious abnormalities or discoloration were not used. The sample was transillumated by a 7-mW He–Ne laser to permit sarcomere length measurement by laser diffraction [30]. Resolution of this method is approximately 5 nm [31]. The system was calibrated with a 2.50-μm plastic blazed diffraction grating prior to experimentation (Diffraction Gratings, Inc., Nashville, TN).

Each segment was brought to slack length (length at which the sample exerted ~2 μN), and sample dimensions were measured optically with a cross-hair reticule mounted on a dissecting microscope and micromanipulators on an x-y mobile stage.

The samples were then loaded with strains of approximately 0.25 μm/sarcomere at 100 fiber lengths/sec. Each stretch was held for 3 minutes to permit stress relaxation before a sequential stretch was made [5]. Segments were stretched in total to approximately 100% strain. Samples were discarded if they did not produce a clear diffraction pattern, if any irregularities appeared along their length during testing, or if they were severed or slipped at either suture attachment point during the test. Two fibers, bundles, and fascicles from different regions of the muscle were tested to avoid regional biases. Following the completion of testing, samples were transferred to microcentrifuge tubes and either suspended in sodium dodecyl sulfate-vertical agarose gel electrophoresis (SDS-VAGE) sample buffer [32] for titin analysis or in an empty tube for hydroxyproline analysis. All samples were stored at -80°C until further testing.

3.3.3 Protein Gels

Titin isoform was analyzed on gels from single fibers, fiber bundles, fascicles, and whole muscle sections (~5-mg wet weight) using SDS-VAGE, and myosin heavy chain (MyHC) content was analyzed from whole muscle sections using sodium dodecyl sulfate-polyacrylamide gel electrophoresis (SDS-PAGE). Samples were homogenized in 1-ml glass homogenization tubes and then boiled for 2 minutes in a 5:1 SDS-VAGE and 40:1 SDS-PAGE sample buffer, respectively.

To quantify titin isoforms, the molecular mass of titin in each sample was determined using SDS-VAGE, as described previously [32]. Titin standards were

obtained from human cadaver soleus (3716 kDa) and rat cardiac muscle (2992 kDa), which had molecular weights based on sequence analysis of the 300 kb titin gene with a coding sequence contained within 363 exons [33, 34]. These tissues were also homogenized and stored at -80°C until analysis. Before loading onto the gel, a titin standard "cocktail" was created with the following ratio: 1-unit human soleus standard:3-units rat cardiac standard:6-units sample buffer. Sample wells were then loaded with both sample and rat cardiac homogenate. Four standard lanes, containing the human soleus and rat cardiac titin homogenates, were evenly distributed throughout the gel. This facilitated titin quantification on each gel. Gels were run on a dual slab gel chamber (C.B.S. Scientific, Del Mar, CA) at 4°C for 5 h at 25-mA constant current.

To quantify MyHC isoform distribution, homogenized protein solution was resuspended to 0.125 μg/μL protein (BCA protein assay, Pierce, Rockford, IL, USA) in a sample buffer. Samples were boiled for 2 min and stored at -80°C. Before loading onto the gel, protein was further diluted 1:15 (0.008 μg/μL) in the same sample buffer to account for the approximately 50-fold greater sensitivity of the silver stain. Ten microliters of each sample were loaded in each lane. Total acrylamide concentration was 4% and 8% in the stacking and resolving gels, respectively (bisacrylamide, 1:50). Gels (16 cm x 22 cm, 0.75 mm thick) were run at a constant current of 10 mA for 1 h, and thereafter, at a constant voltage of 275 V for 22 h at 4°C [35].

Gels were fixed and silver stained according to the Silver Stain Plus procedure (BioRad, Hercules, CA), except that titin gels were dried for approximately 20 h at 40°C immediately after fixing. Relative mobility and intensity of each band was

quantified with Quantity One 1-D Analysis software (Bio-Rad) and denistometry (GS-800, Bio-Rad). The relative mobilities of proteins on the gel were linearly related to the log of their molecular mass. The gel regression relationship for titin and MyHC was calculated based on the standard lanes containing human soleus titin and rat cardiac titin and the lanes containing homogenized adult rat TA muscle (which contains the four adult skeletal muscle myosin isoforms (types 1, 2A, 2X, and 2B)), respectively. The molecular mass of the unknown band was calculated from the relative mobility compared to the standards and the regression equation. As TA contained two bands, the data were averaged by weighting the two bands based on the relative density of each.

3.3.4 Hydroxyproline Assay

Collagen percentage was determined using a colorimetric analysis of hydroxyproline content. Briefly, muscle samples were hydrolyzed in 6-N HCl for 24 h at 110°C, dried, and treated with a chloramine T solution for 20 min at room temperature followed by a solution of p-diaminobenzaldehyde for 30 min at 60°C. Sample absorbance was read at 550 nm in triplicate and compared to a standard curve to determine the hydroxyproline content. Hydroxyproline content was converted to collagen using a constant (7.14; [36]) that defines the number of hydroxyproline residues in a molecule of collagen and then normalized to the specimen wet weight to obtain μg collagen/mg of wet weight [37].

3.3.5 Anatomic Operating Range

Three separate New Zealand White rabbits were anesthetized with isoflurane and sacrificed via pentobarbital injection as previously mentioned. Their hindlimbs were skinned and amputated mid-thigh. Three hindlimbs were pinned to a corkboard at their maximal anatomic dorsiflexion with all toes fully extended and three hindlimbs at their maximum anatomic plantarflexion with all toes fully flexed. The pinned hindlimbs were fixed in 10% buffered formalin for 48 hours. After rinsing in isotonic phosphate-buffered saline, TA, EDL, and EDII were detached and digested in 15% H_2SO_4 for 20 minutes to facilitate muscle fiber bundle microdissection. Muscle architecture was completed according to the methods of Sacks and Roy [38] as modified by Lieber and Blevins [26]. Muscle mass and length was measured for each muscle. Two fiber bundles from three regions (six total) of each muscle were microdissected and sarcomere length (L_s) was measured in each bundle using laser diffraction [30]. The operating range of each muscle was determined by subtracting the L_s of each muscle in full dorsiflexion from the L_s in full plantarflexion. For the muscle halves placed in 10% formalin, muscle architecture was completed in the same manner.

3.3.6 Data Analysis

From the whole muscle experiments, force data were converted to stress by normalizing it to the muscle's physiological cross-sectional area (PCSA) to compare muscles. PCSA (cm^2) was calculated according to the equation $(M \bullet \cos(\theta))/(L_{fn} \bullet \rho)$

where M is measured muscle mass, θ is pennation angle, L_{fn} is fiber length normalized to sarcomere length from muscle architecture, and ρ is an assumed density of 1.0597 g/cm^3 [39]. For fibers, bundles, and fascicles, force data were converted to stress by dividing force by the baseline cross-sectional area value determined assuming a cylindrical sample with an average diameter determined from 3 separate points along the fiber. In all cases, length was converted to strain by normalizing to the slack length of the specimen.

Passive stress-strain curves were fit with a second-order polynomial (r^2: 0.98±0.01 averaged across all size scales). Tangent moduli were evaluated at 90% of the operating range of each muscle (chosen arbitrarily as a value in which passive tension has sufficiently developed) to provide results pertinent to *in vivo* function (Table 3.1). To examine the effect of strain on the predictors of passive tension, tangent moduli were evaluated at a sarcomere length of 2.75 μm (arbitrarily determined as a measure of short sarcomere lengths). Long sarcomere lengths were not listed as the results were similar to the 90% of the operating range data.

Muscle and size scale were compared using a two-way repeated measures ANOVA, and pair-wise comparisons were used to compare all levels (SPSS, Chicago, IL). The correlation between passive moduli at a given size scale and the structural measurements for the three muscles was evaluated using multiple regression analysis. For whole muscle, normalized muscle and fiber lengths, PCSA, pennation angle, fiber area, anatomical operating range length, dorsiflexion L_s, plantarflexion L_s, titin molecular weight, myosin heavy chain isoform distribution, and collagen content were the independent variables included in the analysis. For fascicles, fiber bundles, and

single fibers, the specimen cross-sectional area, slack length, titin molecular weight, and collagen content were the independent variables included. Both step-up and step-down hierarchical regression analyses were used to confirm significant results. Significance was set to $p < 0.05$, and data are presented as mean±SEM (standard error of the mean).

3.4 Results

Specimen diameter and slack sarcomere length were not significantly different among TA, EDL, and EDII at any size scale (Table 3.1). Experimentally-measured muscle architecture data agreed well with literature-reported values (Table 3.1; [10, 25, 26]).

Functionally, passive moduli increased with increasing size scale ($p < 0.001$; Fig. 3.2), and moduli were significantly different among muscles ($p < 0.001$; Fig. 3.3A). Furthermore, moduli at each size scale were found to be muscle dependent ($p < 0.001$; Fig. 3.3A). For TA, passive modulus increased moderately from fiber to bundle (55.707 ± 5.925 kPa to 69.444 ± 5.325 kPa, respectively, $p = 0.068$) and from bundle to fascicle (69.444 ± 5.325 kPa to 79.444 ± 4.426 kPa, respectively, $p = 0.190$), but didn't experience a statistically significant increase until the whole muscle level (598.371 ± 6.325 kPa, $p < 0.001$). EDL and EDII experienced a similar increase to TA from fiber to bundle (EDL: 34.357 ± 7.082 kPa to 62.670 ± 8.638 kPa, respectively, $p = 0.053$; EDII: 41.044 ± 5.875 kPa to 50.535 ± 4.074 kPa, respectively, $p = 0.289$), but their statistically significant increase in modulus occurred at the bundle to fascicle

level (EDL: 62.670 ± 8.638 kPa to 106.460 ± 13.359 kPa, respectively, $p = 0.039$; EDII: 50.535 ± 4.074 kPa to 214.814 ± 36.398 kPa, respectively, $p = 0.004$) and also demonstrated a similar increase at the fascicle to whole muscle level (EDL: 1664.720 ± 108.452 kPa, $p < 0.001$; EDII: 1941.509 ± 73.583 kPa, $p < 0.001$). This suggests that there is an intrinsic scaling difference between TA and EDL/EDII.

To further examine scaling differences, modulus was plotted against the number of fibers in each specimen on a log-log plot (Fig. 3.3B). Due to the nonlinear scaling of the axes, the data were best fit using a power law equation ($y = ax^b$; TA: $r^2 = 0.837$; EDL: $r^2 = 0.928$; EDII: $r^2 = 0.923$), which suggests a nonlinear scaling relationship across size scales. Furthermore, TA exhibits a different scaling pattern than EDL and EDII (b in $y = ax^b$; 0.229 ± 0.015; EDL = 0.366 ± 0.018; EDII = 0.405 ± 0.014; $p < 0.001$), which reinforces the idea that TA scales differently than EDL and EDII.

Muscle-specific differences were also noted at each size scale (Fig. 3.3A). At the fiber level, TA was significantly different from EDL and EDII ($p = 0.006$ and 0.039, respectively). All muscles were similar at the bundle level ($p = 0.232$). At the fascicle level, EDII was significantly different from TA and EDL ($p = 0.010$ and 0.031, respectively) due its distinct rise in passive modulus at this level. Finally, significant differences were revealed among all muscles at the whole muscle level (TA vs EDL, TA vs EDII, and EDL vs EDII: $p = 0.001$, $p < 0.001$, and $p = 0.024$, respectively). These results demonstrate the idea that passive moduli at each size are distinct (Fig. 3.3A); differences between muscles observed at smaller size scales were not simply increased at larger size scales, but rather, a new pattern emerged.

Titin molecular mass, myosin heavy chain isoform distribution, and collagen content of each specimen (MyHC only at the whole muscle level) were analyzed to provide insights into the sources of passive tension (Fig. 3.4). Titin molecular weights were not significantly different across size scales for any of the muscles tested ($p = 0.842$; Fig. 3.4B), but titin isoform size for TA was significantly different from EDL and EDII at all levels ($p < 0.001$; Fig 3.4B). MyHC isoform distribution was also not different among muscles ($p = 0.211$), reaffirming that all three muscles are predominantly fast-fibered muscles (Fig. 3.4C). Collagen content was found to increase with size ($p < 0.001$) and was significantly different across muscles ($p = 0.006$; Fig. 3.4D). Furthermore, the collagen content at a given size scale was dependent on the muscle ($p = 0.046$).

Multiple regression analysis was used to examine the independent variables that best predict passive tension. At the single fiber and fiber bundle level, titin was the significant predictor of passive moduli and yielded an inverse relationship ($r^2 = 0.573$ and 0.225, $p = 0.001$ and 0.047, respectively; Table 3.2). The importance of titin was diminished at the fascicle level, and collagen became the strongest predictor of passive moduli ($r^2 = 0.533$, $p < 0.001$; Table 3.2). At the whole muscle level, both normalized fiber length and collagen acted conjointly to predict passive tension ($r^2 = 0.880$ and 0.608, $p < 0.001$ and $p = 0.023$, respectively; Table 3.2). Although excluded from the model due to colinearity with L_{fn}, pennation angle was also strongly correlated with modulus ($r^2 = 0.808$, $p < 0.001$).

To examine the effect of strain on passive tension predictors, the morphologic predictors of the tangent modulus at 2.75 μm (an arbitrarily chosen short strain) were

determined by multiple regression analysis. For fibers and bundles, titin remained the sole predictor of passive moduli with a strong inverse relationship (r^2 = 0.573 and 0.342, p = 0.001 and 0.013, respectively). Interestingly, at the fascicle and whole muscle level, titin became significant in the modulus prediction, despite collagen still being the main predictor (Fascicles: standardized weight (β) = 0.742 and -0.389 for collagen and titin, respectively; Whole muscle: β = 0.864 and -0.316 for collagen and titin, respectively). These data suggest that titin is important in determining passive stiffness at short strains.

With the modulators of passive identified at long and short strains, we attempted to create a model that captures whole muscle passive stress-strain performance based on the structural and biochemical parameters measured. The passive stress-strain curves were fit with the equation $y = Ax^2 + Bx$ (averaged r^2: 0.98±0.01). The independent variables used in the whole muscle multiple regression (see Methods) were used as independent variables in this multiple regression to determine the best predictors of "A" and "B". A constant was not included in the equation because no stress was assumed to occur at zero strain. Using the multiple regression analysis, "A" and "B" were determined using the following equations:

$$\begin{aligned} A &= 120.29C_{WM} - 12.16L_{fn} - 89.46 \\ B &= -2.50T_{WM} - 19.62L_{fn} + 9511.011 \end{aligned} \quad (1)$$

where C_{WM} is the collagen content at the whole muscle level [in %], L_{fn} is normalized fiber length [in mm], and T_{WM} is the titin molecular weight at the whole muscle level [in kDa]. When comparing the theoretical model with experimentally

measured data, the predicted values agreed strongly for all muscles (TA: ICC = 0.997; EDL: ICC = 0.976; EDII: ICC = 0.975; $p < 0.001$; Fig. 3.5).

3.5 Discussion

These data demonstrate several important concepts. First, the increase in passive tension across size scales is muscle-specific and nonlinear. This suggests that passive tension is mediated, at least at larger scales, by the extracellular matrix. Second, the structures responsible for passive tension change with size scale. Titin was found to be the strongest predictor of passive tension at both the fiber and bundle level; however, collagen surpassed titin as the strongest predictor at the fascicle level. At the whole muscle level, muscle architecture, namely normalized fiber length, became an important indicator of passive tension along with collagen content. Finally, a model of passive tension was developed based on morphological parameters that accurately predict the experimental data for all three muscles. Clinically, these data suggest that a fundamental difference exists between fibers, bundles, fascicles, and whole muscles, and clinicians should not rely on muscle biopsies to infer whole muscle passive mechanical properties.

Magid and Law [40] introduced the idea that fiber and whole muscle have the same passive modulus, suggesting that passive tension is mediated intracellularly. However, these data suggest that that this idea is too simple. Fibers have been shown to have different passive mechanical properties than bundles, which contain a connective tissue matrix layer (i.e., endomysium) that fibers do not [4-6]. The

differences between fibers and bundles manifest themselves functionally as well: bundles exhibit a nonlinear stress-strain response, whereas individual fibers demonstrate a linear response outside of an initial toe region (Fig 3.2; [8, 22, 23]). This nonlinearity results in a much stiffer bundle than their constituent fibers at longer lengths, but similar moduli at shorter strains. By comparing a group of dissected fibers with a fiber bundle, the nonlinearity was shown to be due to the material properties of the ECM [23], which is known to have distinctly nonlinear material properties [41].

Because fibers and bundles contain little to no ECM, titin is thought to be the primary determinant of passive stiffness [2] and slack sarcomere length [20] at these size scales. Titin isoforms in TA were smaller than in EDL or EDII (Fig. 3.4B), and while not significant, TA did have a shorter slack sarcomere length compared to EDL and EDII (Table 3.1). Further, titin size was found to be significantly correlated with modulus and was the dominant predictor of passive tension at the fiber level. Similarly, titin size remained the sole predictor of passive moduli for bundles, which included approximately 20 fibers and their constituent ECM (endomysium). This correlation was weaker than that of the single fibers. One explanation for this result is increased heterogeneity in titin isoform size caused by additional fibers. However, titin size between fibers and bundles was not significantly different, and the variability in titin isoform size decreased with increasing size scale, suggesting that additional fibers did not increase size heterogeneity. A more likely explanation for the reduced predictive power of titin is the partial emergence of a new contributor to passive stiffness (i.e., endomysial collagen). With the addition of interfibrillar connections, they become important to passive stiffness; however, titin size is a significantly

stronger predictor compared to these connections. The inverse correlation between titin size and fiber stiffness is well reported in the literature [2, 42], but other studies have failed to find a significant correlation [4, 22, 43]. This may be explained by the limited range in titin size exhibited in the latter studies (~Δ80 kDa in [22] and ~Δ20 kDa in [4] compared to Δ179.017 kDa in the current study). Thus, evidence suggests that titin is the dominant source of passive tension in both single fibers and fiber bundles.

At larger size scales, addition layers of ECM further increase stress-strain curve nonlinearity, which increases moduli. Fascicles, composed of approximately 300 fibers, contained both endomysium and perimysium. With the addition of a second layer of ECM, collagen became the strongest predictor of modulus, and titin was no longer a significant source of passive tension at 90% of the anatomical range. Thus, the combination of interfascicular connections (i.e., perimysium) and interfibrillar connections (i.e., endomysium) eclipsed titin's ability to predict passive moduli. At the whole muscle level, all levels of ECM are included as well as the organization of muscle fibers (i.e., muscle architecture). Therefore, both muscle architecture and collagen predict whole muscle modulus conjointly, with L_{fn} being the main source of passive tension (standardized weights; Table 3.2).

It has been suggested that the substantial stiffening at larger size scales is necessitated by the anatomical range that these muscles experience *in vivo*. With short fibers and a miniscule operating range (0.167 μm; Table 3.1), EDII is designed to be functionally stiff to protect against overstretching and damage. Due to longer fibers and a medium operating range (0.582 μm; Table 3.1), TA is compliant. However,

EDL has short fibers and the largest operating range (1.187 μm; Table 3.1). Thus, EDL develops passive force slowly throughout its operating range (similar to TA; Fig 3.2B), but at 90% of its anatomical range, EDL is functionally stiff to protect its short fibers (similar to EDII; Fig. 3.3A). These results suggest that muscle architecture and collagen content are intimately linked to dictate muscle excursion and stiffness.

The strain-dependence of the biochemical and architectural parameters were assessed by evaluating the sources of passive tension at different sarcomere lengths. As 90% of the anatomical range was generally a long sarcomere length for each muscle (Table 3.1), the analysis was completed at 2.75 μm. This analysis revealed a similar story of titin dominating passive tension at the fiber and bundle level, but at the fascicle and whole muscle level, titin joined collagen as a significant predictor of passive moduli at shorter sarcomere lengths. Taken together with the anatomic data, these results suggest that titin is functionally important in regulating passive stiffness at short strains, while collagen is functionally important at longer strains. Structurally, these data also concur with the literature. The I-band region of titin generates passive tension during early stretch, but when strained by a factor of 3-4 [44, 45], titin reaches a plateau as it is forcibly detached from its anchor points in the A-band and recruited into the extensible titin pool [44]. In contrast, the contribution of collagen is small at short strains due to crimping of the collagen fibril, but as strain increases, the uncrimping produces tension at higher strains [46-49].

With the main sources of passive tension identified at two different strains, we aimed to develop a model of whole muscle passive tension. Current estimates of whole muscle function either rely on generic models of passive tension [50] that are

unable to capture muscle-specific passive performance [25] or on the extrapolation of muscle function from surgical biopsies (i.e., fiber bundles). However, the results of the current study demonstrate that bundles are fundamentally different from whole muscle, and thus, this extrapolation should be made with caution or avoided altogether. Therefore, a whole muscle passive model was developed using the form $y = Ax^2 + Bx$, where biochemical and architectural parameters predicted "A" and "B". "A" indicates the steepness and direction of the curvature; "B" gives the rate of change when x is equal to zero, or in other words, the initial steepness of the toe region. Therefore, collagen makes sense as a predictor of "A" because it dictates the overall steepness of the passive tension curve, while titin predicts "B", which is the initial stiffness (short strain). This model is limited by the fact that it predicts the curves that it was developed from, and therefore, it requires further validation by altering the predictors of the coefficients and measuring muscle function to determine its usability.

In summary, these data demonstrate that passive moduli scale nonlinearly from fiber to whole muscle, and that passive scaling is muscle-specific. In addition, the structures responsible for mediating passive tension are fundamentally different across size scales and strains. Titin dominates passive tension when minimal amounts of collagen are present (e.g., fibers and bundles) and at short strains, but collagen modulates passive tension once the perimysium is added (e.g., fascicles and whole muscle) and the muscle is stretched to longer strains. At the whole muscle level, architecture and collagen also synergistically regulate in vivo function by dictating stiffness to protect against damage. Finally, a model of passive tension was developed

based on morphologic data and was shown to accurately predict the passive stress-strain curve of all three muscles.

3.6 Acknowledgements

I would like to acknowledge the co-authors of this paper. Chapter 3, is currently being prepared for submission for publication of the material, Winters TM, Lieber RL, Ward SR. We thank Shannon Bremner for her expertise in the development of the LabView program, Mark Chang, Mark Chapman, Tony Choi, Eugene Sato, Tomonori Yamaguchi, and Tatsuhiko Fujiwara for technical assistance. We acknowledge grant support by the Department Veterans Affairs and NIH/NICHD grants HD048501 and HD050837.

3.7 References

1. Brown, I.E., T.L. Liinamaa, and G.E. Loeb, *Relationships between range of motion, lo, and passive force in five strap-like muscles of the feline hind limb.* J Morphol, 1996. **230**(1): p. 69-77.

2. Prado, L.G., et al., *Isoform diversity of giant proteins in relation to passive and active contractile properties of rabbit skeletal muscles.* J Gen Physiol, 2005. **126**(5): p. 461-80.

3. Shah, S.B., et al., *Structural and functional roles of desmin in mouse skeletal muscle during passive deformation.* Biophys J, 2004. **86**(5): p. 2993-3008.

4. Ward, S.R., et al., *Passive mechanical properties of the lumbar multifidus muscle support its role as a stabilizer.* J Biomech, 2009. **42**(10): p. 1384-9.

5. Friden, J. and R.L. Lieber, *Spastic muscle cells are shorter and stiffer than normal cells.* Muscle Nerve, 2003. **27**(2): p. 157-64.

6. Lieber, R.L., et al., *Inferior mechanical properties of spastic muscle bundles due to hypertrophic but compromised extracellular matrix material.* Muscle Nerve, 2003. **28**(4): p. 464-71.

7. Abrams, R.A., et al., *Skeletal muscle recovery after tenotomy and 7-day delayed muscle length restoration.* Muscle Nerve, 2000. **23**(5): p. 707-14.

8. Meyer, G.A. and R.L. Lieber, *Skeletal Muscle Fibrosis Develops in Response to Desmin Deletion.* Am J Physiol Cell Physiol, 2012.

9. Brown, S.H., et al., *ISSLS prize winner: Adaptations to the multifidus muscle in response to experimentally induced intervertebral disc degeneration.* Spine (Phila Pa 1976), 2011. **36**(21): p. 1728-36.

10. Takahashi, M., S.R. Ward, and R.L. Lieber, *Intraoperative single-site sarcomere length measurement accurately reflects whole-muscle sarcomere length in the rabbit.* J Hand Surg [Am], 2007. **32**(5): p. 612-7.

11. Borg, T.K. and J.B. Caulfield, *Morphology of connective tissue in skeletal muscle.* Tissue Cell, 1980. **12**(1): p. 197-207.

12. Trotter, J.A. and P.P. Purslow, *Functional morphology of the endomysium in series fibered muscles.* J Morphol, 1992. **212**(2): p. 109-22.

13. Maruyama, K., *Connectin, an elastic filamentous protein of striated muscle.* Int Rev Cytol, 1986. **104**: p. 81-114.

14. Wang, K., *Sarcomere-associated cytoskeletal lattices in striated muscle. Review and hypothesis.* Cell Muscle Motil, 1985. **6**: p. 315-69.

15. Maruyama, K., et al., *Connectin filaments link thick filaments and Z lines in frog skeletal muscle as revealed by immunoelectron microscopy.* J Cell Biol, 1985. **101**(6): p. 2167-72.

16. Trombitas, K., J.P. Jin, and H. Granzier, *The mechanically active domain of titin in cardiac muscle.* Circ Res, 1995. **77**(4): p. 856-61.

17. Smith, L.R., et al., *Hamstring contractures in children with spastic cerebral palsy result from a stiffer extracellular matrix and increased in vivo sarcomere length.* J Physiol, 2011. **589**(Pt 10): p. 2625-39.

18. Granzier, H.L. and T.C. Irving, *Passive tension in cardiac muscle: contribution of collagen, titin, microtubules, and intermediate filaments.* Biophys J, 1995. **68**(3): p. 1027-44.

19. Bartoo, M.L., W.A. Linke, and G.H. Pollack, *Basis of passive tension and stiffness in isolated rabbit myofibrils.* Am J Physiol, 1997. **273**(1 Pt 1): p. C266-76.

20. Wang, K., et al., *Regulation of skeletal muscle stiffness and elasticity by titin isoforms: a test of the segmental extension model of resting tension.* Proc Natl Acad Sci U S A, 1991. **88**(16): p. 7101-5.

21. Linke, W.A., V.I. Popov, and G.H. Pollack, *Passive and active tension in single cardiac myofibrils.* Biophys J, 1994. **67**(2): p. 782-92.

22. Brown, S.H., et al., *Passive mechanical properties of rat abdominal wall muscles suggest an important role of the extracellular connective tissue matrix.* J Orthop Res, 2011.

23. Meyer, G.A. and R.L. Lieber, *Elucidation of extracellular matrix mechanics from muscle fibers and fiber bundles.* J Biomech, 2011. **44**(4): p. 771-3.

24. Powell, P.L., et al., *Predictability of skeletal muscle tension from architectural determinations in guinea pig hindlimbs.* J Appl Physiol, 1984. **57**(6): p. 1715-21.

25. Winters, T.M., et al., *Whole muscle length-tension relationships are accurately modeled as scaled sarcomeres in rabbit hindlimb muscles.* J Biomech, 2011. **44**(1): p. 109-15.

26. Lieber, R.L. and F.T. Blevins, *Skeletal muscle architecture of the rabbit hindlimb: functional implications of muscle design.* J Morphol, 1989. **199**(1): p. 93-101.

27. Lieber, R.L. and J. Friden, *Muscle damage is not a function of muscle force but active muscle strain.* J Appl Physiol, 1993. **74**(2): p. 520-6.

28. Lieber, R.L., T.M. Woodburn, and J. Friden, *Muscle damage induced by eccentric contractions of 25% strain.* J Appl Physiol, 1991. **70**(6): p. 2498-507.

29. Einarsson, F., E. Runesson, and J. Friden, *Passive mechanical features of single fibers from human muscle biopsies--effects of storage.* J Orthop Surg Res, 2008. **3**: p. 22.

30. Lieber, R.L., Y. Yeh, and R.J. Baskin, *Sarcomere length determination using laser diffraction. Effect of beam and fiber diameter.* Biophys J, 1984. **45**(5): p. 1007-16.

31. Baskin, R.J., K.P. Roos, and Y. Yeh, *Light diffraction study of single skeletal muscle fibres.* Biophys J, 1979. **28**(1): p. 45-64.

32. Warren, C.M., P.R. Krzesinski, and M.L. Greaser, *Vertical agarose gel electrophoresis and electroblotting of high-molecular-weight proteins.* Electrophoresis, 2003. **24**(11): p. 1695-702.

33. Labeit, S. and B. Kolmerer, *Titins: giant proteins in charge of muscle ultrastructure and elasticity.* Science, 1995. **270**(5234): p. 293-6.

34. Freiburg, A., et al., *Series of exon-skipping events in the elastic spring region of titin as the structural basis for myofibrillar elastic diversity.* Circ Res, 2000. **86**(11): p. 1114-21.

35. Talmadge, R.J. and R.R. Roy, *Electrophoretic separation of rat skeletal muscle myosin heavy-chain isoforms.* J Appl Physiol, 1993. **75**(5): p. 2337-40.

36. Etherington, D.J. and T.J. Sims, *Detection and estimation of collagen.* Journal of the Science of Food and Agriculture, 1981. **32**(6): p. 539-546.

37. Edwards, C.A. and W.D. O'Brien, Jr., *Modified assay for determination of hydroxyproline in a tissue hydrolyzate.* Clin Chim Acta, 1980. **104**(2): p. 161-7.

38. Sacks, R.D. and R.R. Roy, *Architecture of the hind limb muscles of cats: functional significance.* J Morphol, 1982. **173**(2): p. 185-95.

39. Mendez, J. and A. Keys, *Density and composition of mammalian muscle.* Metabolism, 1960. **9**: p. 184-188.

40. Magid, A. and D.J. Law, *Myofibrils bear most of the resting tension in frog skeletal muscle.* Science, 1985. **230**(4731): p. 1280-2.

41. Purslow, P.P. and J.A. Trotter, *The morphology and mechanical properties of endomysium in series-fibred muscles: variations with muscle length.* J Muscle Res Cell Motil, 1994. **15**(3): p. 299-308.

42. Thacker, B.E., et al., *Passive mechanical properties and related proteins change with botulinum neurotoxin A injection of normal skeletal muscle.* J Orthop Res, 2011. **30**(3): p. 497-502.

43. Olsson, M.C., et al., *Fibre type-specific increase in passive muscle tension in spinal cord-injured subjects with spasticity.* J Physiol, 2006. **577**(Pt 1): p. 339-52.

44. Wang, K., et al., *Viscoelasticity of the sarcomere matrix of skeletal muscles. The titin-myosin composite filament is a dual-stage molecular spring.* Biophys J, 1993. **64**(4): p. 1161-77.

45. Granzier, H.L. and K. Wang, *Passive tension and stiffness of vertebrate skeletal and insect flight muscles: the contribution of weak cross-bridges and elastic filaments.* Biophys J, 1993. **65**(5): p. 2141-59.

46. Diamant, J., et al., *Collagen; ultrastructure and its relation to mechanical properties as a function of ageing.* Proc R Soc Lond B Biol Sci, 1972. **180**(60): p. 293-315.

47. Franchi, M., et al., *Tendon crimps and peritendinous tissues responding to tensional forces.* Eur J Histochem, 2007. **51 Suppl 1**: p. 9-14.

48. Franchi, M., et al., *Crimp morphology in relaxed and stretched rat Achilles tendon.* J Anat, 2007. **210**(1): p. 1-7.

49. Benjamin, M., E. Kaiser, and S. Milz, *Structure-function relationships in tendons: a review.* J Anat, 2008. **212**(3): p. 211-28.

50. Zajac, F.E., *Muscle and tendon: properties, models, scaling, and application to biomechanics and motor control.* Crit Rev Biomed Eng, 1989. **17**(4): p. 359-411.

Table 3.1: Sample dimensions do not significantly differ between muscles until the whole muscle level. At the fiber, bundle, and fascicle level, diameter and slack sarcomere length did not differ between muscles. At the whole muscle level, the anatomic operating range of TA, EDL, and EDII were evaluated to determine the sarcomere lengths relevant to *in vivo* function. Other architectural parameters are shown below. Data are presented as mean ± SEM.

		TA	EDL	EDII
Single Fiber	Diameter [mm]	0.065 ± 0.005	0.072 ± 0.005	0.064 ± 0.004
	Sarcomere Length [μm]	2.154 ± 0.088	2.322 ± 0.038	2.220 ± 0.080
Fiber Bundle	Diameter [mm]	0.287 ± 0.018	0.239 ± 0.026	0.248 ± .017
	Sarcomere Length [μm]	2.131 ± 0.067	2.291 ± 0.060	2.184 ± 0.057
Fascicle	Diameter [mm]	1.198 ± 0.126	1.308 ± 0.213	0.974 ± 0.176
	Sarcomere Length [μm]	2.009 ± 0.081	2.201 ± 0.064	2.125 ± 0.073
Whole Muscle	Dorsiflexion Sarcomere Length [μm]	2.365 ± 0.175	2.427 ± 0.207	2.773 ± 0.030
	Plantarflexion Sarcomere Length [μm]	2.947 ± 0.007	3.613 ± 0.037	2.940 ± 0.103
	90% of Anatomical Range [μm]	2.889 ± 0.024	3.495 ± 0.012	2.923 ± 0.090
	Normalized Fiber Length [mm]	38.406 ± 1.603	15.425 ± 0.971	10.638 ± 0.818
	Pennation Angle [°]	0.6 ± 0.187	8.7 ± 2.280	18.1 ± 2.909
	PCSA [cm^2]	0.781 ± 0.029	1.927 ± 0.117	0.620 ± 0.064

Values are presented as mean ± SEM

Table 3.2: Multiple regression analysis provides insight into the sources of passive tension at each size scale. At smaller size scales (e.g., fibers and bundles), titin is the dominant source of passive tension. However, at larger size scales (e.g., fascicles and whole muscle), collagen is a dominant source of passive tension. Interestingly, at the whole muscle level, architecture (e.g., normalized fiber length) is significantly important to passive tension. Data are presented as mean ± SEM.

	Parameter	Unstandardized Weights	Standardized Weights	Significance	r^2
Single Fiber	Constant	606.606 ± 121.653	N/A	$p < 0.001$	N/A
	Titin	-0.159 ± 0.034	-0.757	$p < 0.001$	0.573
Fiber Bundle	Constant	394.620 ± 153.978	N/A	$p = .021$	N/A
	Titin	-0.094 ± 0.044	-0.474	$p = 0.047$	0.225
Fascicle	Constant	-38.554 ± 42.492	N/A	$p = .378$	N/A
	Collagen	35.125 ± 8.232	0.73	$p < 0.001$	0.533
Whole Muscle	Constant	1571.711 ± 339.059	N/A	$p < 0.001$	N/A
	Collagen	33.847 ± 13.370	0.26	$p = 0.023$	0.608
	L_{fn}	-37.601 ± 5.068	-0.761	$p < 0.001$	0.880

Values are presented as mean ± SEM

r^2 values represent the explained variation between the parameter and passive modulus

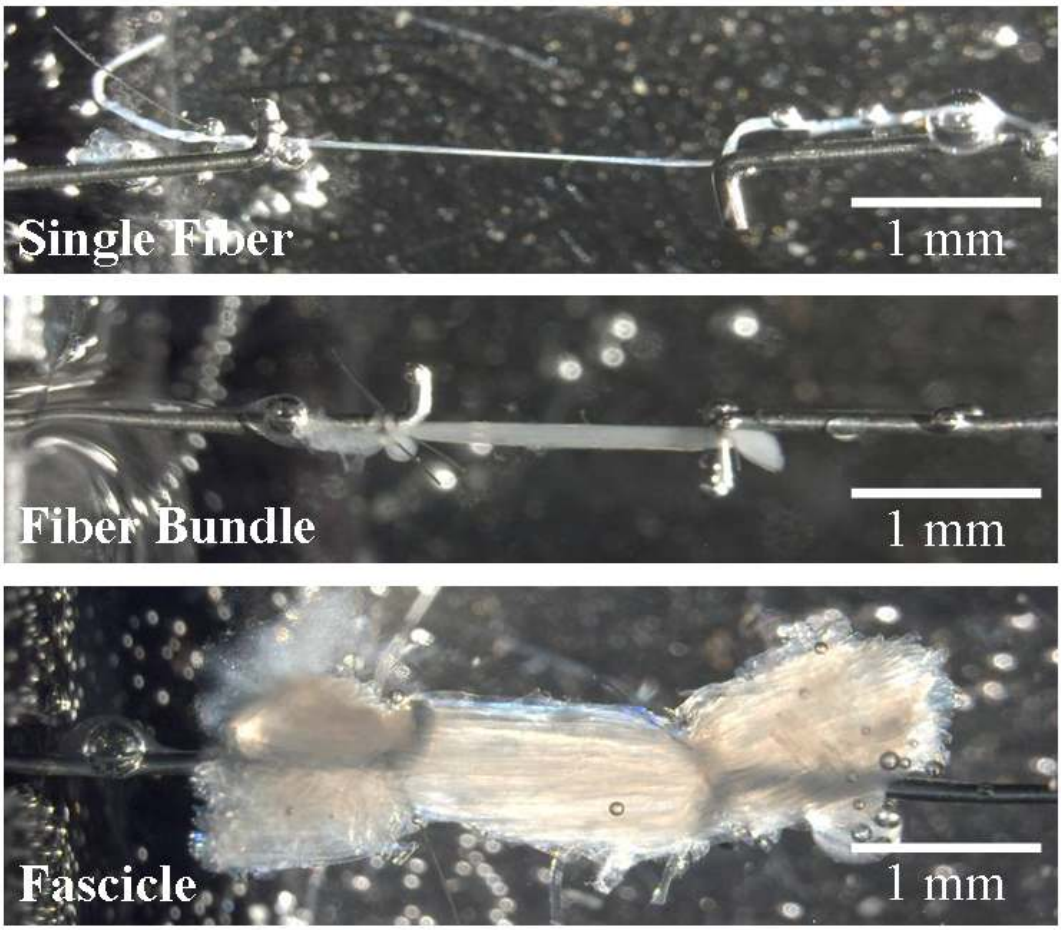

Figure 3.1: Mechanical testing set-up for single fiber, fiber bundle (approximately 20 fibers), and fascicle (approximately 300 fibers and defined by natural ECM divisions) segments and their constitutive ECM. Each sample (1.5-3.0 mm in length) was mounted in a chamber in a custom apparatus at room temperature (20°C). Using 10-0 monofilament nylon suture, samples were secured to a force transducer on one end and to a titanium wire rigidly attached to a rotational bearing on the other end. The samples were then loaded with strains of approximately 0.25 μm/sarcomere at 100 fiber lengths/sec. Each stretch was held for 3 minutes to permit stress relaxation before a sequential stretch was made. Segments were stretched in total to approximately 100% strain.

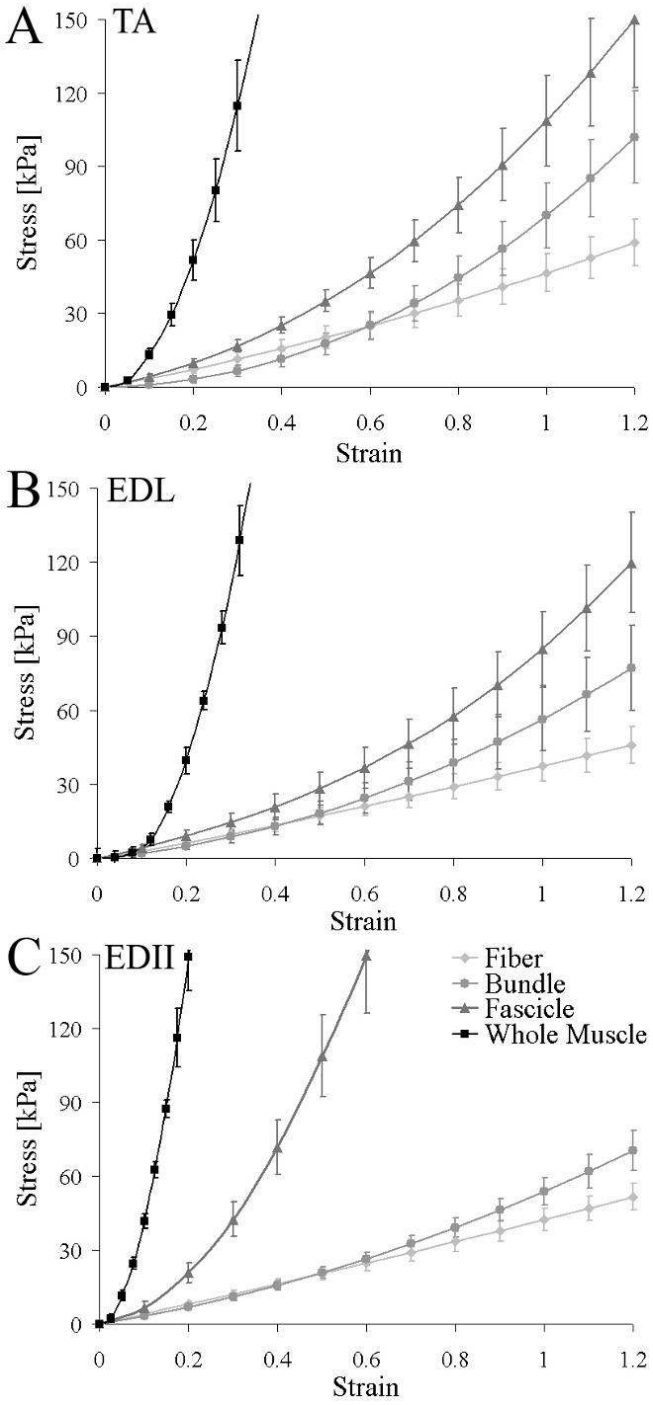

Figure 3.2: Passive stress-strain curves for (A) TA, (B) EDL, and (C) EDII with each curve representing a different size scale: fibers (diamonds), bundles (circles), fascicles (triangles), and whole muscle (squares). Although raw data were fit with quadratic regression, fiber stress-strain curves were nearly linear. As size scale increased, samples increased in stiffness and became highly nonlinear, presumably due to increases in ECM. Data are presented as mean ± SEM.

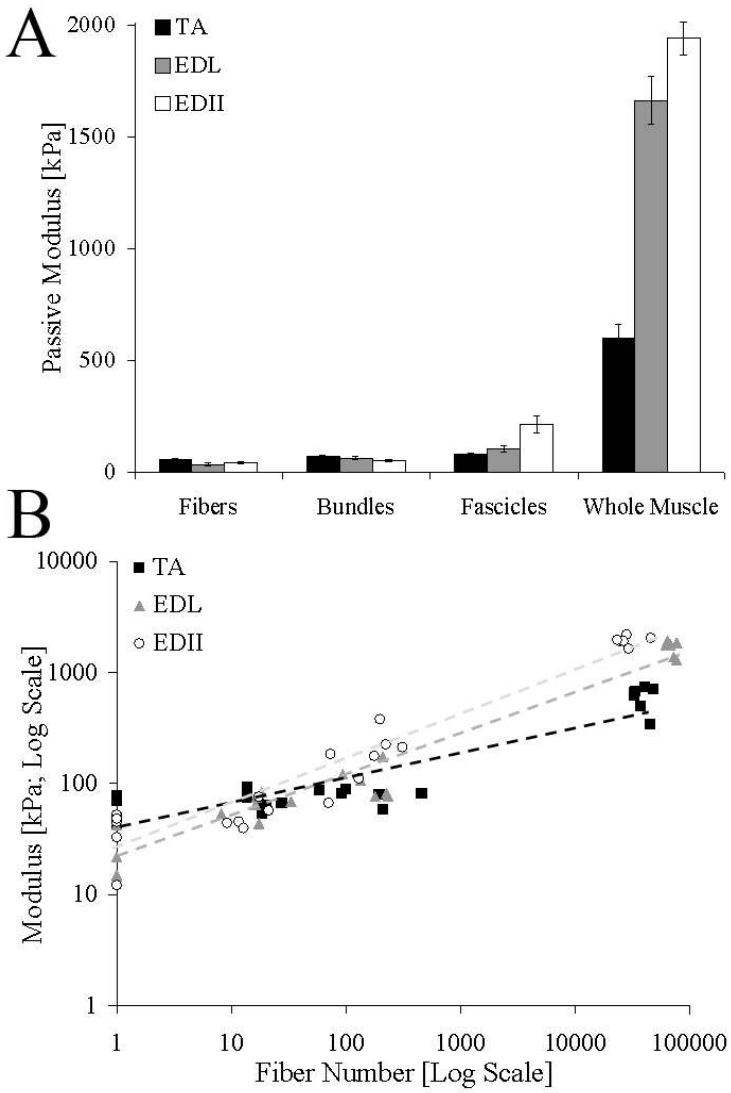

Figure 3.3: The scaling of passive tension modulus across size scales. (A) Passive tangent moduli were calculated from the stress-strain curves in Fig. 2 at 90% of the anatomical range of each muscle (Table 3.1). Moduli increased with size scale ($p < 0.001$) and were significantly different among muscles ($p < 0.001$). Furthermore, the passive moduli at each size scale were muscle dependent ($p < 0.001$). The passive modulus of TA did not change until the whole muscle size scale, while EDL and EDII both demonstrated significant increases in modulus at the fascicle level. (B) The moduli from (A) were replotted on a log-log scale to demonstrate the relationship between fiber number and modulus. Due to the nonlinear scaling of the axes, a linear line represents a power law equation ($y = ax^b$), which suggests a nonlinear scaling relationship across size scales (TA: $r^2 = 0.837$; EDL: $r^2 = 0.928$; EDII: $r^2 = 0.923$). Furthermore, TA exhibited a different scaling pattern than EDL and EDII (b in $y = ax^b$; TA = 0.229 ± 0.015; EDL = 0.366 ± 0.018; EDII = 0.405 ± 0.014; $p < 0.001$), suggesting that scaling is muscle-specific. Data are presented as mean ± SEM.

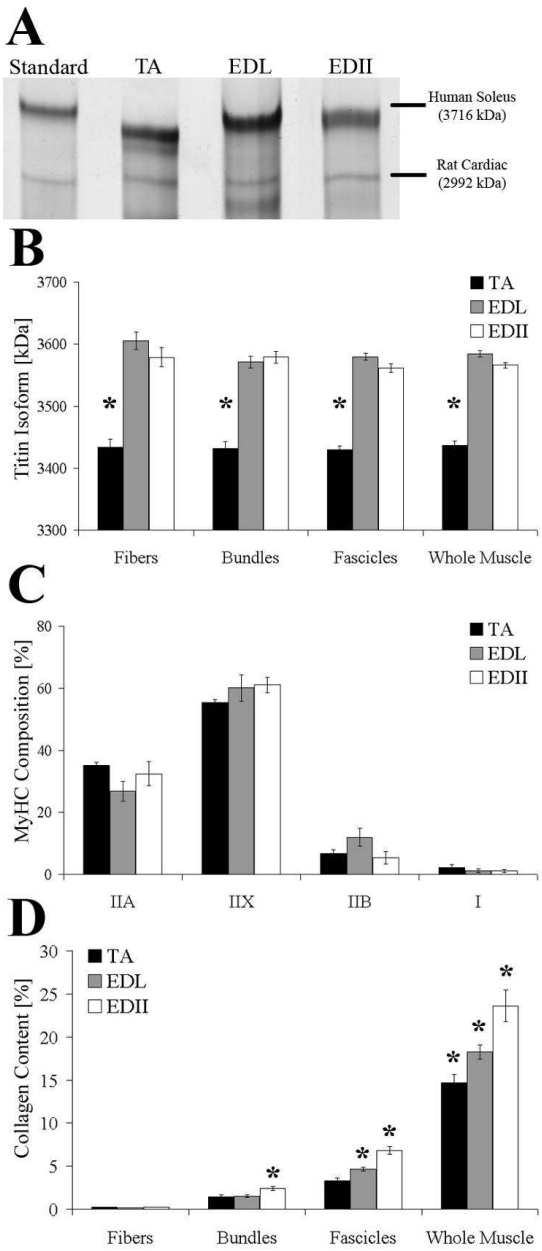

Figure 3.4: Biochemical properties of the muscles were analyzed to provide insights into the sources of passive tension. (A) Representative titin gel. (B) Titin molecular weight is not significantly different across size scales for any of the muscles tested ($p = 0.842$). However, titin isoform size for TA was significantly different from EDL and EDII ($p < 0.001$). (C) Because all three muscles are predominantly fast-fibered muscles, MyHC isoform distribution was also not significantly different among muscles ($p = 0.211$). (D) Collagen content was found to increase with size ($p < 0.001$) and was significantly different across muscles ($p = 0.006$). Furthermore, the collagen content at a given size scale was dependent on the muscle ($p = 0.046$). Collagen content is expressed as % wet weight. Asterisk indicates significant difference other muscles ($p < 0.001$). Data are presented as mean ± SEM.

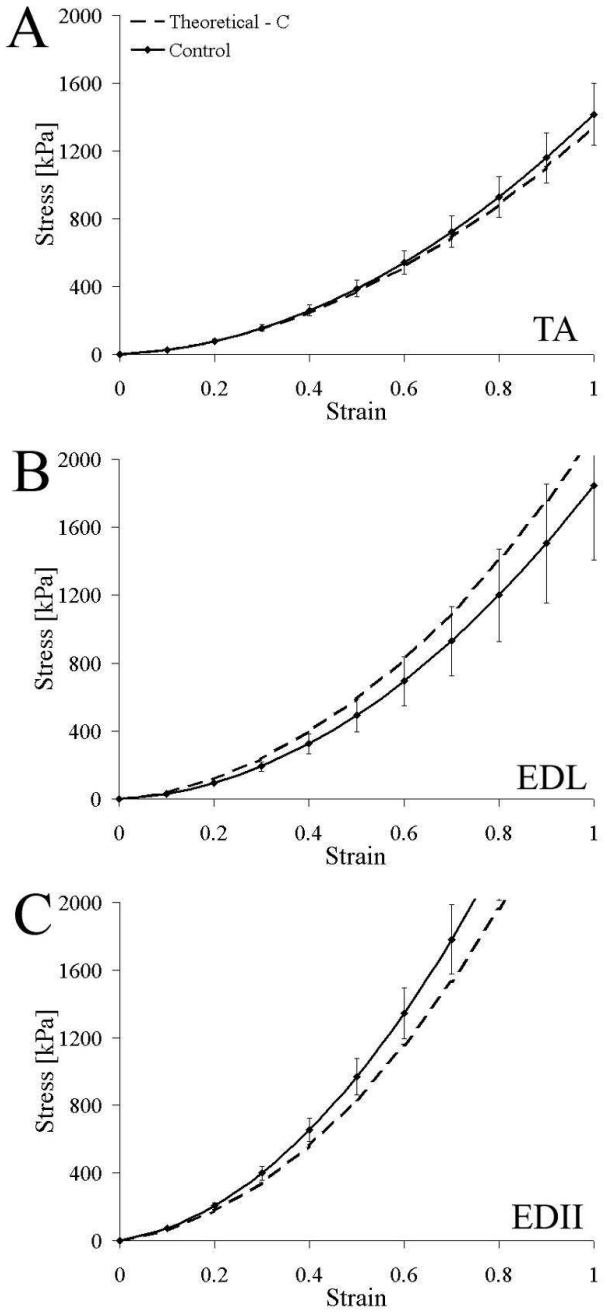

Figure 3.5: The passive model accurately predicts experimental data for (A) TA, (B) EDL, and (C) EDII. Whole muscle experimental passive tension curves were fit with the equation $y = Ax^2 + Bx$, where y was stress in kPa, x was strain, and A and B were unknown coefficients. Using multiple regression analysis, A was found to depend on collagen content and L_{fn}, and B was found to depend on titin isoform size and L_{fn} (see Results for equation). The theoretical model (dashed lines) and experimentally measured data (black solid line) agreed well suggesting that this model may be applicable to predicting whole muscle passive tension curves. Data are presented as mean ± SEM.

CHAPTER 4

DETERMINANTS OF ACTIVE AND PASSIVE TENSION FOLLOWING TENOTOMY

4.1 Abstract

Structure-function relationships are paramount to predicting *in vivo* function. Using architectural relationships, a scaled sarcomere model was previously able to accurately predict whole muscle active function. However, architecture alone was unable to predict passive tension data, suggesting the need for a model that includes load-bearing protein differences. A muscle-specific model based on both load-bearing proteins and architectural data was developed, but has not yet been robustly validated against experimental data. To accomplish this goal, three architecturally diverse muscles were tenotomized, and muscle remodeling was allowed to occur. The contralateral leg served as a control. After six weeks, whole muscles were mechanically tested actively and passively, and single fibers, fiber bundles, and fascicles were passively tested from the same muscles. Biochemical, histological, and architectural analyses were completed. For active tension, architecture alone was unable to predict the length-tension curve following tenotomy (averaged: $p = 0.366$),

which was a result of an uncoupling of architectural structure-function relationships. Therefore, a new model was developed that incorporated changes in collagen and fiber area to accurately predict FWHM and peak force, respectively, under both control and tenotomy conditions (ICC = 0.971 and 0.644, $p < 0.001$, respectively). For passive tension, the model of passive tension relied on collagen content, normalized fiber length, and titin isoform size to accurately predict the passive curves for control and tenotomy experimental data (ICC > 0.95 for all muscles, $p < 0.001$), which validates the use of the model. Therefore, this study provides a robust model for understanding both active and passive tension and identifying key mediators of function following tenotomy.

4.2 Introduction

Skeletal muscle represents the classic biological example of a structure-function relationship. Muscle architecture (the number and orientation of fibers within a muscle) is the key structural determinant of active function [1, 2]. Serial sarcomere number (i.e., normalized fiber length) predicts with muscle excursion [3], while physiological cross-sectional area (PCSA) predicts maximum tetanic tension (P_o) [4]. Using only muscle architecture, whole muscle active tension was accurately modeled by scaling up the contractile function of a sarcomere [3]. Thus, architectural measurements provide a useful tool for accurately predicting active muscle function.

However, current models of passive tension [5] are not generalizable across muscles [3] and rely mainly on muscle architecture, not load-bearing protein

differences [6, 7]. The disconnect between model and experiment may be caused by the muscle- [8], size-scale- [9], and strain-dependence [10] of collagen and titin (Chapter 3). This forces clinicians to rely on the properties of muscle biopsies (i.e., fiber bundles) to infer whole muscle function and prescribe the appropriate treatment, which is not advised due to nonlinear scaling from bundle to whole muscle (Chapter 3). To correct this deficiency, a passive tension model was recently developed based on both architectural parameters and load-bearing proteins to produce muscle-specific models of passive tension (Chapter 3). However, this model has not been robustly validated.

Functional changes at the fiber and/or bundle level have been shown to occur with pathology, such as cerebral palsy [9], desminopathy [11], intervertebral disc degeneration [12], spasticity [13], and botulinum neurotoxin [14]. These changes have been attributed to changes in collagen and titin, but their dependence has not been explicitly tested. Furthermore, a disconnect between structure and function was found after tendon transfer (Takahashi, 2011). Despite an increase in serial sarcomere number and a maintenance in PCSA compared to controls, both muscle excursion and maximum tetanic tension (P_0) were reduced, suggesting that the current dogma regarding structure-function relationships may be inherently altered with pathology.

Tenotomy is an important clinical phenomena that results from surgical manipulation (e.g., tendon transfer or lengthening), trauma (e.g., tendon lacerations or insertion avulsions), or degenerative processes (e.g., rotator cuff, distal biceps, or Achilles rupture). Tenotomized muscle is characterized by both functional and structural changes [15]. Functionally, peak active tension declines by over 50% [16,

17], while the muscle becomes passively stiffer [18, 19]. These functional changes are accompanied by ECM proliferation [20], declines in PCSA, mass, and fiber area [17, 20, 21], and reduced serial sarcomere number [16, 22]. However, it is unclear whether the functional changes are a direct cause of post-tenotomy sarcomere or extracellular protein remodeling.

Therefore, the purpose of the current study is to produce a functional change in a well-understood system and assess the robustness of the strongest structural predictors of function at four different size scales and validate the use of both an active and passive model to accurately predict whole muscle function.

4.3 Materials

4.3.1 Aseptic Surgery

The tibialis anterior (TA; n=6), extensor digitorum longus (EDL; n=6), and extensor digitorum of the second toe (EDII; n=6) muscles of New Zealand White rabbits (mass=2.68±0.04 kg) were chosen due to their varied architecture [23, 24]). The distal tendon of these muscles was tenotomized using aseptic technique (sterile instruments, gloves, face mask, and scrubs) in a room suitable for aseptic surgery. The animal was anesthetized using a subcutaneous injection of a ketamine-xylazine cocktail (35 and 5 mg/kg, respectively) and maintained on 2% isoflurane (IsoFlo; Abbott Laboratories, North Chicago, IL) at 2 L/min through a 2.5-mm endotracheal tube. In this 15-minute procedure, the hair surrounding the ankle was clipped and the site scrubbed with Betadine. A 1 to 2-cm incision was made distal to the extensor

retinaculum for TA and EDL and 20-mm proximal to the medial malleolus for EDII. The tendon of interest (one per animal) was clamped with a hemostat, and a 5-mm section was excised via cuts flanking the clamped area. The wound was then closed subcutaneously using 4-0 Vicryl and dressed with Nexaband. For the contralateral leg, the same methods were used to expose the tendon, clear the fascia, and close the incision; this sham operation served as a control. Six rabbits were included in each group (TA tenotomy, EDL tenotomy, and EDII tenotomy) for a total of 18 animals. The animal's heart rate and respiratory rate was monitored peri-operatively and post-operatively until the animal was awake and alert. Metacam (0.2 mg/kg) and Cefazolin (22 mg/kg) were given subcutaneously immediately following anesthetic induction and then every 8-12 hours for 3 days.

4.3.2 Whole Muscle Mechanical Testing

Animal preparation and measurement of isometric contractile properties were performed as previously described [25, 26]. Six weeks after tenotomy, rabbits (mass = 3.71±0.05 kg) were re-anesthetized using a subcutaneous injection of a ketamine-xylazine cocktail (35 and 5 mg/kg, respectively) and maintained on 2% isoflurane (IsoFlo; Abbott Laboratories, North Chicago, IL) at 2 L/min through a face-mask. Heart rate and oxygen saturation were monitored (VetOx, Heska Co., Fort Collins, CO) throughout the test. A mid-line incision was made from the mid-thigh to the ankle to expose the muscle. The muscle's retraction was quantified as the difference between control and tenotomized muscle length while the muscle was in the neutral

position (the hip and knee at 90° and the ankle at 0° dorsiflexion). To immobilize the leg, it was secured to a custom jig via tightened screws at the lateral femoral condyle and malleoli. Suture markers were placed at the distal and proximal muscle-tendon junctions to define muscle length (L_m). For the TA and EDL, the biceps femoris was split, exposing the peroneal nerve; for the EDII, the tibial nerve was exposed. A cuff electrode was placed around the nerve for direct stimulation (Pulsar 6 bp Stimulator; FHC, Bowdoinham, ME). The tenotomized or control tendon was released from its surrounding scar tissue or transected distally, respectively. For TA and EDL testing, both tendons were cut to avoid confounding effects of the other muscle. Subsequently, it was clamped to a servomotor (Cambridge Model 310B; Aurora Scientific, Aurora, ON, Canada) at the muscle-tendon junction and aligned with the force-generating axis of the motor [26]. Muscle temperature was maintained at 37°C with radiant heat and a servo-temperature controller (Model 73A; YSI, Yellow Springs, OH). Muscle and tendon tissue were regularly irrigated with isotonic saline to prevent dehydration.

The length-tension protocol consisted of a series of 100-Hz tetanic contractions (pulse width: 0.3 ms; amplitude: 10 V) over a 640-ms period. Three-minute rest intervals were interposed between contractions to minimize fatigue and allow for passive stress relaxation. Measurements began at the neutral position and ranged from −25 to 25% L_{fn} in increments of 5% L_{fn} (L_{fn}: normalized fiber length). Passive tension at each muscle length was obtained by measuring the baseline (preactivation) force. Force and length were acquired for each contraction using a data acquisition board (610E series; National Instruments, Austin, TX) and a custom-written LabView

program (National Instruments) at 4 kHz per channel. After the experimental leg was tested, the contralateral leg was tested in the same manner.

Upon completion of testing, animals were euthanized with pentobarbital (Euthasol; Virbac AH, Fort Worth, TX) and the tenotomized and control muscles were removed. Muscles were blotted dry and weighed for mass. The muscles were then divided longitudinally into two sections, and one section was fixed for 3-5 days in 10% buffered formalin for architectural determination. From the other section, the distal one-third was removed and placed into a glycerinated storage solution (composed of 170.0-mM KPropionate, 5.0-mM K_3EGTA, 5.3-mM $MgCl_2$, 10.0-mM imidazole, 21.2-mM Na_2ATP, 1.0-mM NaN_3, 2.5-mM glutathione, 50-μM leupeptin, and 50% (v/v) glycerol) at -20°C for up to four weeks [13, 27]. The remainder of the muscle was snap frozen in isopentane chilled by liquid nitrogen (-159°C) and stored at -80°C.

4.3.3 Fiber, Bundle, and Fascicle Mechanical Testing

The muscle section was removed from the storage solution and transferred to a chilled relaxing solution maintained at pCa 8.0 and pH 7.1, consisting of the following: 59.4-mM imidazole, 86.0-mM KCH_4O_3S, 0.13-mM $Ca(KCH_4O_3S)_2$, 10.8-mM $Mg(KCH_4O_3S)_2$, 5.5-mM K_3EGTA, 1.0-mM KH_2PO_4, 5.1-mM Na_2ATP, and 50.0-μM leupeptin. Single fiber, fiber bundle (approximately 20 fibers), and fascicle (approximately 300 fibers; defined by natural ECM divisions) segments and their constitutive ECM were carefully dissected from the same muscle. Each sample (1.5-

3.0 mm in length) was mounted in a chamber in a custom apparatus at room temperature (20°C). Using 10-0 monofilament nylon suture, samples were secured to a force transducer (Model 405A for fibers and bundles and 404A for fascicles, Aurora Scientific, Ontario, Canada) on one end and to a titanium wire rigidly attached to a rotational bearing (Newport MT-RS; Irvine, CA) on the other end. Segments displaying obvious abnormalities or discoloration were not used. The sample was transillumated by a 7-mW He–Ne laser to permit sarcomere length measurement by laser diffraction [28]. Resolution of this method is approximately 5 nm [29]. The system was calibrated with a 2.50-μm plastic blazed diffraction grating prior to experimentation (Diffraction Gratings, Inc., Nashville, TN).

Each segment was brought to slack length (length at which the sample exerted ~2 μN), and sample dimensions were measured optically with a cross-hair reticule mounted on a dissecting microscope and micromanipulators on an x-y mobile stage. The samples were then loaded with strains of approximately 0.25 μm/sarcomere at 100 fiber lengths/sec. Each stretch was held for 3 minutes to permit stress relaxation before a sequential stretch was made [13]. Segments were stretched in total to approximately 100% strain. Samples were discarded if they did not produce a clear diffraction pattern, if any irregularities appeared along their length during testing, or if they were severed or slipped at either suture attachment point during the test. Two fibers, bundles, and fascicles from different regions of the muscle were tested to avoid regional biases. Following the completion of testing, samples were transferred to microcentrifuge tubes and either suspended in sodium dodecyl sulfate-vertical agarose gel electrophoresis (SDS-VAGE) sample buffer [30] for titin analysis or in an empty

tube for hydroxyproline analysis. All samples were stored at -80°C until further testing.

4.3.4 Protein Gels

Titin isoform was analyzed on gels from single fibers, fiber bundles, fascicles, and whole muscle sections (~5-mg wet weight) using SDS-VAGE, and myosin heavy chain (MyHC) content was analyzed from whole muscle sections using sodium dodecyl sulfate-polyacrylamide gel electrophoresis (SDS-PAGE). Samples were homogenized in 1-ml glass homogenization tubes and then boiled for 2 minutes in a 5:1 SDS-VAGE and 40:1 SDS-PAGE sample buffer, respectively. To quantify titin isoforms, the molecular mass of titin in each sample was determined using SDS-VAGE, as described previously [30]. Titin standards were obtained from human cadaver soleus (3716 kDa) and rat cardiac muscle (2992 kDa), which had molecular weights based on sequence analysis of the 300 kb titin gene with a coding sequence contained within 363 exons [31, 32]. These tissues were also homogenized and stored at -80°C until analysis. Before loading onto the gel, a titin standard "cocktail" was created with the following ratio: 1-unit human soleus standard:3-units rat cardiac standard:6-units sample buffer. Sample wells were then loaded with both sample and rat cardiac homogenate. Four standard lanes, containing the human soleus and rat cardiac titin homogenates, were evenly distributed throughout the gel. This facilitated titin quantification on each gel. Gels were run on a dual slab gel chamber (C.B.S. Scientific, Del Mar, CA) at 4°C for 5 h at 25-mA constant current.

To quantify MyHC isoform distribution, homogenized protein solution was resuspended to 0.125 μg/μL protein (BCA protein assay, Pierce, Rockford, IL, USA) in a sample buffer. Samples were boiled for 2 min and stored at -80°C. Before loading onto the gel, protein was further diluted 1:15 (0.008 μg/μL) in the same sample buffer to account for the approximately 50-fold greater sensitivity of the silver stain. Ten microliters of each sample were loaded in each lane. Total acrylamide concentration was 4% and 8% in the stacking and resolving gels, respectively (bisacrylamide, 1:50). Gels (16 cm x 22 cm, 0.75 mm thick) were run at a constant current of 10 mA for 1 h, and thereafter, at a constant voltage of 275 V for 22 h at 4°C [33]. Gels were fixed and silver stained according to the Silver Stain Plus procedure (BioRad, Hercules, CA), except that titin gels were dried for approximately 20 h at 40°C immediately after fixing. Relative mobility and intensity of each band was quantified with Quantity One 1-D Analysis software (Bio-Rad) and denistometry (GS-800, Bio-Rad). The relative mobilities of proteins on the gel were linearly related to the log of their molecular mass. The gel regression relationship for titin and MyHC was calculated based on the standard lanes containing human soleus titin and rat cardiac titin and the lanes containing homogenized adult rat TA muscle (which contains the four adult skeletal muscle myosin isoforms (types 1, 2A, 2X, and 2B)), respectively. The molecular mass of the unknown band was calculated from the relative mobility compared to the standards and the regression equation. As TA contained two bands, the data were averaged by weighting the two bands based on the relative density of each.

4.3.5 Hydroxyproline Assay

Collagen percentage was determined using a colorimetric analysis of hydroxyproline content. Briefly, muscle samples were hydrolyzed in 6-N HCl for 24 h at 110°C, dried, and treated with a chloramine T solution for 20 min at room temperature followed by a solution of p-diaminobenzaldehyde for 30 min at 60°C. Sample absorbance was read at 550 nm in triplicate and compared to a standard curve to determine the hydroxyproline content. Hydroxyproline content was converted to collagen using a constant (7.14; [34]) that defines the number of hydroxyproline residues in a molecule of collagen and then normalized to the specimen wet weight to obtain μg collagen/mg of wet weight [35]. Because the assay was not sensitive enough for fibers, ~2 mg of fibers were collected and analyzed. Further, whole muscle blocks were carefully sectioned to include all levels of ECM.

4.3.6 Histology

Muscle sections previously snap frozen in isopentane chilled in liquid nitrogen were used for histology. Cross-sections (10-μm thick) taken from the midportion of the tissue block were cut on a cryostat at −25°C (Microm HM500, Walldorf, Germany). Serial sections were stained with hematoxylin & eosin to observe general tissue morphology. To investigate the collagen area fraction, sections were stained with picosirius red according to the Picosirius Red Stain Kit (Polysciences, Inc., Warrington, PA). Samples were visualized with polarized light to identify collagen location and area fraction. To examine fiber and ECM area fraction, sections were

labeled with 1:200 wheat germ agglutinin (WGA; Alexa Fluor® 680 Conjugate, Life Technologies, Grand Island, NY) for 10 minutes at 20°C. WGA binds to carbohydrates (glycoproteins), which includes collagens (ECM), laminin (basal lamina), and fibronectin, and thus, is a strong tool for quantifying ECM proliferation [36, 37].

Fiber cross-sectional areas were measured from WGA-stained slides using a custom-written macro in ImageJ (NIH, Bethesda, MD). Filtering criteria were applied to insure measurement of actual muscle fibers. These criteria rejected regions with areas below 50 μm^2 or above 5,600 μm^2 to eliminate neurovascular structures and "optically fused" fibers, respectively. Fibers touching the edge of the field were excluded as they were assumed to be incomplete. Regions with circularity below 0.30 or above 1.0 were excluded to prevent inclusion of fibers that were obliquely sectioned. Over 70% of the muscle section was included to avoid sample bias. To assess endomysial changes, images were taken at 10X and cropped to avoid the presence of perimysium. Images were then taken at 4X magnification to appropriately assess perimysial changes after tenotomy.

4.3.7 Muscle Architecture

The muscle halves were removed from 10% formalin, rinsed in isotonic phosphate-buffered saline, and digested in 15% H_2SO_4 for 20 minutes to facilitate muscle fiber bundle microdissection. Muscle architecture was completed according to the methods of Sacks and Roy [38] as modified by Lieber and Blevins [23]. Muscle

length was measured for each muscle. Two fiber bundles from three regions (six total) of each muscle were microdissected and sarcomere length (L_s) was measured in each bundle using laser diffraction [3, 28].

4.3.8 Data Analysis

PCSA (cm^2) was calculated according to the equation $(M \bullet \cos(\theta))/(L_{fn} \bullet \rho)$ where M is measured muscle mass, θ is pennation angle, L_{fn} is fiber length normalized to sarcomere length from muscle architecture, and ρ is an assumed density of 1.0597 g/cm^3 [39]. To include only the contractile area fraction, an adjusted PCSA was calculated by subtracting out the ECM fraction calculated from WGA-stained cross-sections. Thus, whole muscle stress was determined by normalizing force to adjusted PCSA to compare muscles, while passive stress was determined from unadjusted PCSA [40]. Furthermore, because tenotomized muscles have been known to fatigue quicker than control muscles, active force was corrected by via a muscle-specific equation dependent on contraction number. For fibers, bundles, and fascicles, force data were converted to stress by dividing force by the baseline cross-sectional area value determined assuming a cylindrical sample with an average diameter determined from 3 separate points along the fiber. In all cases, length was converted to strain by normalizing to the slack length of the specimen.

For active tension, the experimental data from control and tenotomized muscles were compared to the theoretical model used previously in [3] using intraclass correlation coefficients (ICC) (20.0 SPSS, Armonk, NY). In addition, excursion was

quantified by the full-width-at-half-maximum (FWHM; [3]) and compared to L_{fn} in both control and tenotomized muscles via linear regression. However, data were not captured at exactly 50% of peak force for all trials, thus raw data were fit to a second-order polynomial (r^2=0.93±0.02 & 0.94±0.01 for control and tenotomy muscles, respectively) to permit the calculation of FWHM. To examine the effect of pathology on specific tension [4], peak force was linearly regressed against PCSA in both control and tenotomized muscles.

For passive tension, passive stress-strain curves were fit with a second-order polynomial (r^2: 0.98±0.01 & 0.99±0.01 for control and tenotomy, respectively, averaged for fibers, bundles, fascicles, and whole muscle). Tangent moduli were evaluated at 3.5 μm (chosen arbitrarily as a value in which passive tension has sufficiently developed). Data from control and tenotomized muscles were compared to the structural passive model developed in Chapter 3 using ICC. Briefly, theoretical data was fit with the equation $y = Ax^2 + Bx$, where y is stress in kPa, x is strain, and A and B are coefficients determined by the following equations:

$$\begin{aligned} A &= 120.29C_{WM} - 12.16L_{fn} - 89.46 \\ B &= -2.50T_{WM} - 19.62L_{fn} + 9511.011 \end{aligned} \quad (1)$$

Where C_{WM} is the collagen content at the whole muscle level [in %], L_{fn} is normalized fiber length [in mm], and T_{WM} is the titin molecular weight at the whole muscle level [in kDa].

ECM material properties were determined using the theory of composites, which states that the elastic modulus of a composite material is the sum of the elastic modulus of each component multiplied by its volume fraction [41]. This relationship

is mathematically defined by the rule of mixtures, and has been used previously to define the contribution of ECM to muscle passive mechanics [42, 43].

$$E_{ecm} = \frac{E_m - E_f(1 - A_{ecm})}{A_{ecm}} \quad (2)$$

where E_{ecm} is the modulus of the ECM, E_f is the fiber modulus, E_m is the modulus of the whole muscle (composite), and A_{ecm} is the ECM area fraction in the whole muscle.

Muscle, treatment, and size scale were compared using a three-way repeated-measures ANOVA, and pair-wise comparisons were used to compare all levels. The correlation between passive moduli at a given size scale and the structural predictors for the three muscles was evaluated using multiple regression analysis. For whole muscle, normalized muscle and fiber lengths, PCSA, fiber area, pennation angle, titin molecular weight, myosin heavy chain isoform distribution, and collagen content were included as independent variables in the analysis. For fascicles, fiber bundles, and single fibers, the specimen cross-sectional area, slack length, titin molecular weight, and collagen content were included. Both step-up and step-down hierarchical regression analyses were used to confirm significant results. Significance was set to $p < 0.05$, and data are presented as mean±SEM (standard error of the mean).

4.4 Results

Six week post-tenotomy, muscles declined in mass by over a quarter of their control values (Table 4.1, $p < 0.001$). This was matched by a decline in normalized fiber length (L_{fn})/ sarcomere number. The decline in both L_{fn} and mass resulted in no

change in PCSA for TA ($p = 0.858$) and EDII ($p = 0.144$) and an increase in PCSA for EDL ($p < 0.001$; Table 4.1). This trend was not altered when PCSA was adjusted to include only the contractile area fraction. Furthermore, to quantify the retraction of each muscle, the muscle length was measured *in vivo* and *ex vivo* during muscle architecture measurements and was found to be significantly shorter after tenotomy (Fig. 4.1, Table 4.1; $p < 0.001$).

To test the active scaled sarcomere model established in [3], predicted values from the model were compared to control and tenotomy active tension data (Fig. 4.2). The theoretical model and experimentally measured data agreed well for control data (TA: ICC = 0.840; EDL: ICC = 0.781; EDII: ICC = 0.788; $p < 0.001$ for all muscles). However, following tenotomy, active tension declined moderately in TA (23.6 ± 7.0%) and more substantially in EDL and EDII (56.7 ± 5.4% and 43.0 ± 9.0%, respectively) (Fig. 4.2). Furthermore, EDL and EDII both experienced a broadening of the length tension curve (quantified by an increase in FWHM by 51.8 ± 18.3% and 33.7 ± 12.2% for EDL and EDII, respectively), while TA remained constant (-4.3 ± 10.8%). Thus, the model was still able to accurately predict the length-tension curve for TA (ICC = 0.681, $p < 0.001$), but failed to do so for EDL and EDII (EDL: ICC = 0.093, $p = 0.532$; EDII: ICC = 0.052, $p = 0.567$).

To better understand the disconnect between the model and active tension following tenotomy for two of the three muscles, the ability of muscle architecture to predict function was examined. For control data, the relationship between excursion (quantified as FWHM) and L_{fn} ($r^2 = 0.958$, $p < 0.001$) strongly agreed with previously reported data (ICC = 0.976, $p < 0.001$; [3]) . However, L_{fn} was unable to predict

FWHM following tenotomy (TA: ICC = 0.151, p = 0.242; EDL: ICC = 0.001, p = 0.493; EDII: ICC = 0.012, p = 0.333; Fig. 4.3A). Similarly, the relationship between control peak force and PCSA (r^2 = 0.982, p < 0.001) also strongly agreed with previously reported data in healthy muscle (ICC = 0.943, p < 0.001; [4]). However, PCSA was unable to predict function following tenotomy (TA: ICC = 0.305, p = 0.139; EDL: ICC = 0.007, p = 0.444; EDII: ICC = 0.048, p = 0.378; Fig. 4.3B).

Because architecture was unable to predict function, multiple regression was used to identify the structural or biochemical variables that could explain the change in peak force and FWHM. Under normal conditions, L_{fn} was the best predictor of FWHM (slope = 0.68 ± 0.05) and adjusted PCSA was the best predictor of peak force (slope = 22.4 ± 1.3 N/cm^2). Therefore, to appropriately assess post-tenotomy changes, we focused on understanding the change in tenotomy data compared to controls. For the change in FWHM, the change in L_{fn} (ΔL_{fn}) was the strongest contributor to predicting FWHM (standardized weight (β) = 1.23). The change in adjusted PCSA ($\Delta PCSA_{adj}$) further contributed to increasing FWHM (β = 0.43), while the change in collagen (ΔCollagen) acted to resist FWHM increases (β = -0.62). To predict the change in muscle force, $\Delta PCSA_{adj}$ remained the strongest contributing variable (β = -0.78), but displayed the opposite correlation as the control data, revealing that adjusted PCSA actually served to decrease peak force under tenotomy conditions. Examining this further, specific tension ($P_0/PCSA_{adj}$) of the tenotomized muscles (123.3 ± 14.6 kPa) was approximately 40% lower compared to control muscles (223.6 ± 12.6 kPa), indicating decreased force-generating capacity after tenotomy. This decrease in peak force compared to controls was accentuated by ΔL_{fn} (β = -0.395), while the combined

changes in fiber area ($\Delta Area_{fiber}$; $\beta = 0.49$) and $\Delta Collagen$ ($\beta = 0.49$) served to increase peak force. Taken together, the modification of FWHM and peak force suggest that the architectural data that predict function under normal conditions are no longer the sole determinant of function, and the changes in other structural variables alter function based on muscle-specific morphologic differences.

In an attempt to develop a robust model for predicting active tension under pathologic conditions, the structural parameters discussed above were merged with the control architectural relationships to predict altered function following tenotomy. The results yielded the following equations:

$$\begin{aligned} FWHM &= 0.68L_{fn} + 2.15\Delta L_{fn} + 9.60\Delta PCSA_{Adj} - 0.42\Delta Collagen + 21.96 \\ Force_{Peak} &= 22.4PCSA_{Adj} - 28.04\Delta PCSA_{Adj} - 1.11\Delta L_{fn} + 0.54\Delta Collagen + 0.01\Delta Area_{Fiber} - 11.39 \end{aligned} \quad (3)$$

where L_{fn} is the normalized fiber length of the control muscle [mm], $PCSA_{Adj}$ is the adjusted PCSA of the control muscle [cm^2], and ΔL_{fn}, $\Delta PCSA_{Adj}$, $\Delta Collagen$, and $\Delta Area_{Fiber}$ are the difference between tenotomy and control normalized fiber length [mm], adjusted PCSA [cm^2], collagen content [% μg collagen/mg wet weight], and fiber area [μm^2], respectively (FWHM and peak force: $p < 0.003$ and $p < 0.005$ for all coefficients and constants, respectively). Under control conditions, these equations simplify to the architectural relationships between FWHM & L_{fn} and peak force & PCSA found for the control data. By fitting a second order polynomial to the three points defined by the peak force and FWHM, the theoretical model matched the

experimental data for both control (TA: ICC = 1.00, $p < 0.001$; EDL: ICC = 0.934, $p < 0.001$; EDII: ICC = 0.981, $p < 0.001$) and tenotomy (TA: ICC = 0.965, $p < 0.001$; EDL: ICC = 0.509, $p < 0.001$; EDII: ICC = 0.460, $p < 0.001$) data (Fig. 4.4).

To appropriately validate the passive tension model under pathologic conditions, it is important to first understand how the structural predictors of passive tension change with tenotomy. Passive tangent moduli were calculated from stress-strain curves at 3.5 μm for fibers, bundles, fascicles, and whole muscle. As reported previously (Chapter 3), control moduli increased nonlinearly with size scale ($p < 0.001$) and were significantly different among muscles ($p < 0.001$; Fig. 4.5). Following tenotomy, moduli increased significantly ($p < 0.001$), and this increase was dependent on size scale ($p < 0.001$) and muscle ($p < 0.001$). As a control to make sure that specimen size was not a confounding effect, single fiber, bundle, or fascicle CSA were not significantly different between control and tenotomy groups ($p = 0.231$).

To explain the passive functional changes observed after tenotomy, titin isoform size, myosin heavy chain isoform distribution, and collagen content were examined. Average titin molecular weight was determined from the previously tested fibers, bundles, and fascicles and a whole muscle homogenate. For EDL and EDII, titin size increased with tenotomy ($p < 0.001$), but no change in titin isoform was noted in TA ($p = 0.284$; Fig. 4.6B). For myosin heavy chain isoform distribution, muscles did not experience any change in MyHC isoform due to all control muscles being fast initially ($p = 0.427$, Fig. 4.6C). Average collagen content was determined for fibers, bundles, fascicles, and whole muscle homogenate using a hydroxyproline assay. Collagen content was found to increase with size ($p < 0.001$), was significantly

different across muscles ($p < 0.001$), and was muscle-dependent at each size scale ($p < 0.001$; Fig. 4.6D) for both control and tenotomy data.

To further probe passive changes, multiple regression analysis was used to examine the structural variables best responsible for predicting passive moduli (Table 4.2). For control data, titin was the only significant predictor at the single fiber and bundle level ($p < 0.001$ and $p = 0.009$, respectively). At the fascicle level, collagen replaced titin as the strongest predictor ($p = 0.001$). Finally, at the whole muscle, L_{fn}, collagen, and PCSA all contributed to predicting the passive modulus with all factors contributing equally ($\beta = -0.488$, 0.464, and -0.457; $p = 0.001$, $p = 0.001$, $p < 0.001$, respectively). With tenotomy, all of the previous strongest predictors were maintained. Despite not reaching significance, titin was still the best predictor at the fiber and bundle level ($p = 0.099$ and 0.209, respectively). Collagen remained the strongest (and became the only) predictor at both the fascicle and whole muscle level ($p = 0.001$ and $p < 0.001$, respectively), suggesting that the increase in collagen dominated over any architectural predictors that were previously present.

The importance of collagen for passive stiffness was highlighted for both control and tenotomy data at large size scales, but it is unclear whether the increase in modulus is a direct result of a change in ECM material properties or the result of collagen proliferation at a given level. To test these hypotheses, the rule of mixtures for composites (Eq. 2) was utilized to determine the modulus of the ECM. ECM modulus was approximately 1 GPa for all muscles ($p = 0.209$) and was not affected by tenotomy ($p = 0.629$; Fig. 4.7C), suggesting that the material properties of the ECM were not altered following tenotomy. Therefore, the increased modulus is most likely

a result of ECM proliferation. This begs the question if the addition of ECM is uniformly distributed across layers or concentrated at a single level. To answer this question, a wheat germ agglutinin (WGA) stain was used to examine the collagen area fraction at both the endomysial and perimysial levels (Fig. 4.7A). The endomysial area fraction was not significantly different among muscles ($p = 0.617$) and did not change with tenotomy ($p = 0.770$). However, perimysial area fractions were significantly different among muscles ($p < 0.001$) and increased after tenotomy ($p < 0.001$; Fig. 4.7B). This result suggests that the increase in passive modulus is a result of perimysial proliferation. To further validate this result, the WGA data was found to correlate strongly with the quantification of collagen from the picosirius red stain (ICC = 0.776 and 0.787, $p < 0.001$ for control and tenotomy, respectively).

As the predictors of passive tension remained the same for control and tenotomized muscles, the passive model established in Chapter 3 was applied to the control and tenotomy data to test its robustness under pathological conditions. The theoretical model and experimentally measured data agreed well for both control (TA: ICC = 0.997; EDL: ICC = 0.976; EDII: ICC = 0.975; $p < 0.001$ for all muscles) and tenotomy (TA: ICC = 0.997; EDL: ICC = 0.993; EDII: ICC = 0.955; $p < 0.001$ for all muscles) data, suggesting that this model may be used to predict passive tension in both control and pathologic states (Fig. 4.8).

4.5 Discussion

The most important finding was that structurally-based models for active and passive tension were able to accurately predict the length tension relationship under both control and tenotomy conditions (Fig. 4.4 and 4.8). For active tension, the scaled sarcomere model was unable to predict the length-tension curve following tenotomy (Fig. 4.2). This was a direct result of an uncoupling of muscle architecture and function. Therefore, a new model was developed that incorporates changes in collagen and fiber area to better predict FWHM and peak force, respectively. For passive tension, the same structural predictors were found to be important at each size scale in control and tenotomized muscles (e.g., titin at the fiber and bundle level, collagen at the fascicle and whole muscle level), providing strong evidence that alterations in these variables were responsible for the change in passive tension with pathology. Therefore, this study provides a robust model for understanding how structural parameters affect both active and passive tension with pathology. Clinically, these data suggest that using morphological measurements to infer function after adaption may be suitable for both active and passive tension.

Similar to [3], the scaled sarcomere model accurately predicted the experimentally measured active length-tension curve under normal conditions (Fig. 4.2). Following tenotomy, the model was able to predict TA due to its moderate decline in active stress and constant FWHM, but it could not predict EDL and EDII. This result suggests the effect of tenotomy was muscle-specific and that the uncoupling of architecture and function was most predominant in EDL and EDII.

Because L_{fn} is the main determinant of excursion under normal conditions, it is logical to hypothesize that changes in L_{fn} following tenotomy would accurately predict the altered muscle excursion. A previous study [18] had suggested that after a tendon lengthening, newly synthesized sarcomeres were not yet functional, and these less functional sarcomeres might negatively affect the muscle's contractile function. However, we reported a similar uncoupling after the deletion of functional sarcomeres, suggesting that the addition of sarcomeres is not the cause of the disconnect. A second explanation hypothesized that the structure-function relationship had not stabilized following adaption. This is based on the idea that intramuscular remodeling occurs during 4 weeks after altered muscle use [44-46]. However, six weeks of recovery was chosen in this study to provide adequate time for remodeling to stabilize before testing occurred. Although unlikely, it is not clear if a later time point would provide a stronger correlation between structure and function. These conclusions suggest that the altered excursion is a result of remodeling in structural variables in addition to L_{fn}.

Therefore, a new model was developed that relied on morphologic measurements to predict the active length tension relationship (Fig. 4.4). Under control conditions, the model simplifies to predict excursion based on L_{fn} with the same slope as [3] (Fig. 4.3A). Moreover, after tenotomy, the addition of tenotomy-control differences in L_{fn}, adjusted PCSA, and collagen content produced a model that was able to accurately predict muscle excursion. As hypothesized above, ΔL_{fn} was the strongest contributor to the model. $\Delta PCSA_{adj}$ further contributed to increasing FWHM, while increases in collagen resisted increases in FWHM. Based on these results, we hypothesize two mechanisms for the changes in excursion: 1) functional stiffening

caused by an increased in collagen content may ultimately change the load-bearing structure within whole muscle during active contraction, or 2) ECM-fiber connections (i.e., costameric proteins) may be altered with remodeling resulting in a compliant fiber that "floats" within a stiffer ECM. Both of these hypotheses share the idea that specimen strain is a reflection of a stretch in the ECM, leaving sarcomere length relatively unchanged, which would result in a broader length tension curve. The relationship between FWHM and collagen content support these hypotheses, but to appropriately validate these results, sarcomere length would need to be measured *in vivo* as the muscle is stretched.

Similar to FWHM, simplification of the model for predicting peak force yields a specific tension of 22.4 N/cm^2 under normal conditions (compare to 22.5 N/cm^2 in [4]). Following tenotomy, $\Delta PCSA_{adj}$ inversely affected peak force, suggesting that despite increases in contractile area fraction, force is decreased. This is unlikely to be the result of altered intrinsic properties of the fiber itself because $\Delta Area_{fiber}$ is a significant positive predictor of force. Therefore, we hypothesize that the decline in force is a result of impaired force transmission either by disruption of ECM-fiber connections or by neuromuscular junction modulation. The former hypothesis is supported by result that increased collagen content increases peak force by aiding in force transmission, and increased L_{fn} decreases peak force by providing a longer path of transmission. Impaired excitation-contraction coupling has been suggested as a source of declined tension previously [16], but as the current study only focused on structural parameters, we cannot currently comment on this. Furthermore, it is important to note that these results may be impacted by limitations in PCSA. PCSA is

a computed value that relies heavily on mass and L_{fn}. Therefore, a larger decline in L_{fn} compared to mass or an overestimation in mass will produce an artificially large PCSA. Despite taking extra care to blot the muscle dry, muscle mass was measured wet, and thus, a tenotomized muscle may hold more water compared to controls. However, it is unlikely that the disconnect would be caused solely by an overestimation of mass.

Passively, muscles became stiffer following tenotomy, and it was size-scale and muscle dependent (Fig. 4.5). This increase is consistent with results reported from rotator cuff tears [19], intervertebral disc degeneration [12], desmin knockout bundles [11]. To probe the structures responsible to the changes in passive tension at each size scale, titin isoform, myosin heavy chain isoform distribution, and collagen content was examined (Fig. 4.6). Similar to active tension, TA exhibited a mild phenotype after tenotomy with no change in titin isoform and a moderate increase in collagen content. Conversely, EDL and EDII revealed increased titin isoform sizes and increases in collagen content. No muscles experienced a shift in MyHC isoform, which is likely due to the relatively small number of slow fibers in each muscle under control conditions.

The idea that titin isoform is altered with pathology is debatable (isoform altered: [12], [14]; no change: [9, 47]). Furthermore, many studies do not observe any correlation between titin and modulus after pathology [12, 47]. In the current study, the alteration in titin size was unable to account for the increase in passive tension for EDL and EDII and the decrease in passive tension for TA at the fiber level. Despite not reaching significance, titin size remained the strongest predictor of passive moduli

from the independent variables we examined at the fiber and bundle level (Table 4.2). This suggests that other intracellular proteins or the reorganization of fiber materials that were not measured in the current study may have replaced titin as the main determinant of passive tension at smaller size scales following tenotomy, but further research is needed to determine a significant predictor at these size scales. At larger size scales, collagen remained the strongest predictor of passive moduli for both fascicle and whole muscle size scale (Table 4.2). Furthermore, the predictors of whole muscle function for control muscles matched well with the predictors reported in Chapter 3 (L_{fn} and collagen were reported as significant predictors).

As fascicle and whole muscle stiffness was shown to be predominantly determined by the amount of connective tissue (Table 4.2, Chapter 3), WGA staining was used to further probe ECM proliferation (Fig. 4.7B) and ECM modulus (Fig. 4.7C). The ECM passive modulus agrees with values reported in the literature [11, 27, 43]. Furthermore, the idea that perimysial proliferation is responsible for the increase in passive moduli has been reported previously [18], although ECM wasn't explicitly measured in this study. Perimysium is a complex load-bearing structure that can transmit contraction forces [48, 49] and produce passive tension at focal attachment sites, known as perimysial junction plates [49, 50]. Although little is known regarding their contribution to passive tension, increases in perimysium, and subsequent increases in perimysial junction plates, will provide more "struts" to resist passive stretch. Further research will be needed to determine the exact contribution of these perimysial junction plates in mediating passive tension.

The passive model established in Chapter 3 was applied to the control and tenotomy passive tension data (Eq. 1, Fig. 4.8). The model was able to accurately capture the performance of both control and tenotomy data suggesting that the model can be robustly applied to control muscles and pathologic muscles affected by fibrosis or serial sarcomere deletion. This model improves over current passive tension models that typically rely on a generic curve [5] that is scaled by a muscle's architectural parameters. These models fail to accurately predict passive tension because they fail to incorporate any mechanism of load-bearing [6, 7] and do not consider load-bearing protein differences among muscles [8]. The current model demonstrates that the model is over three times more sensitive to collagen than L_{fn} (standardized coefficients: collagen = 0.687, L_{fn} = -0.183) and relies on muscle-specific collagen contents.

It is important to note that both active and passive models were developed and validated in rabbit. Therefore, extrapolation of the model to other species will require further validation. Furthermore, the passive model was developed from control data and validated on tenotomy data. The active data, however, was developed simultaneously on control and tenotomy data, and thus, has not been explicitly validated outside the current system. Explicit testing in other species and on different muscles is needed to extrapolate the current results. However, the two models presented in this paper do identify key structural parameters mediating both active and passive tension following tenotomy and this result will be paramount to identifying the mechanism of length tension remodeling during pathology.

In summary, these data demonstrate that control and tenotomy whole muscle passive tension curves can be well modeled using muscle-specific biochemical and

architectural parameters. Despite the failure of architectural parameters to accurately predict active length tension curves, a model based on morphological structural measurements was developed that was able to accurately predict active tension. Clinically, these data identify key structures responsible for the alteration in function and suggest that inferring function from morphological data is suitable for both active and passive tension.

4.6 Acknowledgements

I would like to acknowledge the co-authors of this paper. Chapter 4 is currently being prepared for submission for publication of the material, Winters TM, Yamaguchi T, Masuda K, Lieber RL, Ward SR. We thank Shannon Bremner for her expertise in the development of the LabView program, Mark Chang for his assistance during surgeries, Mark Chapman for is help developing the hydroxyproline assay, Tony Choi for helping run the titin gels, Mary Burrows for her help running the myosin heavy chain gels, Tatsuhiko Fujiwara for help suturing during the survival surgery, and Eugene Sato for his helpful discussions. The authors have no conflicts of interest to disclose. We acknowledge grant support by the Department Veterans Affairs and NIH/NICHD grants HD048501 and HD050837.

4.7 References

1. Gans, C., *Fiber architecture and muscle function.* Exerc Sport Sci Rev, 1982. **10**: p. 160-207.

2. Lieber, R.L. and J. Friden, *Functional and clinical significance of skeletal muscle architecture.* Muscle Nerve, 2000. **23**(11): p. 1647-66.

3. Winters, T.M., et al., *Whole muscle length-tension relationships are accurately modeled as scaled sarcomeres in rabbit hindlimb muscles.* J Biomech, 2011. **44**(1): p. 109-15.

4. Powell, P.L., et al., *Predictability of skeletal muscle tension from architectural determinations in guinea pig hindlimbs.* J Appl Physiol, 1984. **57**(6): p. 1715-21.

5. Zajac, F.E., *Muscle and tendon: properties, models, scaling, and application to biomechanics and motor control.* Crit Rev Biomed Eng, 1989. **17**(4): p. 359-411.

6. Delp, S.L., et al., *An interactive graphics-based model of the lower extremity to study orthopaedic surgical procedures.* IEEE Trans Biomed Eng, 1990. **37**(8): p. 757-67.

7. Delp, S.L., et al., *OpenSim: open-source software to create and analyze dynamic simulations of movement.* IEEE Trans Biomed Eng, 2007. **54**(11): p. 1940-50.

8. Prado, L.G., et al., *Isoform diversity of giant proteins in relation to passive and active contractile properties of rabbit skeletal muscles.* J Gen Physiol, 2005. **126**(5): p. 461-80.

9. Smith, L.R., et al., *Hamstring contractures in children with spastic cerebral palsy result from a stiffer extracellular matrix and increased in vivo sarcomere length.* J Physiol, 2011. **589**(Pt 10): p. 2625-39.

10. Granzier, H.L. and T.C. Irving, *Passive tension in cardiac muscle: contribution of collagen, titin, microtubules, and intermediate filaments.* Biophys J, 1995. **68**(3): p. 1027-44.

11. Meyer, G.A. and R.L. Lieber, *Skeletal Muscle Fibrosis Develops in Response to Desmin Deletion.* Am J Physiol Cell Physiol, 2012.

12. Brown, S.H., et al., *ISSLS prize winner: Adaptations to the multifidus muscle in response to experimentally induced intervertebral disc degeneration.* Spine (Phila Pa 1976), 2011. **36**(21): p. 1728-36.

13. Friden, J. and R.L. Lieber, *Spastic muscle cells are shorter and stiffer than normal cells.* Muscle Nerve, 2003. **27**(2): p. 157-64.

14. Thacker, B.E., et al., *Passive mechanical properties and related proteins change with botulinum neurotoxin A injection of normal skeletal muscle.* J Orthop Res, 2011. **30**(3): p. 497-502.

15. Jamali, A.A., et al., *Skeletal muscle response to tenotomy.* Muscle Nerve, 2000. **23**(6): p. 851-62.

16. Abrams, R.A., et al., *Skeletal muscle recovery after tenotomy and 7-day delayed muscle length restoration.* Muscle Nerve, 2000. **23**(5): p. 707-14.

17. Buller, A.J. and D.M. Lewis, *Some Observations on the Effects of Tenotomy in the Rabbit.* J Physiol, 1965. **178**: p. 326-42.

18. Takahashi, M., et al., *Muscle excursion does not correlate with increased serial sarcomere number after muscle adaptation to stretched tendon transfer.* J Orthop Res, 2012.

19. Safran, O., et al., *Changes in rotator cuff muscle volume, fat content, and passive mechanics after chronic detachment in a canine model.* J Bone Joint Surg Am, 2005. **87**(12): p. 2662-70.

20. Jozsa, L., et al., *The effect of tenotomy and immobilisation on intramuscular connective tissue. A morphometric and microscopic study in rat calf muscles.* J Bone Joint Surg Br, 1990. **72**(2): p. 293-7.

21. Barry, J.A., et al., *The effect of immobilization on the recovery of rabbit soleus muscle from tenotomy: modulation by chronic electrical stimulation.* Exp Physiol, 1994. **79**(4): p. 515-25.

22. Baker, J.H. and E.C. Hall-Craggs, *Changes in sarcomere length following tenotomy in the rat.* Muscle Nerve, 1980. **3**(5): p. 413-6.

23. Lieber, R.L. and F.T. Blevins, *Skeletal muscle architecture of the rabbit hindlimb: functional implications of muscle design.* J Morphol, 1989. **199**(1): p. 93-101.

24. Takahashi, M., S.R. Ward, and R.L. Lieber, *Intraoperative single-site sarcomere length measurement accurately reflects whole-muscle sarcomere length in the rabbit.* J Hand Surg [Am], 2007. **32**(5): p. 612-7.

25. Lieber, R.L. and J. Friden, *Muscle damage is not a function of muscle force but active muscle strain.* J Appl Physiol, 1993. **74**(2): p. 520-6.

26. Lieber, R.L., T.M. Woodburn, and J. Friden, *Muscle damage induced by eccentric contractions of 25% strain.* J Appl Physiol, 1991. **70**(6): p. 2498-507.

27. Lieber, R.L., et al., *Inferior mechanical properties of spastic muscle bundles due to hypertrophic but compromised extracellular matrix material.* Muscle Nerve, 2003. **28**(4): p. 464-71.

28. Lieber, R.L., Y. Yeh, and R.J. Baskin, *Sarcomere length determination using laser diffraction. Effect of beam and fiber diameter.* Biophys J, 1984. **45**(5): p. 1007-16.

29. Baskin, R.J., K.P. Roos, and Y. Yeh, *Light diffraction study of single skeletal muscle fibres.* Biophys J, 1979. **28**(1): p. 45-64.

30. Warren, C.M., P.R. Krzesinski, and M.L. Greaser, *Vertical agarose gel electrophoresis and electroblotting of high-molecular-weight proteins.* Electrophoresis, 2003. **24**(11): p. 1695-702.

31. Labeit, S. and B. Kolmerer, *Titins: giant proteins in charge of muscle ultrastructure and elasticity.* Science, 1995. **270**(5234): p. 293-6.

32. Freiburg, A., et al., *Series of exon-skipping events in the elastic spring region of titin as the structural basis for myofibrillar elastic diversity.* Circ Res, 2000. **86**(11): p. 1114-21.

33. Talmadge, R.J. and R.R. Roy, *Electrophoretic separation of rat skeletal muscle myosin heavy-chain isoforms.* J Appl Physiol, 1993. **75**(5): p. 2337-40.

34. Etherington, D.J. and T.J. Sims, *Detection and estimation of collagen.* Journal of the Science of Food and Agriculture, 1981. **32**(6): p. 539-546.

35. Edwards, C.A. and W.D. O'Brien, Jr., *Modified assay for determination of hydroxyproline in a tissue hydrolyzate.* Clin Chim Acta, 1980. **104**(2): p. 161-7.

36. Gulati, A.K. and A.A. Zalewski, *An immunofluorescent analysis of lectin binding to normal and regenerating skeletal muscle of rat.* Anat Rec, 1985. **212**(2): p. 113-7.

37. Gosselin, L.E., et al., *Interstitial space and collagen alterations of the developing rat diaphragm.* J Appl Physiol, 1993. **74**(5): p. 2450-5.

38. Sacks, R.D. and R.R. Roy, *Architecture of the hind limb muscles of cats: functional significance.* J Morphol, 1982. **173**(2): p. 185-95.

39. Mendez, J. and A. Keys, *Density and composition of mammalian muscle.* Metabolism, 1960. **9**: p. 184-188.

40. Gokhin, D.S., et al., *Quantitative analysis of neonatal skeletal muscle functional improvement in the mouse.* J Exp Biol, 2008. **211**(Pt 6): p. 837-43.

41. Jones, R., *Mechanics of Composite Materials*, ed. T.F. Inc. 1999.

42. Purslow, P.P. and J.A. Trotter, *The morphology and mechanical properties of endomysium in series-fibred muscles: variations with muscle length.* J Muscle Res Cell Motil, 1994. **15**(3): p. 299-308.

43. Meyer, G.A. and R.L. Lieber, *Elucidation of extracellular matrix mechanics from muscle fibers and fiber bundles.* J Biomech, 2011. **44**(4): p. 771-3.

44. Eisenberg, B.R., J.M. Brown, and S. Salmons, *Restoration of fast muscle characteristics following cessation of chronic stimulation. The ultrastructure of slow-to-fast transformation.* Cell Tissue Res, 1984. **238**(2): p. 221-30.

45. Eisenberg, B.R. and S. Salmons, *The reorganization of subcellular structure in muscle undergoing fast-to-slow type transformation. A stereological study.* Cell Tissue Res, 1981. **220**(3): p. 449-71.

46. Kernell, D., et al., *Effects of physiological amounts of high- and low-rate chronic stimulation on fast-twitch muscle of the cat hindlimb. I. Speed- and force-related properties.* J Neurophysiol, 1987. **58**(3): p. 598-613.

47. Olsson, M.C., et al., *Fibre type-specific increase in passive muscle tension in spinal cord-injured subjects with spasticity.* J Physiol, 2006. **577**(Pt 1): p. 339-52.

48. Huijing, P.A., G.C. Baan, and G.T. Rebel, *Non-myotendinous force transmission in rat extensor digitorum longus muscle.* J Exp Biol, 1998. **201**(Pt 5): p. 683-91.

49. Passerieux, E., et al., *Physical continuity of the perimysium from myofibers to tendons: involvement in lateral force transmission in skeletal muscle.* J Struct Biol, 2007. **159**(1): p. 19-28.

50. Passerieux, E., et al., Structural organization of the perimysium in bovine skeletal muscle: Junctional plates and associated intracellular subdomains. J Struct Biol, 2006. **154**(2): p. 206-16.

Table 4.1: Muscle architecture is significantly altered following tenotomy. Muscles all retracted similar amounts, quantified by the change in L_{mn}. Due to this retraction, L_{fn} and correspondingly, sarcomere number, decreased. Furthermore, pennation angle increased, while mass decreased. These data result in a maintenance or increase (for EDL) in the muscle's PCSA. Data are presented as mean ± SEM.

Parameter	TA		EDL		EDII	
	Control	Tenotomy	Control	Tenotomy	Control	Tenotomy
L_{mn} [mm]	57.713 ± 2.505	44.355 ± 3.7233*	71.194 ± 3.436	57.935 ± 2.932*	56.354 ± 1.918	42.158 ± 2.936*
L_{fn} [mm]	38.406 ± 0.005	28.389 ± 1.124*	15.425 ± 0.971	7.869 ± 0.346*	10.638 ± 0.818	4.973 ± 0.521*
Sarcomere Number	15522 ± 353	12343 ± 223*	6250 ± 212	3421 ± 151*	4015 ± 247	2162 ± 226*
Pennation Angle [deg]	0.6 ± 0.2	5.8 ± 0.6*	8.7 ± 0.8	23.8 ± 2.7*	18.1 ± 2.9	33.1 ± 2.1*
Mass [g]	3.17 ± 0.06	2.45 ± 0.10*	3.18 ± 0.06	2.37 ± 0.07*	0.73 ± 0.03	0.48 ± 0.03*
PCSA [cm^2]	0.781 ± 0.0295	0.808 ± 0.033	1.927 ± 0.117	2.548 ± 0.113*	0.619 ± 0.064	0.779 ± 0.0756

Values are mean ± SEM; L_{mn}: Normalized muscle length; L_{fn}: Normalized fiber length

*Significantly different from control data, $p < 0.001$

Table 4.2: Multiple regression analysis on control and tenotomy data confirms that titin and collagen are the main sources of passive tension at small and large size scales, respectively. For control data, titin was the only significant predictor at the single fiber and bundle level, and collagen was the main source at the fascicle level. At the whole muscle, L_{fn}, collagen, and PCSA all contributed to predicting the passive modulus with all factors contributing equally With tenotomy, all of the previous strongest predictors were maintained. Despite not reaching significance, titin was still the best predictor at the fiber and bundle level, and collagen remained the strongest predictor at both the fascicle and whole muscle level, suggesting that the increase in collagen dominated over any architectural predictors that were previously present. Data are presented as mean ± SEM.

Size	Treatment	Parameter	Unstandardized Weights	tandardized Weight	Significance	r^2
Single Fiber	Control	Titin	-0.178 ± 0.37	0.769	$p < 0.001$	0.592
		Constant	679.690 ± 131.162	N/A	$p < 0.001$	N/A
	Tenotomy	Titin	0.078 ± 0.044	0.402	$p = 0.099$	0.161
		Constant	-244.877 ± 158.821	N/A	$p = 0.176$	N/A
Fiber Bundle	Control	Titin	-0.190 ± 0.064	-0.595	$p = 0.009$	0.354
		Constant	749.299 ± 226.754	N/A	$p = 0.004$	N/A
	Tenotomy	Titin	0.107 ± 0.082	0.311	$p = 0.209$	0.097
		Constant	-254.857 ± 292.572	N/A	$p = 0.397$	N/A
Fascicle	Control	Collagen	49.585 ± 10.507	0.763	$p = 0.001$	0.582
		Constant	-36.625 ± 54.234	N/A	$p = 0.509$	0
	Tenotomy	Collagen	116.123 ± 26.781	0.735	$p = 0.001$	0.54
		Constant	-187.213 ± 214.081	N/A	$p = 0.395$	N/A
Whole Muscle	Control	L_{fn}	-39.976 ± 9.543	-0.488	$p = 0.001$	0.469
		Collagen	100.272 ± 24.639	0.464	$p = 0.001$	0.768
		PCSA	-768.432 ± 145.008	-0.457	$p < 0.001$	0.166
		Constant	1985.349 ± 737.851	N/A	$p = 0.018$	N/A
	Tenotomy	Collagen	101.318 ± 21.925	0.0756	$p < 0.001$	0.572
		Constant	108.900 ± 676.722	N/A	$p = 0.874$	N/A

Values are presented as mean ± SEM

r^2 values represent the explained variation between the parameter and passive modulus; L_{fn}: Normalized fiber length; PCSA: Physiological cross-sectional area

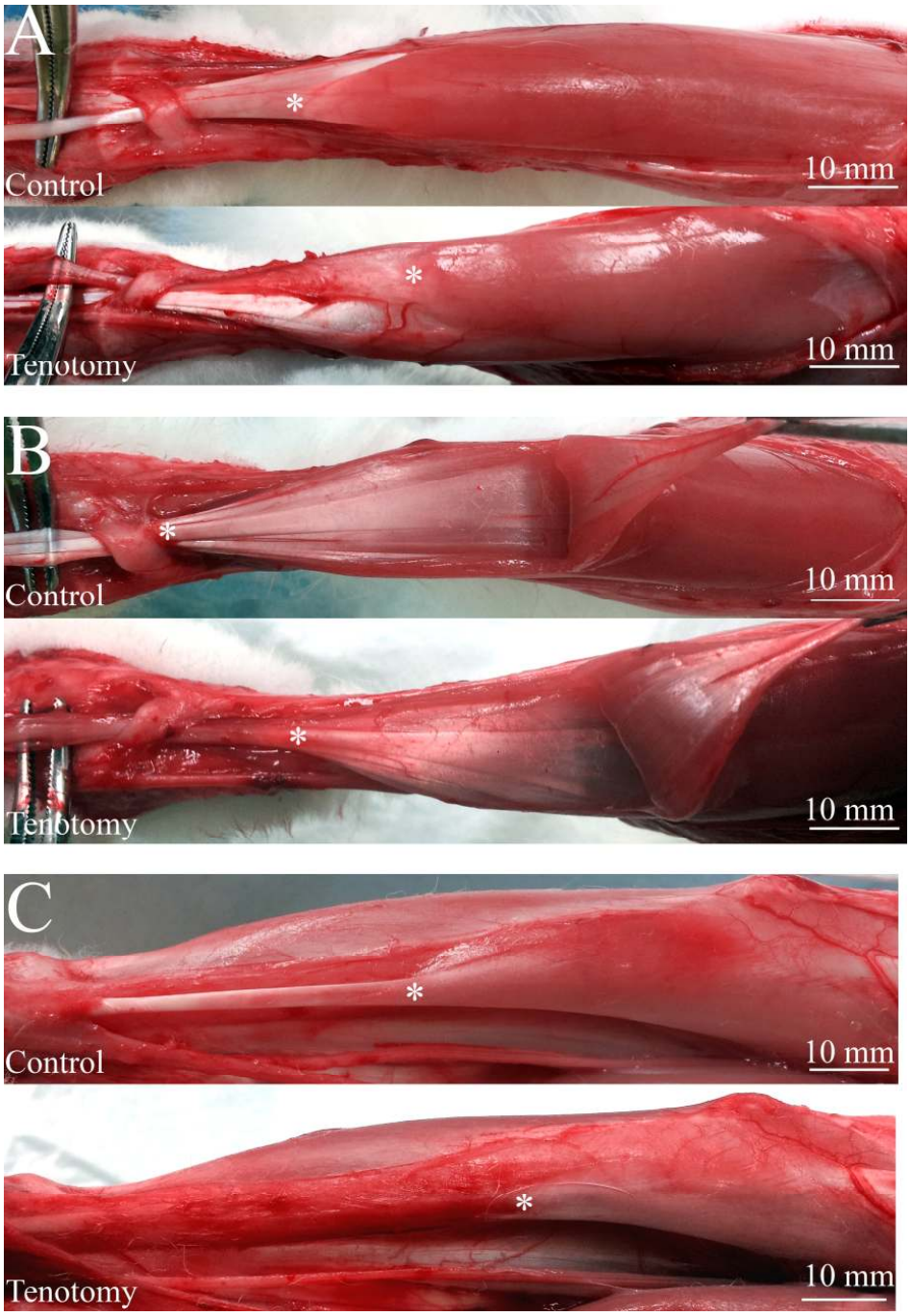

Figure 4.1: Following tenotomy, macroscopic muscular remodeling is observed. Control and tenotomy muscles are shown for (A) TA, (B) EDL, and (C) EDII. Qualitatively, tenotomized muscles appear to be flatter, paler, and covered in a thicker layer of fascia. Furthermore, the pearlescent tendon is now replaced by a connective tissue sheath ending in scar tissue (not shown). For EDII, the connective tissue sheath was so intimately associated with the tibia that surgical dissection was unable to separate the two. Finally, the most distal fibers have retracted (i.e., shortened) compared to controls. Asterisk denotes the most distal muscle fibers.

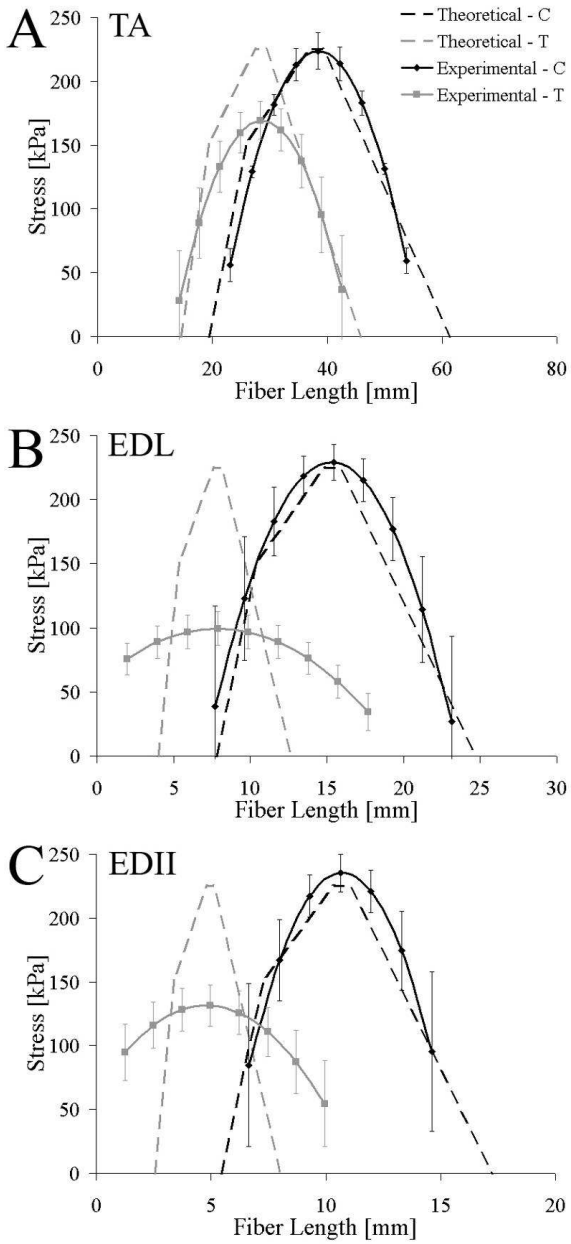

Figure 4.2: Active length-tension relationships do not match the scaled sarcomere model following tenotomy for (A) TA, (B) EDL, and (C) EDII. The scaled sarcomere model established in [3] (dashed lines) was compared to control (black diamonds; solid black line) and tenotomy (grey squares; solid grey line) data. The theoretical model and experimentally measured data agreed well for control data. However, following tenotomy, peak stress declined moderately in TA and more substantially in EDL and EDII. Furthermore, EDL and EDII both experienced a broadening of the length tension curve, while TA remained constant. Thus, the model was able to accurately predict the length tension curve for TA, but failed to do so for EDL and EDII. C and T in legend represent Control and Tenotomy, respectively. Data are presented as mean ± SEM.

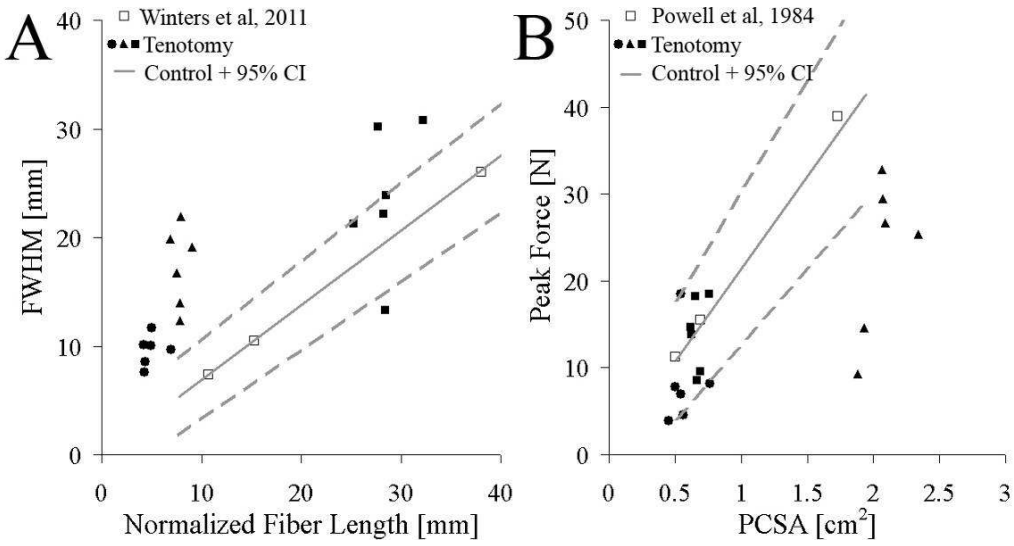

Figure 4.3: Tenotomy alters known architectural relationships. (A) The relationship between excursion (quantified as FWHM) and normalized fiber length (grey line with 95% confidence interval) strongly agrees with previously reported data ([3], open squares) . However, this relationship is not maintained following tenotomy (Black circles, triangles, and squares represent EDII, EDL, and TA, respectively). (B) The relationship between peak force and PCSA (gray line with 95% confidence interval) also strongly agrees with data calculated using a specific tension of 22.5 N/cm^2 ([4], open squares). Similarly, the tenotomy data does not match the reported relationship. These data suggest that a fundamental shift in the muscle structure-function relationship occurs following tenotomy.

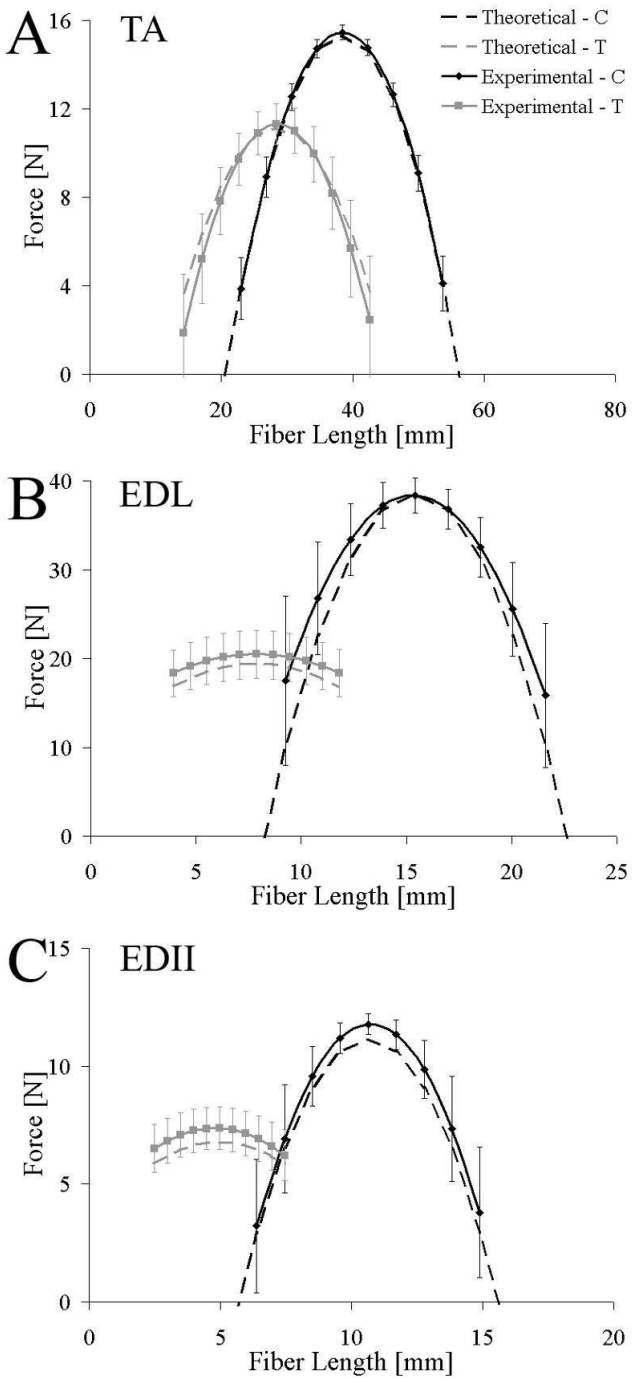

Figure 4.4: The new active tension model accurately predicts both control and tenotomy length tension curves for (A) TA, (B) EDL, and (C) EDII. Based on structural properties, a theoretical model (dashed lines) was found to agree well with experimentally measured control (black diamonds; solid black line) and tenotomy (grey squares; solid grey line) data. This new active tension model was developed from changes in architectural and biochemical properties following tenotomy (see Results for equation). Data are presented as mean ± SEM.

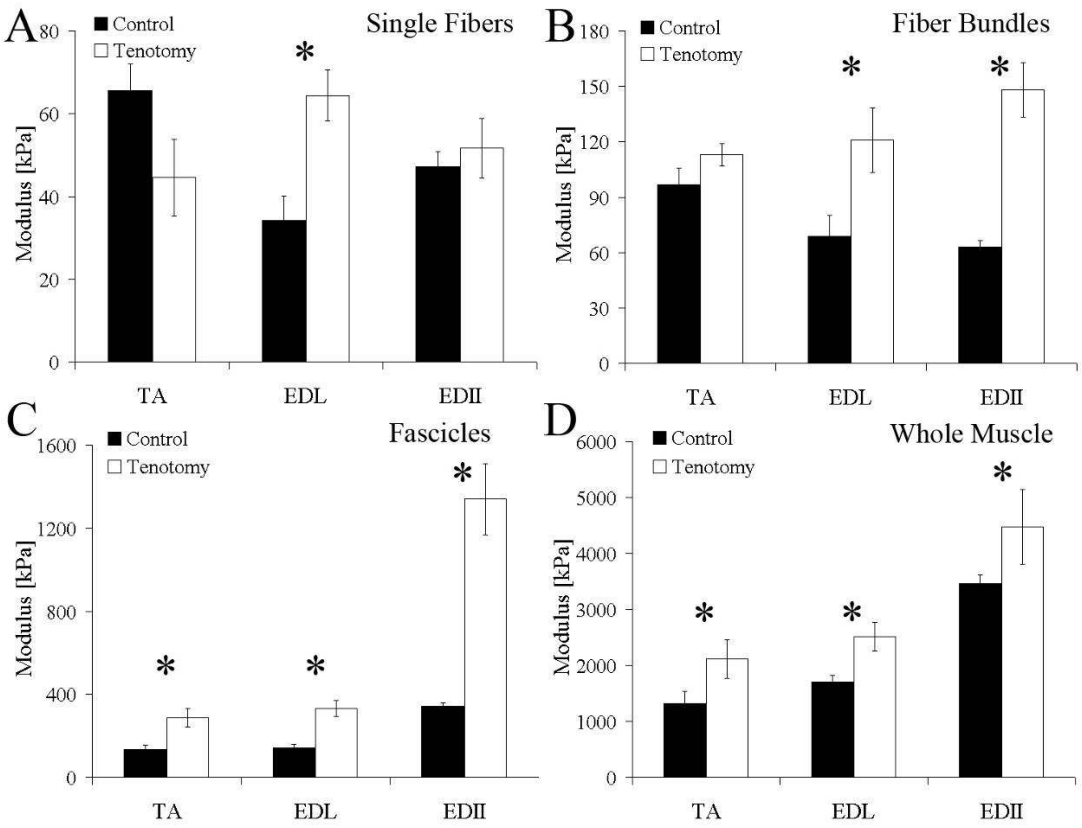

Figure 4.5: The effect of tenotomy on passive moduli is size-scale dependent. Passive tangent moduli were calculated from the stress-strain curves at 3.5 µm for (A) fibers, (B) bundles, (C) fascicles, and (D) whole muscle. With tenotomy, moduli at the single fiber level were altered in a muscle-specific manner. However, as size scale increased, tenotomy produced an increase in passive moduli for all muscles. This suggests that different structures mediate passive tension at the various size scales and that, at least at the fiber level, tenotomy affects them in a muscle-specific manner. Data are presented as mean ± SEM and asterisk (*) indicates significant difference between control and tenotomy.

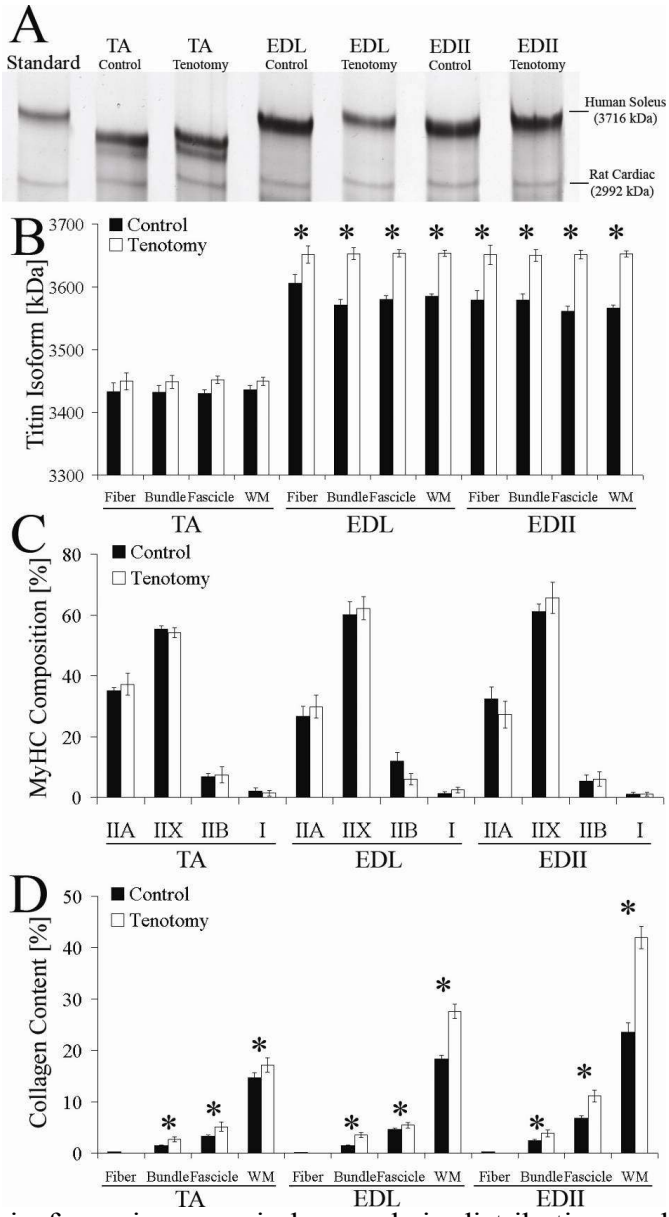

Figure 4.6: Titin isoform size, myosin heavy chain distribution, and collagen content are altered with tenotomy. (A) A representative titin gel. (B) Average titin molecular weight is shown from the passively tested fibers, bundles, and fascicles and a whole muscle homogenate. Titin molecular weight was not significantly different across size scales for any of the muscles tested, but increased with tenotomy for EDL and EDII but not TA. (C) Muscles did not experience any change in MyHC isoform due to all control muscles being fast initially. (D) Average collagen content was determined for fibers, bundles, fascicles, and whole muscle homogenate using a hydroxyproline assay. Collagen content was found to increase with size and was significantly different across muscles. Following tenotomy, collagen was found to increase compared to controls. Collagen content is expressed as % wet weight. Data are presented as mean ± SEM, and asterisk (*) indicates significant difference between control and tenotomy.

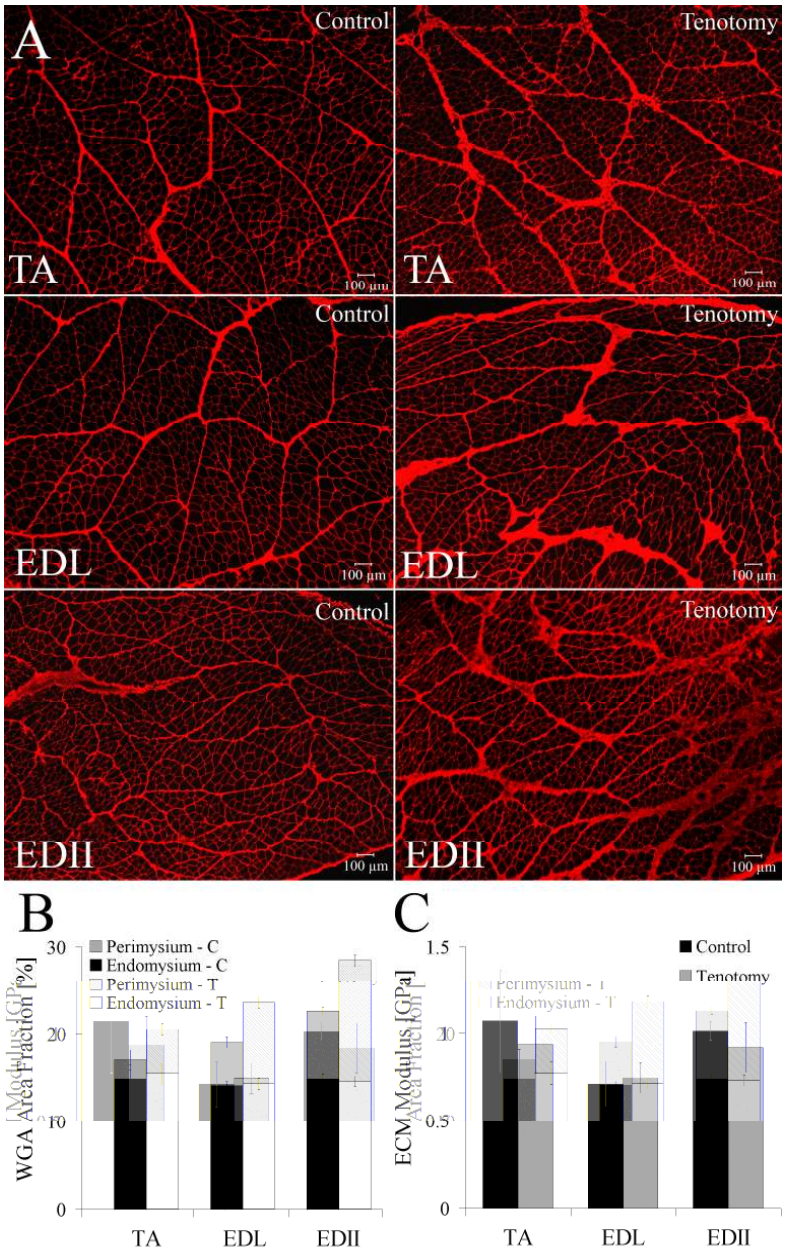

Figure 4.7: Wheat germ agglutinin (WGA) stain reveals proliferation of the perimysium in tenotomized muscles. (A) WGA stain of control and tenotomy TA, EDL, and EDII muscles. Qualitatively, tenotomy sections have more ECM, which appears to be concentrated at the perimysial level. (B) Quantification of the sections in (A). Endomysial area fraction was not significantly different among muscles or between control and tenotomy. However, the perimysial area fraction was significantly different among muscles and increased after tenotomy. (C) Using the rule of mixtures for composites (See Eq. 2 in Methods), the modulus of the ECM was determined. ECM modulus was not statistically different across muscles and was not altered after tenotomy, suggesting that ECM proliferated, but did not alter its material properties. Data are presented as mean ± SEM.

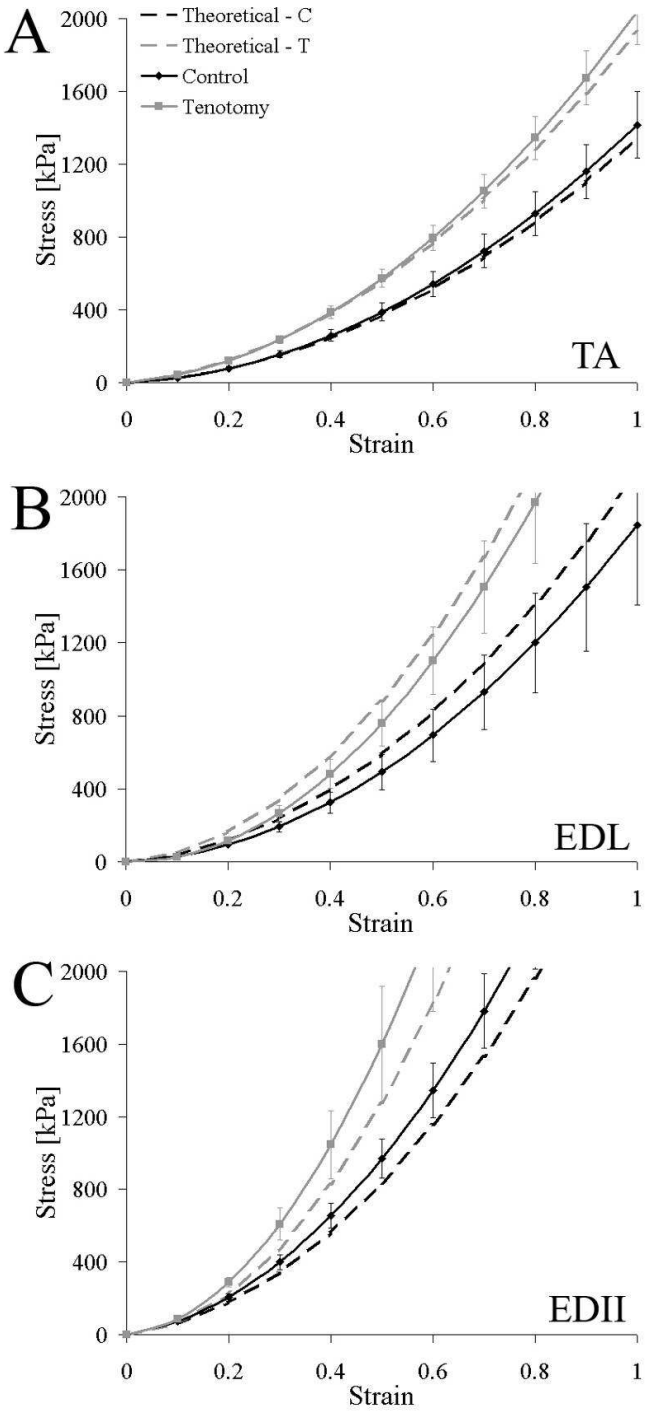

Figure 4.8: The passive model accurately predicts experimental data under both control and tenotomy conditions for (A) TA, (B) EDL, and (C) EDII. The passive model established in Chapter 3 (dashed lines) agreed well with control (black diamonds; black solid line) and tenotomized (grey squares; grey solid line) data, suggesting that this model may be used to predict passive tension in both healthy and pathologic states. Data are presented as mean ± SEM.

CHAPTER 5

CONCLUSIONS

The work in this dissertation provided a structural basis for the prediction of whole muscle active and passive tension in healthy and pathological states. Using relatively simple models to predict function, active and passive length-tension curves of three architecturally distinct muscles were accurately predicted. Under normal conditions, active function relied on myofilament dimensions and architectural parameters, highlighting the importance of intra- and extra-cellular components. Moreover, the passive model, as well as the active model following tenotomy, relied on inputs from architecture, morphologic parameters, and intra- and extra-cellular protein data, suggesting that structures from different size scales and from distinct locations are paramount to passive function. This also reinforces the idea that scaling across size scales is non-linear, suggesting that whole muscle performance is dependent on structures from all size scales. Thus, to appropriately understand the pathology of skeletal muscle, to prescribe a treatment or therapy, or to model the properties of muscle, it is not sufficient to take a static view where only one predictor/one muscle level is considered.

5.1 Success of the Scaled Sarcomere Model

The need for added complexities in a model is a prevalent theme in the literature [1]. However, the results of this dissertation debunk this idea, at least for the prediction of active tension. As seen in Chapter 2 and Chapter 4 (Fig. 2.2 and 4.2), under normal conditions, normalized fiber length, PCSA, and myofilament dimensions are the only parameters that are needed to accurately predict whole muscle performance.

5.2 Scaling of Passive Tension: Fiber to Whole Muscle

To investigate the scaling of passive tension moduli, fibers, bundles, fascicles, and whole muscles were passively stretched. Fundamental differences were noted between fibers/bundles and fascicles, and all scales and whole muscle. These data suggest that the sources of passive tension differ between these scales and these sources are muscle-specific. Clinically, these results demonstrate that bundles are fundamentally different from whole muscles, and thus, this extrapolation should be made with caution or avoided altogether.

5.3 Sources of Passive Tension

The structure-function relationship for active tension is well accepted in the literature [5, 6], while the source(s) of passive tension are highly debated [7, 8]. Chapter 3 was thus completed to provide an objective analysis of the morphologic and

architectural parameters involved in function. Titin was found to be the main source of passive tension at the fiber level, which contained little to no ECM presence. At the bundle level (with the addition of interfibrillar ECM connections), titin remained the strongest predictor. Despite not reaching significance, these results were maintained after tenotomy. These results demonstrate that titin is the dominant predictor of function at size scales with minimal ECM; however, other proteins (i.e., intermediate filaments) may have increased roles following tenotomy [9]. Furthermore, these results suggest that the endomysium may play only a minor role in passive load-bearing.

The first functional difference was observed at the fascicle level, which corresponds with the addition of the perimysium. With two layers of ECM at this level, collagen is functionally relevant. Taken together, these data suggest that the perimysium functions as the main extracellular load-bearing structure. This hypothesis is further supported by the fact that, with tenotomy, preferential perimysial proliferation was observed. Further research is needed to determine the exact mechanism in which the perimysium provides the increased load-bearing. A closer examination of ECM organization after tenotomy may provide insights into this. One potential mechanism is increased perimysial junction plates that could provide more anchoring connections that resist stretch [10].

At the whole muscle level, the synergistic actions of collagen, titin, and normalized fiber length acted to define the passive tension curve. Titin appeared to be functionally relevant during short strains, while collagen provided passive resistance at longer strains. These results are consistent with the structure of the two proteins: the A-band region is recruited into the extensible pool at high strains [11], while the crimp pattern of collagen provides slack at short strains [12-15]. Interestingly, normalized

fiber length appeared to be inversely related to function at all strains, suggesting that passive moduli are designed to prevent overextension of muscle fibers, and thus, damage.

5.4 Morphologic Models of Active and Passive Tension

By identifying key predictors of passive tension, the models from Chapter 2 and Chapter 3 were developed. However, these models were validated on experimental data they were derived from. Furthermore, these models were only applicable to normal conditions, which generally, is not clinically relevant. Therefore, the same system used in Chapters 2 and 3 was perturbed via tenotomy and after 6 weeks of muscle remodeling, the models were retested under new conditions.

The active tension model was unable to predict whole muscle function, reiterating the idea that an uncoupling of architecture and function occurs after pathologic remodeling [16]. This allowed for the refinement of the model, identifying fiber area and collagen to be important contributors to peak force. Regarding excursion, normalized fiber length remained the dominant predictor, while the fibrotic response altered FWHM by resisting stretch.

The model of passive tension was able to accurately match the experimental data, suggesting that the main functionally relevant alterations following tenotomy occurred with titin, collagen, and normalized fiber length. This also validates the model, but further studies are needed to validate it following other pathologies and in other systems.

5.5 Summary

By identifying the key determinants of active and passive tension, a robust model for each was developed that is able to accurately predict whole muscle function under both normal and pathologic conditions. Moreover, both models are relatively simple compared to the range of complexity in the literature. Actively, muscle architecture proved to be the strongest predictor of active force. Passively, the synergistic combination of intracellular proteins, extracellular proteins, and muscle architecture acted to dictate function. Following tenotomy, the resulting fibrotic response stiffened the muscle, which was proposed to be a protective mechanism to prevent overextension of the muscle fibers. Finally, the non-linear scaling across size scales suggests that whole muscle performance is dependent on the combined function of all size scales, and cannot be extrapolated among levels. These models of muscle function provide a new tool for muscle modeling as well as providing a unique perspective into the morphologic and biochemical parameters that modulate active and passive function during normal and pathologic conditions.

5.6 References

1. Blemker, S.S. and S.L. Delp, *Rectus femoris and vastus intermedius fiber excursions predicted by three-dimensional muscle models.* J Biomech, 2006. **39**(8): p. 1383-91.

2. Delp, S.L., et al., *OpenSim: open-source software to create and analyze dynamic simulations of movement.* IEEE Trans Biomed Eng, 2007. **54**(11): p. 1940-50.

3. Delp, S.L. and J.P. Loan, *A graphics-based software system to develop and analyze models of musculoskeletal structures.* Comput Biol Med, 1995. **25**(1): p. 21-34.

4. Delp, S.L., et al., *An interactive graphics-based model of the lower extremity to study orthopaedic surgical procedures.* IEEE Trans Biomed Eng, 1990. **37**(8): p. 757-67.

5. Powell, P.L., et al., *Predictability of skeletal muscle tension from architectural determinations in guinea pig hindlimbs.* J Appl Physiol, 1984. **57**(6): p. 1715-21.

6. Winters, T.M., et al., *Whole muscle length-tension relationships are accurately modeled as scaled sarcomeres in rabbit hindlimb muscles.* J Biomech, 2011. **44**(1): p. 109-15.

7. Magid, A. and D.J. Law, *Myofibrils bear most of the resting tension in frog skeletal muscle.* Science, 1985. **230**(4731): p. 1280-2.

8. Prado, L.G., et al., *Isoform diversity of giant proteins in relation to passive and active contractile properties of rabbit skeletal muscles.* J Gen Physiol, 2005. **126**(5): p. 461-80.

9. Granzier, H.L. and T.C. Irving, *Passive tension in cardiac muscle: contribution of collagen, titin, microtubules, and intermediate filaments.* Biophys J, 1995. **68**(3): p. 1027-44.

10. Passerieux, E., et al., *Structural organization of the perimysium in bovine skeletal muscle: Junctional plates and associated intracellular subdomains.* J Struct Biol, 2006. **154**(2): p. 206-16.

11. Wang, K., et al., *Viscoelasticity of the sarcomere matrix of skeletal muscles. The titin-myosin composite filament is a dual-stage molecular spring.* Biophys J, 1993. **64**(4): p. 1161-77.

12. Benjamin, M., E. Kaiser, and S. Milz, *Structure-function relationships in tendons: a review.* J Anat, 2008. **212**(3): p. 211-28.

13. Diamant, J., et al., *Collagen; ultrastructure and its relation to mechanical properties as a function of ageing.* Proc R Soc Lond B Biol Sci, 1972. **180**(60): p. 293-315.

14. Franchi, M., et al., *Crimp morphology in relaxed and stretched rat Achilles tendon.* J Anat, 2007. **210**(1): p. 1-7.

15. Franchi, M., et al., *Tendon crimps and peritendinous tissues responding to tensional forces.* Eur J Histochem, 2007. **51 Suppl 1**: p. 9-14.

16. Takahashi, M., et al., *Muscle excursion does not correlate with increased serial sarcomere number after muscle adaptation to stretched tendon transfer.* J Orthop Res, 2012.